2019

# Optimal dispatch of uncertain energy resources

Mahraz Amini
*University of Vermont*

# Optimal dispatch of uncertain energy resources

A Dissertation Presented

by

Mahraz Amini

to

The Faculty of the Graduate College

of

The University of Vermont

In Partial Fullfillment of the Requirements
for the Degree of Doctor of Philosophy
Specializing in Electrical Engineering

May, 2019

Defense Date: March 26, 2019
Thesis Examination Committee:

Mads Almassalkhi, Ph.D., Advisor
Taras Lakoba, Ph.D., Chairperson
Paul Hines, Ph.D.
Hamid Ossareh, Ph.D.
Cynthia J. Forehand, Ph.D., Dean of the Graduate College

# Abstract

The future of the electric grid requires advanced control technologies to reliably integrate high level of renewable generation and residential and small commercial distributed energy resources (DERs). Flexible loads are known as a vital component of future power systems with the potential to boost the overall system efficiency. Recent work has expanded the role of flexible and controllable energy resources, such as energy storage and dispatchable demand, to regulate power imbalances and stabilize grid frequency. This leads to the DER aggregators to develop concepts such as the virtual energy storage system (VESS). VESSs aggregate the flexible loads and energy resources and dispatch them akin to a grid-scale battery to provide flexibility to the system operator. Since the level of flexibility from aggregated DERs is uncertain and time varying, the VESSs' dispatch can be challenging. To optimally dispatch uncertain, energy-constrained reserves, model predictive control offers a viable tool to develop an appropriate trade-off between closed-loop performance and robustness of the dispatch. To improve the system operation, flexible VESSs can be formulated probabilistically and can be realized with chance-constrained model predictive control.

The large-scale deployment of flexible loads needs to carefully consider the existing regulation schemes in power systems, i.e., generator droop control. In this work first, we investigate the complex nature of system-wide frequency stability from time-delays in actuation of dispatchable loads. Then, we studied the robustness and performance trade-offs in receding horizon control with uncertain energy resources. The uncertainty studied herein is associated with estimating the capacity of and the estimated state of charge from an aggregation of DERs.

The concept of uncertain flexible resources in markets leads to maximizing capacity bids or control authority which leads to dynamic capacity saturation (DCS) of flexible resources. We show there exists a sensitive trade-off between robustness of the optimized dispatch and closed-loop system performance and sacrificing some robustness in the dispatch of the uncertain energy capacity can significantly improve system performance. We proposed and formulated a risk-based chance constrained MPC (RB-CC-MPC) to co-optimize the operational risk of prematurely saturating the virtual energy storage system against deviating generators from their scheduled set-point. On a fast minutely timescale, the RB-CC-MPC coordinates energy-constrained virtual resources to minimize unscheduled participation of ramp-rate limited generators for balancing variability from renewable generation, while taking into account grid conditions. We show under the proposed method it is possible to improve the performance of the controller over conventional distributionally robust methods by more than 20%.

Moreover, a hardware-in-the-loop (HIL) simulation of a cyber-physical system consisting of packetized energy management (PEM) enabled DERs, flexible VESSs and transmission grid is developed in this work. A predictive, energy-constrained dispatch of aggregated PEM-enabled DERs is formulated, implemented, and validated on the HIL cyber-physical platform. The experimental results demonstrate that the existing control schemes, such as AGC, dispatch VESSs without regard to their energy state, which leads to unexpected capacity saturation. By accounting for the energy states of VESSs, model-predictive control (MPC) can optimally dispatch conventional generators and VESSs to overcome disturbances while avoiding undesired capacity saturation. The results show the improvement in dynamics by using MPC over conventional AGC and droop for a system with energy-constrained resources.

# Citations

Material from this dissertation has been published in the following forms:

Amini, M., and Almassalkhi, M.. (2018). Trading off robustness and performance in receding horizon control with uncertain energy resources. 2018 IEEE Power Systems Computation Conference (PSCC).

AND

Amini, M., and Almassalkhi, M.. (2016). Investigating delays in frequency-dependent load control. 2016 IEEE Innovative Smart Grid Technologies-Asia (ISGT).

AND

Amini, M., Khurram, A., Klem, A., Almassalkhi, M., and Hines, P.. (2019). A Model-Predictive Control Method for Coordinating Virtual Power Plants and Packetized Resources, with Hardware-in-the-Loop Validation. 2019 IEEE Power and Energy Society General Meeting (PES-GM).

AND

Material from this dissertation has been submitted for publication in IEEE Transactions on Smart Grid on March, 15, 2019 in the following form:

Amini, M., and Almassalkhi, M.. (2019). Corrective dispatch of uncertain energy resources using chance-constrained receding horizon control. IEEE Transactions on Smart Grid.

*To my parents, and my lovely wife, Shima*

# Acknowledgements

During my doctoral studies, I have been very fortunate to get support from many people, some of whom are acknowledged below.

First of all, I want to gratefully acknowledge my advisor, Professor Mads Almassalkhi, for his excellent mentorship and support. Over the past four and a half years, his office door was always open to me and he has been tremendously resourceful, supportive and encouraging. During my time at the University of Vermont, he supported me to attend fascinating conferences and a summer school that helped considerably in my research and also in shaping my future career. He is an excellent advisor and an amazing friend, always willing to do his best whenever his help is needed. He has been a living role model to me and I will never find words to tell what I owe to him, and if I start doing it, I would not know where to stop... thanks for everything Sir... to me, you are *"perfection personified"*. I also like to thank his wife Brittney for being kind and supportive to me and my wife.

I am also thankful to my dissertation committee members: Professors Taras Lakoba, Hamid Ossareh, and Paul Hines. I truly appreciate all the time and effort they put to help me finish my dissertation. Also, many thanks to Professors Paul Hines, Luis Duffaut Espinosa and Pavan Nandan Racherla for their fruitful sharing of their experience on several parts of this dissertation. Several other Professors at the University of Vermont have been inspiring me in teaching and research, and I am grateful to all of them, especially Professor Taras Lakoba who is a very inspirational teacher and continually supported me during my career applications.

I am also very lucky to work with amazing fellows at the energy system lab (TESLa) and UVM IGERT Smart Grid team. They are vibrant colleagues who made our office a brighter and happier place. I like to especially thank Adil Khurram and Andrew Klem, not only for their friendship but also for collaborating on the ARPA-E project.

I could not have a better experience at the University of Vermont without Sam Chevalier. He and his family have assisted me in many ways from the first moment I came to Vermont. Many respects to my friends scattered all around the world, especially Seyyed Amir Ali Javadinia, Farid Farmani, Seyyed Mahdi Jafari, and Mohammad Ahmadzadeh, for all of their companionships, sympathies,

suggestions, and great wishes during my hardship and prosperity.

Finally, I want to thank my loved ones for always believing in me. My parents have always provided their unconditional support in my life. They taught me the value of education and they never stopped encouraging me to continue my studies even at the price of being thousands of miles distant from them. Thanks to my sister, Mahnoosh, and my brother, Mahyar, who have offered invaluable support and humor ever since I first opened my eyes and never let me down in any stage of my life. My family will always be the main reason for my happiness.

Most importantly, I want to thank my amazing wife Shima. She has been an open ear for all my worries, encouraged me substantially during my work, helped me whenever needed, accompanied me in my career decisions and given me a warm and loving home. More importantly, She has inspired me to be truly "myself". Without you, I would have probably still gotten my PhD, but without me, you would never have gone through all these difficulties, especially living far away from your beloved family. I love you.

# Table of Contents

# List of Figures

# List of Tables

# 1 Chapter I: Introduction

## 1.1 Motivation and overview

The quality of delivered electrical power and safety of electrical facilities are related to the nominal system frequency (e.g., 60 Hz in the U.S.). If the balance between supply and demand is not reached the system frequency will deviate from its nominal at a rate determined by the inertia of the total system. In the standard appertain of a power system, the imbalances are regulated by fast acting reserves from generators, such as gas turbines or hydro storage power plants. However, in recent years, due to environmental and energy concerns and decrease in the cost of renewable generation such as solar photovoltaic and wind generation, integration of renewables into the grid has became a growing trend in the world [6]. The capacity of solar photovoltaic generation increased by 25% and capacity of wind generation increased by 10% in 2018 compared to the previous year [7]. This faces grid operator both opportunity and challenges.

In contrast to the dispatchable conventional generators which can be precisely scheduled and controlled, the intermittent renewables resources needs to be forcasted which are involved significant forecasting errors. These forecast errors can be quite considerable with substantial change over relatively short duration of time. Figure. 1.1 illustrates wind and solar PV generation variability for normalized measured Belgian data for a 14 days period.

To enable reliable operation of the power system, supply and demand must always match continuously. Any supply-demand imbalances leads to frequency variation where the rate of variation is determined by the total inertia of the power system. Traditionally, the power system inertia is determined as the combined inertia of the conventional generators and loads. Because the distributed energy resources (DERs) are electrically connected to the power system, these resources typically do not provide any rotational inertia and power systems, resulting in an overall lower inertia in the power system. This makes frequency dynamics much faster in power system and traditional frequency control scheme becomes too slow regarding the disturbance dynamics [8, 9]. Figure 1.2 illustrates the effect of declining inertia, caused in particularly by high shares of wind generation in the power system.

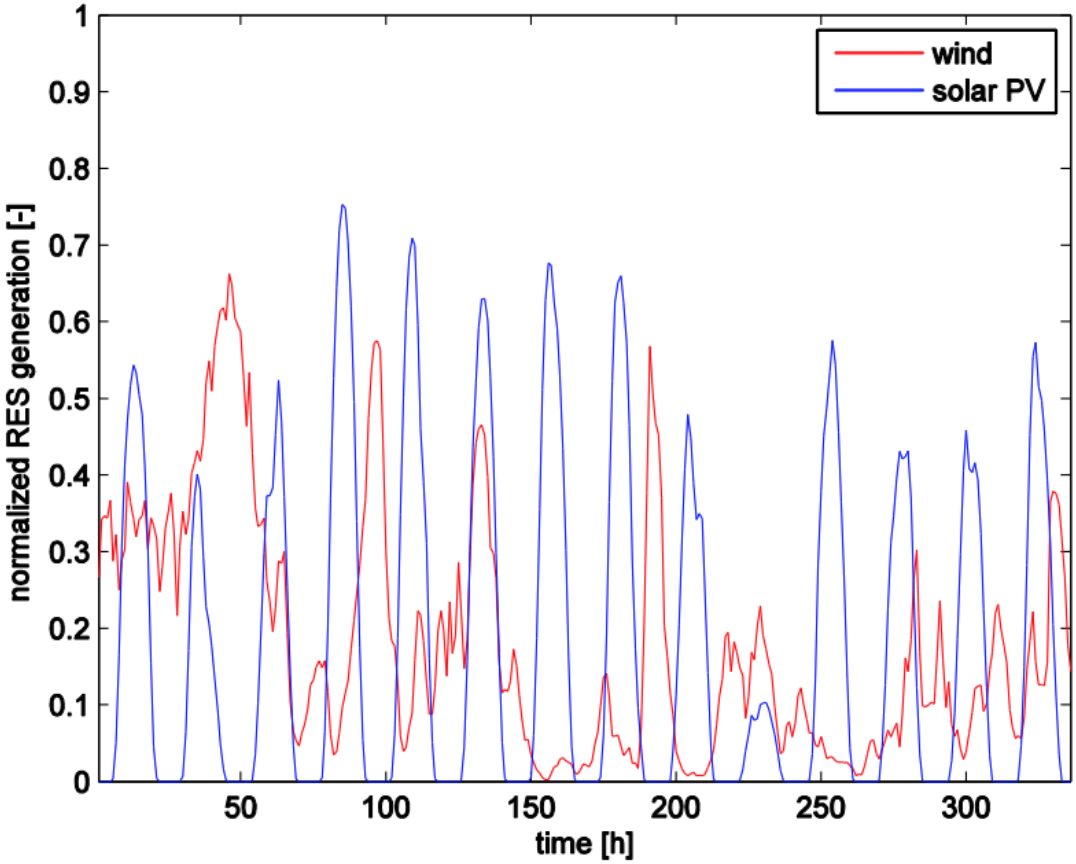


Figure 1.1: Normalized hourly measured data of wind and solar PV generation for a 14 days period [1]

In most power systems, a control system operator, or balancing authority controlled the power plants to match the electrical demand which has been always variable. However, the intermittent of renewable energy sources as well as forecast uncertainties in renewable in-feed profiles, makes matching electrical demand and generation more challenging. This calls for more conventional generators become online which leads to more generators idling, more fuel consumption, and more pollution. Therefore, the traditional form of ensuring reliability should be shifted toward active participation of the controllable and flexible energy resources at the consumer level. Flexible loads are expected to support the system stability according to their characteristic and technical capabilities.

Current DR programs are typically limited to traditional peak shaving or indirect peak pricing schemes. However, appropriate control schemes can be employed to exploit the DERs' full flexibility.

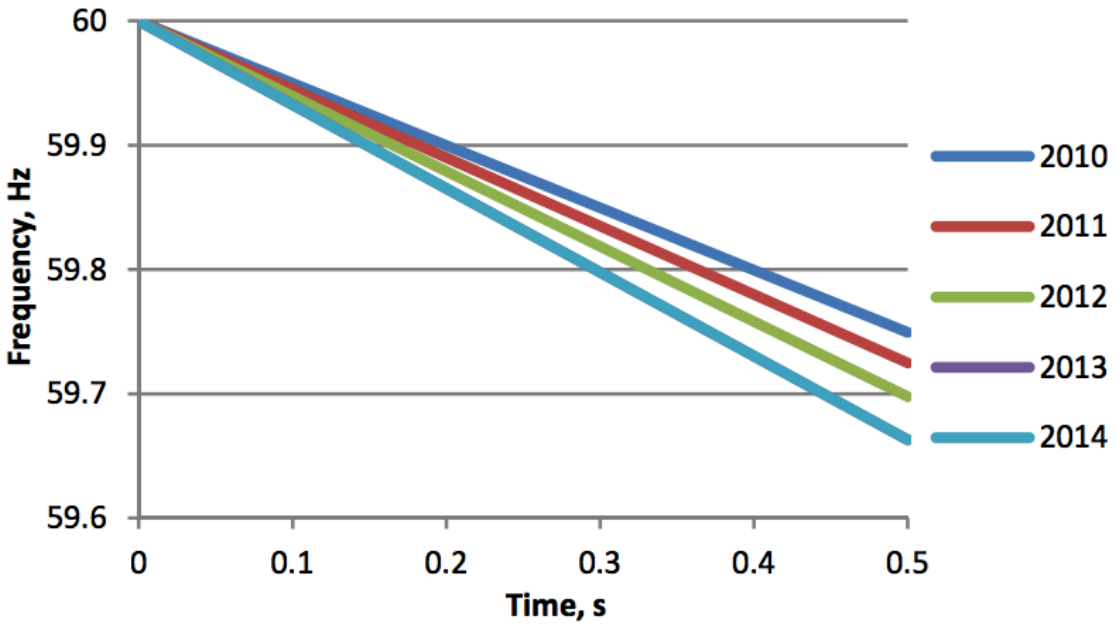


Figure 1.2: Effect of declining system inertia due to increased penetration of renewables on the frequency responses of the power system following a frequency event of 2750 MW generation trip [2].

Since they can be dispatched very quickly to provide wide range of operation time from a few seconds to several minutes, they are considered as an alternative to the conventional spinning reserves. While the concept of DR have been proposed decades ago [10, 11], the DR technology available today is still in its early stages, but maturing rapidly [12–14].

This dissertation expands upon the UVM project "Packetized energy management: coordinating transmission and distribution" which focused on aggregating and coordinating flexible resources to provide required reserves for integrating renewable into the power grid. The Virtual Power Plants (VPPs) as a novel technology for aggregating and coordinating a large fleet of residential flexible energy resources, including electric battery storage, thermostatically controlled loads (TCLs), and deferrable loads, offers the flexibility to the system operator as a synthetic reserve to preserve grid stability [15]. When called upon, the VPP can rapidly respond to changes in net-load by quickly coordinating its fleet of assets to provide requested balancing reserves [16, 17]. Since the level of offered flexibility from aggregated DERs can not be measured directly, dynamic state estimators and simplified model must be employed which introduce uncertainty. To accomplish optimal dis-

patch of these uncertain energy resources, a risk based chance constrained MPC is developed. Our interdisciplinary research lies at the intersection of power systems and optimizations.

## 1.2 Background and related work

### 1.2.1 Demand Response

Residential sector consumes around 40% of the total energy which form the substantial part of the seasonal and daily peak demand [18]. According to the most recent data published by the U.S. Energy Information Administration, U.S. electric utilities had about 80 million advanced metering infrastructure (AMI) installation where about 88% of them are residential advanced meters. These AMI (also known as smart meter) which are capable of two-way communication between costumers and electric utilities, cover almost 50% the 150 million electricity costumers in the U.S. [19]. State of Vermont is one of the leaders in the deployment of smart meters with smart meter penetration rate of over 81% [20]. Increased penetration of smart meters enables higher active participation of consumer in DR program. DR can be defined as the change in the electric consumption from their normal consumption in response to the control signal by end use costumers. The control signal can be designed with respect to the electricity price or reliability of the system [3]. Costumers are offered incentive by utility companies to participate in the DR program [21].

Since consumers are more flexible under DR program, the elasticity of the demand is higher as shown in Fig. 1.3. With no DR program, the demand is shown as vertical line while with the DR program, the demand curve has negative slope compared to the original curve. Therefore, small reduction in demand leads to a large reduction in the total price.

Stability of the power system must be maintained with respect to two operating points of voltage and frequency. Traditionally, conventional power plants are dispatched in a load-following manner. High integration of uncertain renewbale resources and DR makes the voltage/frequency stability problem more complicated. DR can be used in a fast and corrective manner to respond to uncertain and intermittent characteristic of the renewable. Load frequency control (LFC) and corrective voltage control (CVC) have been used for decades to maintain the frequency and voltage of the power system. The impact of integrating renewbales and DR program on LFC and CVC have to

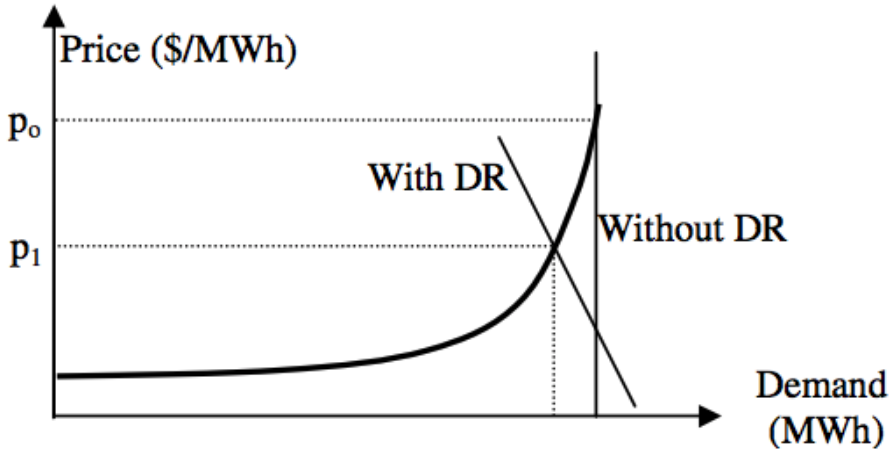


Figure 1.3: Effect of DR on electricity market price [3]

been carefully taken into account [22].

The performance and efficiency of coordinating flexible loads to reduce the total energy cost that costumers should pay is studied in [23]. It has been shown that appropriate coordinating of the flexible resources improves the efficiency of the power system operation [24–27]. Flexible loads aggregators, not only can deliver the valuable electricity service that traditionally provided by conventional generators, but also their distributed nature make them capable of new services [28]. New independent aggregators are blooming in U.S. market due to the true value they bring to the market and not regulatory arbitrage [29].

The DR program two main categories illustrated in Fig 1.4 can be explained as follows:

- Price based program: Send electricity prices via communication channels to the consumers and they will decide whether or not respond to the signals [30]. These types of program only participate in energy market as the system operator can not control the devices directly.

- Incentive based program: End-consumers receives a defined reward for a specific shift or curtailment of the load. These types of program are usually pre-defined contracts and give some level of control to the system operator. Therefore, they can participate in the energy, capacity and ancillary markets [21].

DR can have various benefits and its benefit are not limited to the participants only. Since the

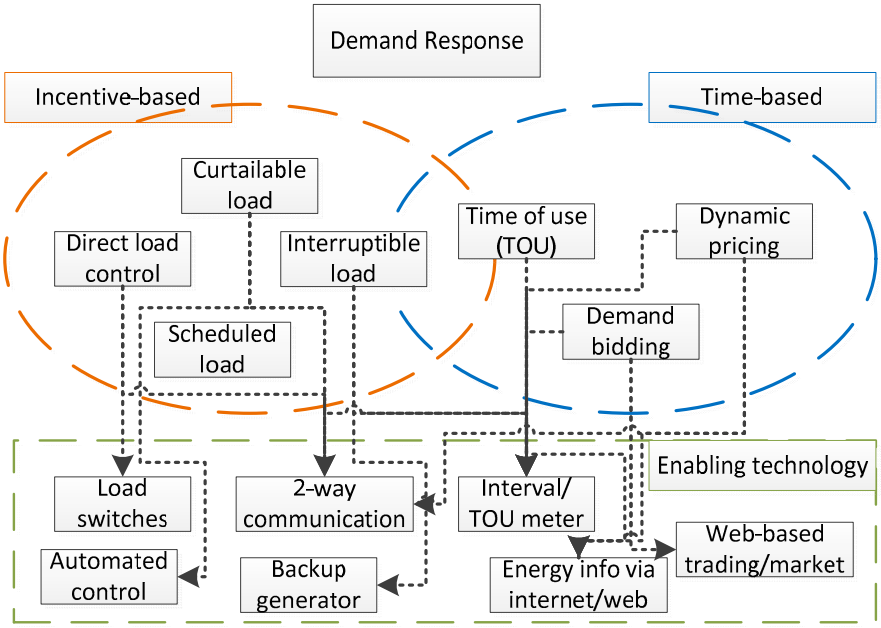


Figure 1.4: Demand response categories and enabling technologies [4].

Table 1.1: Demand response benefits

| Consumers | Market-Wide | Reliablity | Environmental |
|---|---|---|---|
| Lower bill<br>Incentive payments | Lower price<br>Higher capacity<br>Defer new investment | Less outage<br>Diverse resources | More renewables<br>Better land utilization<br>Better water quality<br>Less pollution |

demand peak can be shaved using DR, the available infrastructure can be used more efficiently, the needed electricity from expensive generation units reduce, and consequently the overall electricity price goes down [31]. Moreover, new investment in generation and transmission area can be avoided or at least deferred. In a well designed DR program, costumers participate in reducing risk of outage while the grid operator has wider range of resources to maintain system's reliability. In addition, environmental benefits associated with DR program are achieved by providing reserves for the grid operator and accelerates integration of renewables into the power grid. Some of the DR program's benefit are listed in Table. 1.1.

### 1.2.2 Virtual energy storage system

DR and energy storage system (ESS) are two main tools that improve the power system reliability and flexibility by matching the electricity demand to the uncertain renewable generation. DR program shifts the consumption time while the storage can shift both consumption and generation. Increased penetration of renewables makes the role of these tools, which can be accessed from a number of technologies, more important. Since both of these technologies have the ability of shifting the net-demand over desired period of the time, they are usually evaluated with the common framework. Different types of the energy storage system are shown in table 1.2 which can be classified into two groups based on their power ratings and energy rating and are utilized in power and energy management applications [32].

ESS have been employed for grid frequency regulation since 1980s [33–35]. Conventional generators can be replaced by large scale ESS which can provide reserve to the power grid. Despite the declination in the cost of the electrical storage technologies over the last decades, the main challenge of the large deployment of the energy storage system is their high cost and their large scale deployment is not feasible yet. Various studies discussed the role of integrating DR and battery storage and with numerical studies showed that coordinating the flexible resource under DR program results in considerable reduction in the size of required energy storage [36, 37]. Under DR program, electrical demand can be shifted over time in a smart manner such that resembles the same charging or discharging behaviour of the ESS. By careful coordinating the existing flexible loads in the power system such as thermostatically controllable loads (TCL), DR can be implemented in a lower cost compared to the ESS. Electric water heaters, refrigerators, heat pumps and heating ventilation and air conditions are among the most common TCLs that their temperature can be set so that increase or decrease their demand for balancing purposes [38, 39]. It is estimated that 1.5 million

Table 1.2: Different types of energy storage system [5]

| Electrochemical | Mechanical | Electrical | Thermal |
|---|---|---|---|
| Battery | Pump hydro | Capacitor | Hot water storage |
| Hydrogen | Flywheels | Superconductive magnetic | Thermal fluid storage |
| Flow batteries | Compressed air | | Ceramic thermal storage |

refrigerators can provide approximately 20 MW of response which cost less than \$4m while to have same response power with Flywheel energy storage system would cost approximately $\$33 - 37$m. It is estimated that the energy storage market size will reduce by 50% due to DR program [40].

A virtual energy storage system (VESS) is formed by aggregation of different flexible, controllable or dispatchable devices including conventional ESS, flexible loads such as TCLS and distributed generators (DG) as a single ESS with high power/energy ratings and feasible cost [41]. A VESS is integrated to the power system and vary its consumption level based on the control signal provided by the grid operator to provide service on the transmission level or distribution level with different capacity. In contrast to the ESS, VESS can be formed such that demonstrate both high power and high energy rating with reduced cost and be utilized for wide range of applications accordingly [42]. An overview of a VESS is shown in Fig. 1.5.

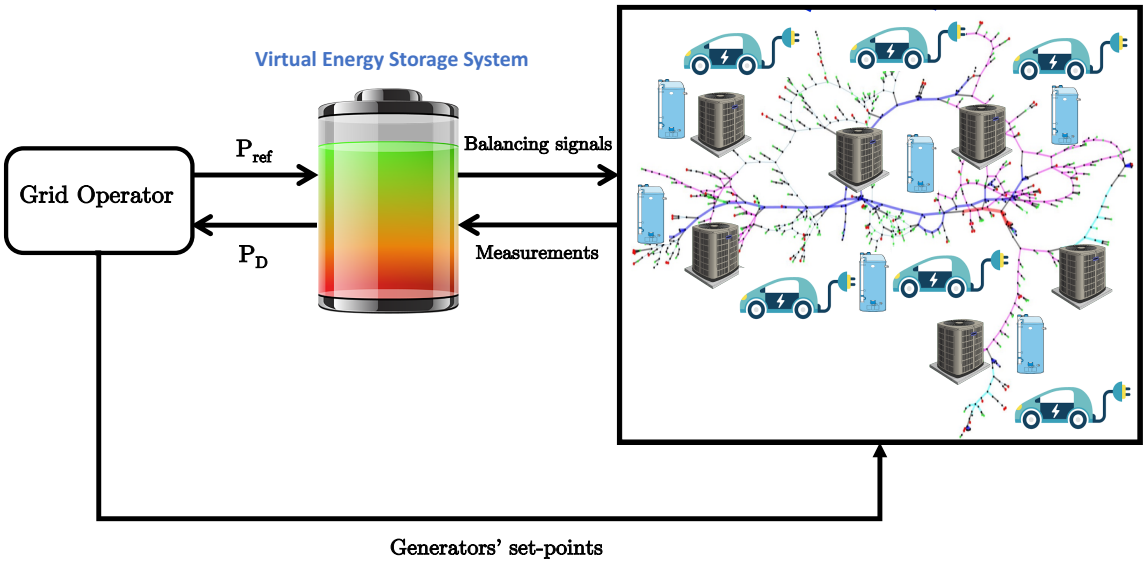


Figure 1.5: Overview of the virtual energy storage system.

Since VESSs can provide charging/discharging functions, by responding properly to the renewable generation output, they can increase the distribution network capacity for renewable generation and smooth the power output [43]. The cluster of the aggregated flexible loads has a baseline consumption equals to the sum of the baseline consumption of individual devices. Actions that increase the total consumption relative to the baseline consumption are charging the VESS and on the hand, actions

that decrease the total consumption relative to the baseline consumption are emptying the VESS. Therefore, the evolution of the state of the charge of a VESS, $S$, can be modeled as follows:

$$S[l+1] = s[l] + (P_C[l] - P_T[l])\Delta\tau \tag{1.1}$$

$$P_C^{\min} \leq P_C[l] \leq P_C^{\max} \tag{1.2}$$

$$0 \leq S[l] \leq S_{max} \tag{1.3}$$

where $P_C$ and $P_T$ represent the aggregated power consumption and the aggregated scheduled baseline consumption and $\Delta\tau$ is the length of time step.

Additionally, they can provide immediate corrective actions following occurrence of a contingency in the power system and mitigate the probable congestion [5, 44]. Moreover the reserve service offered by VESS, decreases the required reserve that traditionally should be provided by conventional generators. Less required reserves from conventional generators means generators can work closer to their maximum capacity [44].

To summarize, the main four potential advantages of VESS can be listed as [45]:

- Facilitate the penetration of renewables into the power grid
- provide ancillary services
- Avoid/Defer needed investments in the power system's infrastructures
- Increase the generators loading capacity

The number of the controllable load and the flexibility they can offer is a function of time and human usage which are uncertaint variable. Therefore, The capacity of the VESS and upper and lower bound of the power consumption are estimated with respect to the different parameters such as human usage pattern and outdoor temperature which are uncertain and time-varying.

## 1.3 Research Objective and Organization

The main objective of this dissertation is to provide a theoretical framework for utilizing the flexibility offered by VESS under DR program to facilitate integration of uncertain, intermittent renewables

to the power grid. Since the flexibility offered by VESSs are also uncertain, in both energy state and energy capacity, a probabilistic optimization framework has been developed on the transmission level. The challenge is to manage flexible resources reliably whit minimal impact on the quality of the server. By corrective dispatch of energy resources on a minute-by-minute time scale, transmission lines congestion and overload are managed via feedback under temperate based rating of transmission lines. Also, since, significant variable or constant time delays are observed in DR program, the effects of these delays on system-wide frequency stability is investigated. Additionally a realistic hardware-in-the-loop platform has been developed. Chapter 2 introduces the basic of the power system. Chapters $3-6$ are presented as published or submitted publications. Chapter 7 discusses the conclusion and avenues for future works. Each chapter is summarized as follow:

- **Chapter** 2 give introduction on the basic power system models.
- **chapter** 3 studies the impact of time-delays on frequency dependent load control scheme for a power system with the droop-controlled generators and describes the conditions under which the instability can occur and how injecting additional delays to an unstable power system can bring back that power system to the stable region.
- **chapter** 4 formulates a chance-constrained optimization problem to integrate the uncertain energy resources into the power system. The chance constrained problem is solved via the scenario approach to dispatch energy resources robust against constraint violation. We showed there exist a sensitive trade-off between robustness of the optimized dispatch and closed-loop system performance and the popular approach of robustifying the chance-constraints may lead to conservative solution exacerbating the system performance.
- We extend the results of **chapter** 4 to to develop an analytical reformulation of the VESSs' uncertainty and formulate a risk-based, chance constrained problem which co-optimizes the tracking performance of the control system and operational risk of the power system in **chapter** 5. The results in **chapter** 5 show that to dispatch uncertain energy resources under high penetration of renewables, the risk-based chanced constrained approach outperforms the deterministic and the robust approaches by reaching a balance between using energy resources and being robust against uncertainties.

- **Chapter** 6 presents a hardware-in-the-loop platform for validation of cyber-physical-system consisting of real-time flexible load aggregator realized by a web-server and a transmission level power system implemented on a real-time simulator. Moreover, we develop a model predictive control scheme as an alternative to the PI-control-based AGC and we show that energy-aware controller dispatch energy-constrained resources more efficiently over the time.

- **Chapter** 7 concludes the dissertation and gives avenues for future work.

# 2 Chapter 2: Power system models

## 2.1 Power flow problem

This chapter gives a brief introduction on the basic of the power system models. The models explain how the power flows from generators to the loads and succinctly derive the algebraic equations associated with the physics of the power flow. The power system can be modeled by graph theory $\mathcal{E} = (\mathcal{N}, \mathcal{L})$ with bus $i \in \mathcal{N}$ and line $ij \in \mathcal{L}$. An example of an actual real-world power system based on the provided data by a transmission utility is illustrated in Fig. 2.1.

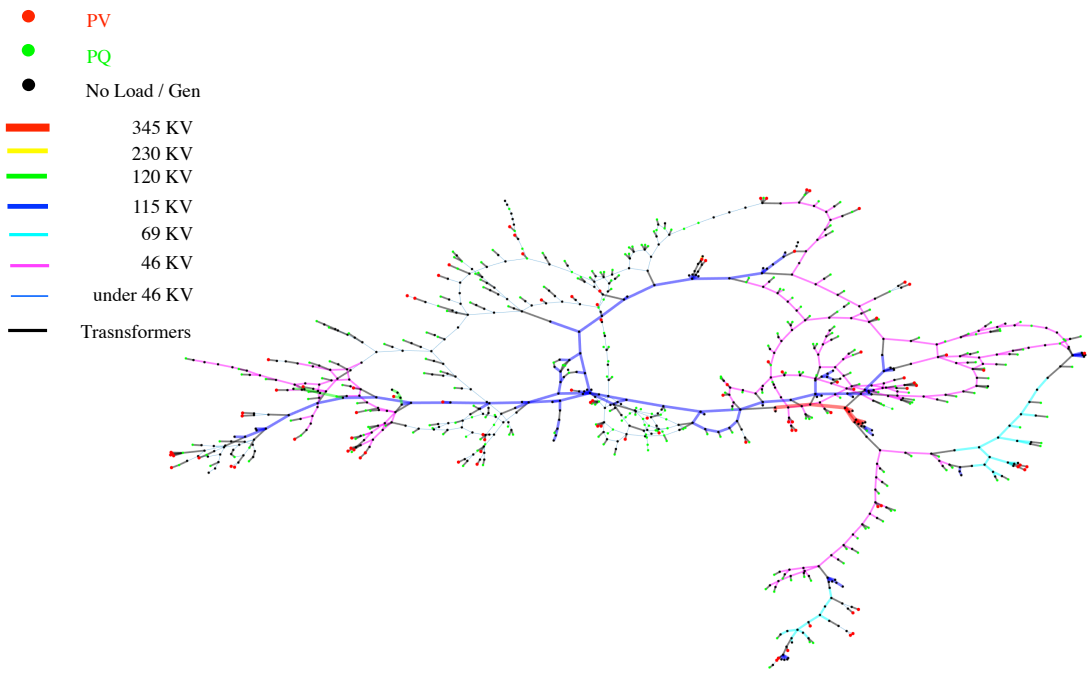


Figure 2.1: An actual power system can be modeled as graph with nodes (representing buses) and vertices (representing transmission lines or transformers)

All transmission lines, phase shifters and transformers can be modeled with a standard $\pi$ transmission line model (also known as unified branch model) which places a series impedance between the buses and distributes one half of the shun capacitance of the line on each bus as shown in Fig. 2.2.

The series admittance of the line is defined as

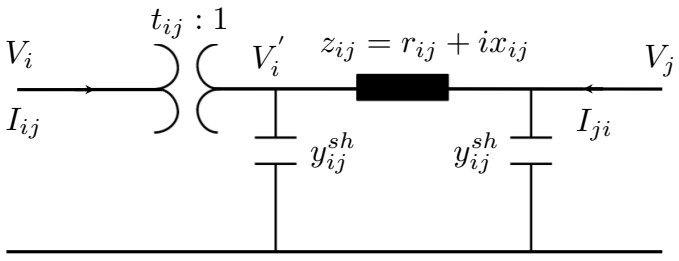


Figure 2.2: The $\pi$-model of the transmission line

$$y_{ij} = g_{ij} + ib_{ij} = \frac{1}{z_{ij}} = \frac{1}{r_{ij} + ix_{ij}} \tag{2.1}$$

while $V, I$ and $t$ represent complex node voltages, complex branch current and complex transformer tap ratio. By considering transformer's equations the currents and voltage of on different sides of the transformer can be derived as

$$\frac{V_i}{t_{ij}} = \frac{V_i^{'}}{1} \rightarrow V_i^{'} = \frac{V_i}{t_{ij}} \tag{2.2}$$

$$I_{ij}^{'} = I_{ij} t_{ij}^{*} \tag{2.3}$$

where the $()^*$ denotes phasor conjugate. By applying Kirchhoff's law, the relationship of the voltage and current can be derived as follows:

$$I_{ij}^{'} = V_i^{'} y_{ij}^{sh} + (V_i^{'} - V_j) y_{ij} \tag{2.4}$$

$$I_{ji} = V_j y_{ij}^{sh} + (V_j - V_i^{'}) y_{ij} \tag{2.5}$$

By substituting (2.2) and (2.3) in (2.4) and (2.5), we can show

$$I_{ij} = \frac{\frac{V_i}{t_{ij}} y_{ij}^{sh} + (\frac{V_i}{t_{ij}} - V_j) y_{ij}}{t_{ij}^*} \tag{2.6}$$

$$I_{ji} = V_j y_{ij}^{sh} + (V_j - \frac{V_i}{t_{ij}}) y_{ij} \tag{2.7}$$

The relationship between voltage and current now can be placed in matrix form:

$$\begin{bmatrix} I_{ij} \\ I_{ji} \end{bmatrix} = \begin{bmatrix} \frac{y_{ij}+y_{ij}^{sh}}{t_{ij}t_{ij}^*} & -\frac{y_{ij}}{t_{ij}^*} \\ -\frac{y_{ij}}{t_{ij}} & y_{ij} + y_{ij}^{sh} \end{bmatrix} \begin{bmatrix} V_i \\ V_j \end{bmatrix} \tag{2.8}$$

Different types of branch can be captured within (2.8):

- Transmission line and nominal transformers: $t_{ij} = 1\angle 0$
- in-phase transformer (IPT) and set $y_{ij}^{sh} = 0$; $t_{ij} = a_{ij}\angle 0$
- phase-shifting transformers (PST): set $y_{ij}^{sh} = 0$; $t_{ij} = 1\angle \psi_{ij}$

Notes that if the transformer does not cause phase shifting, matrix in (2.8) remains symmetric ($t_{ij} = t_{ij}^*$).

Now we can form $N \times N$ dimensional admittance matrix *Y-bus* in the following way:

$Y_{i,i}$ = sum of admittance connected to bus i

$Y_{i,j}$ = negative sum of admittance's connected between bus i and j

The injected current into each node, also known as nodal current, can be found by applying Kirchhoff's Current Law as follows:

$$I_i = \sum_{k \in \mathcal{N}} y_{ik}(V_i - V_k) + V_i y_{ik}^{sh} \tag{2.9}$$

where $\Omega_N$ represent set of adjacent nodes at node $i$. By rearranging (2.9) as follows:

$$I_i = V_i \sum_{k\in\mathcal{N},k\neq i} (y_{ik} + y_{ik}^{sh}) + \sum_{k\in\mathcal{N},k\neq i} V_k(-y_{ik}) \tag{2.10}$$

and then, based on the definition of the *Y-bus* we can show

$$I_i = \sum_{k\in\mathcal{N}} V_k Y_{ik} \tag{2.11}$$

The expression shown in (2.11) is valid for all the nodes in the power system and can be vectorized as follows:

$$\mathbf{I} = Y\mathbf{V} \tag{2.12}$$

where $\mathbf{I}$ and $\mathbf{V}$ are $N$-dimensional vectors.

By multiplying voltage and complex conjugate of the injected current at each node, the complex injected power at each node can be derived as follows:

$$\begin{aligned} S_{ij} = P_{ij} + iQ_{ij} &= V_i I_{ij}^* \\ &= V_i\big(\sum_{k\in\mathcal{N}} V_k Y_{ik}\big)^* \end{aligned} \tag{2.13}$$

By substituting the phasor notation of the voltage, $V_i = \mathrm{V}_i\angle\theta_i$, and admittance values in rectangular coordination we can show:

$$P_i + iQ_i = \mathrm{V}_i \sum_{k\in\mathcal{N}} \mathrm{V}_k e^{i(\theta_i-\theta_k)}(G_{ik} - iB_{ik}) \tag{2.14}$$

By writing $\theta_i - \theta_k$ as $\theta_{ik}$ and transforming the voltage phasor from polar coordination to rectangular coordination it can be shown as:

$$P_i + iQ_i = V_i \sum_{k \in \mathcal{N}} V_k(cos(\theta_{ik}) + isin(\theta_{ik}))(G_{ik} - iB_{ik})$$
$$= Vi \sum_{k \in \mathcal{N}} V_k(G_{ik}cos(\theta_{ik}) + B_{ik}sin(\theta_{ik}) + iG_{ik}sin(\theta_{ik}) - iB_{ik}cos(\theta_{ik})) \quad (2.15)$$

By decomposing the above expression to real and imaginary parts, the injected active and reactive power can be derived as follows:

$$P_i = V_i \sum_{k \in \mathcal{N}} V_k(G_{ik}cos(\theta_{ik}) + B_{ik}sin(\theta_{ik})) \quad (2.16)$$

$$Q_i = V_i \sum_{k \in \mathcal{N}} V_k(G_{ik}sin(\theta_{ik}) - B_{ik}cos(\theta_{ik})) \quad (2.17)$$

This AC power flow model relates the voltage magnitude and voltage phase angle to the active and reactive power injecting to each node. Since the injected active and reactive power to each bus are known based on the generation (positive injected power to the bus) and load (negative injected power to the bus) existed on that bus,$P_i^{sp}$ and $Q_i^{sp}$, the mismatches function are formed as follows:

$$\Delta P_i(\theta, V) = P_i^{sp} - V_i \sum_{k \in \mathcal{N}} V_k(G_{ik}cos(\theta_{ik}) + B_{ik}sin(\theta_{ik})) \quad (2.18)$$

$$\Delta Q_i(\theta, V) = Q_i^{sp} - V_i \sum_{k \in \mathcal{N}} V_k(G_{ik}sin(\theta_{ik}) - B_{ik}cos(\theta_{ik})) \quad (2.19)$$

The AC power flow problem solvers find voltage magnitude and phase angle of all buses, such that all the mismatches functions become equal to zero. The equation above can be expressed in the vector form as follows:

$$f(x) = \begin{bmatrix} \Delta P(\theta, V) \\ \Delta Q(\theta, V) \end{bmatrix} = 0 \quad (2.20)$$

where x is the vector of unknowns, voltage magnitude and phase angles. The solution of the (2.20)

can not be solved in closed form and should be solved in an iterative manner employing a Jacobian matrix:

$$J(x) = \begin{bmatrix} \frac{\partial P(x)}{\theta} & \frac{\partial P(x)}{V} \\ \frac{\partial Q(x)}{\theta} & \frac{\partial Q(x)}{V} \end{bmatrix} \tag{2.21}$$

Applying the Newton-Raphson (NR) method to the power flow equation (2.20) leads to the following non-linear equation

$$\begin{bmatrix} \Delta P \\ \Delta Q \end{bmatrix} = J \begin{bmatrix} \Delta \theta \\ \Delta V \end{bmatrix} \tag{2.22}$$

If the initial guess of the solution picked close to the solution, the NR method converges to the solution very fast with less iteration. However, computing full Jacobian matrix at each iteration is computationally expensive.

## 2.2 Transmission lines temprature model

To include the effects of phase shifting transformers (PST) and in phase transformers (IPT) with complex tap ratio $t_{ij} = a_{ij}\angle\psi_{ij}$, unified branch model is employed in which transmission lines ($a_{ij} = 1, \psi_{ij} = 0$), PSTs ($a_{ij} = 1$) and IPTs ($\psi_{ij} = 0$) can be represented in a unified manner. As mentionde, power flow equations in the electrical power system are set of nonlinear non-convex algebraic equations. The power flow on the line connecting bus $i$ to bus $j$ can be shown as:

$$p_{ij} = \frac{V_i^2}{a_{ij}^2} g_{ij} - \frac{V_i V_j}{a_{ij}} \Big[ g_{ij} \cos(\theta_{ij} - \psi_{ij}) + b_{ij} \sin(\theta_{ij} - \psi_{ij}) \Big] \tag{2.23}$$

The nonlinearity of AC power flow equations make multi period AC-OPF problem computationally intractable. To enable a computationally feasible solution approach, suitable linear approximation of the AC power flow equation (i.e., "DC" ) has been adopted while ensuring the convexity of optimization problem.

under standard DC assumptions:

- The voltage magnitude of the every buses remains constant at 1 p.u.
- Phase angle difference along the branches is small ( $\ll \pi/2$)
- The active power losses is negligible
- Line's reactance, $x_{ij}$, is much greater than its resistance, $r_{ij}$

Under these simplifications, the non-linear AC power flow can be reduced into the DC power flow equations:

$$p_{ij} \approx \frac{\theta_{ij} - \psi_{ij}}{a_{ij} x_{ij}} = \frac{\hat{\theta_{ij}}}{\hat{x_{ij}}} \tag{2.24}$$

where $\hat{x_{ij}} = a_{ij} x_{ij}$ and $\hat{\theta_{ij}} = \theta_{ij} - \psi_{ij}$ represent lumped reactance and phase angle difference along the line.

To prevent excessive sagging and to ensure safety of the transmission lines, power flows on the lines are enforced to be within power limits (MWA). The power carrying capacity of the transmission lines are determined based on the thermal rating of the conductors. Considering such power limits for hourly energy management schedule is reasonable. However, in short term planning of the system the power flows on the lines can exceed the determined power limit without violating the thermal limits of the lines. Since MPC reinitializes every minute, considering thermal limits instead of the power limits, can increase transmission capacity significantly.

The DC formulation presented in (2.24) is based on lossless network assumption. However, heat gain due to electrical and consequently temperature of the transmission line is a function of line resistive losses (i.e. $RI^2$). To ensure satisfying of the thermal limits, it is needed to include line losses in power flow. Basically, line losses can be calculated as difference in active power at sending and receiving nodes

$$p_{ij}^{\text{loss}} = p_{ij} + p_{ji} \tag{2.25}$$

By substituing (2.23) in (2.25) line losses can be described as

$$p_{ij}^{\text{loss}} = g_{ij}\left(\frac{{V_i}^2}{{a_i}^2} + V_j^2 - 2\frac{V_i V_j}{a_{ij}}\cos\hat{\theta_{ij}}\right) \tag{2.26}$$

Under assumption of voltage magnitudes are 1 p.u., $\hat{\theta_{ij}}$ are small, nominal tap ratios are close to 1 and by employing second-order Taylor series approximation of $\cos\hat{\theta_{ij}}$, (2.26) can be manipulated as it shown in [46] to give

$$p_{ij}^{\text{loss}} \approx \frac{r_{ij}\hat{\theta ij}^2}{a_{ij}x_{ij}^2} = a_{ij}r_{ij}p_{ij}^2 \tag{2.27}$$

Since line losses is not linear in $\hat{\theta_{ij}}$ (i.e. quadratic), it can not be used in linear constraint formulation. Therefore, a peicewise linear approximation is applied to (2.27) as it has been done in [46]. IEEE 738 standard [47], a standard for calculating the current-temperature of bare overhead conductors, has been used to calculate the conductor temperature. The rate of change in temperature of a conductor can be calculated by the following heat balance equation (HBE)

$$mC_p\dot{T}(t) = Q_{\text{sun}}(t) + Q_{\text{Loss}}(t) - Q_{\text{conv}}(t) - Q_{\text{rad}}(t) \tag{2.28}$$

where $Q_{\text{sun}}$, $Q_{\text{Loss}}$, $Q_{\text{conv}}$ and $Q_{\text{rad}}$ represent the heat gained by solar radiation, the heat gained due to resistive losses, the heat lost by convection and the heat lost by radiation receptively. Also $mC_p$ represents per unit length conductor heat capacity [J/m-°C]. According to the IEEE 738 standard [47], a standard for calculating the current-temperature of bare overhead conductors, (2.28) can be approximated as

$$\begin{aligned} mC_p\dot{T_{ij}}(t) = Q_{ij}^{\text{sun}}(t) + p_{ij}^{\text{loss}}(t) - \eta_c(T_{ij}(t) - T_{\text{amb}}(t)) \\ -\eta_r((T_{ij}(t)+273)^4 - (T_{\text{amb}}(t)+273)^4) \end{aligned} \tag{2.29}$$

where $T_{ij}$ and $T_{\text{amb}}$ represent conductor $(i,j)$ and ambient temperatures [°C]. Also $p_{ij}^{\text{loss}}$ and $Q_{ij}^{\text{sun}}$

represent resistive loss per unit length [W/m] and solar heat gain rate [W/m] where the later is a function of conductor diameter and solar input. Furthermore, values $\eta_c$ and $\eta_r$ represent conductive heat loss rate coefficient [W/m-°C], and radiative heat loss rate coefficient [w/m-°C$^4$], where both are function of conductor characteristics.

The non-linear continuous-time temperature dynamic in (2.29) should be discretized and linearized around the equilibrium point (i.e $T^*_{ij} = T^{\lim}_{ij}$) to become applicable for linear constraint formulations. While $T^{\lim}_{ij}$ is computed based on steady-state conditions with line current at ampacity, $Q^{\text{sun}*}_{ij}$ and $T^*_{\text{amb}}$ are related to the ambient condition and can be obtained directly from measurements, forecast and historical data. According to [46], linearizing (2.29) with forward Euler discretization can be shown by the following equations:

$$\Delta T_{ij}[k+1] = \tau_{ij}\Delta T_{ij}[k] + \rho_{ij}\Delta p^{\text{loss}}_{ij}[k] + \delta_{ij}\Delta d_{ij}[k] \tag{2.30}$$

$$\tau_{ij} = 1 - \frac{T_s\bar{\gamma}_c}{mC_p} \tag{2.31}$$

$$\bar{\gamma}_c = \eta_c + 4\eta_r(T^{\lim}_{ij} + 273)^3 \tag{2.32}$$

$$\delta_{ij} = [\rho_{ij} \quad \gamma_{ij}] \tag{2.33}$$

$$\rho_{ij} = \frac{T_s}{mC_p} \tag{2.34}$$

$$\gamma_{ij} = \frac{T_s\bar{\gamma}_a}{mCp}, \qquad \bar{\gamma}_a = \eta_c + 4\eta_r(T^*_{\text{amb}} + 273)^3 \tag{2.35}$$

$$\Delta d_{ij} = \text{col}(\Delta Q^{\text{sun}}_{ij}, \Delta T_{\text{amb}}) \tag{2.36}$$

The ampacity of a three phase transmission line (i.e., current capacity) $I_{\lim}(A)$ is related to the base voltage, $V_b(V)$ and power limit of that line, $u_{\lim}(VA)$ as follows:

$$I_{\lim} = \frac{u_{\lim}}{\sqrt{3}V_b} \tag{2.37}$$

As an example, the three phase transmission line rating is given as $u_{ij} = 175MVA$ and, the conductor ampacity is calculated as $I_{\lim} = 439.25(A)$ (i.e., 5 pu at $V_b = 230$ kV) and associated temperature limit of $T_{\lim} = 83$°C. Then, the nonlinear model is linearized with respect to the

operating point. The conductor current is changed from 0 to twice of the $I_{\text{lim}}$ and the linear and the non-linear models of the current are calculated. As it shown in Fig. 2.3, the linearized model accurately approximates the nonlinear model around the operating point.

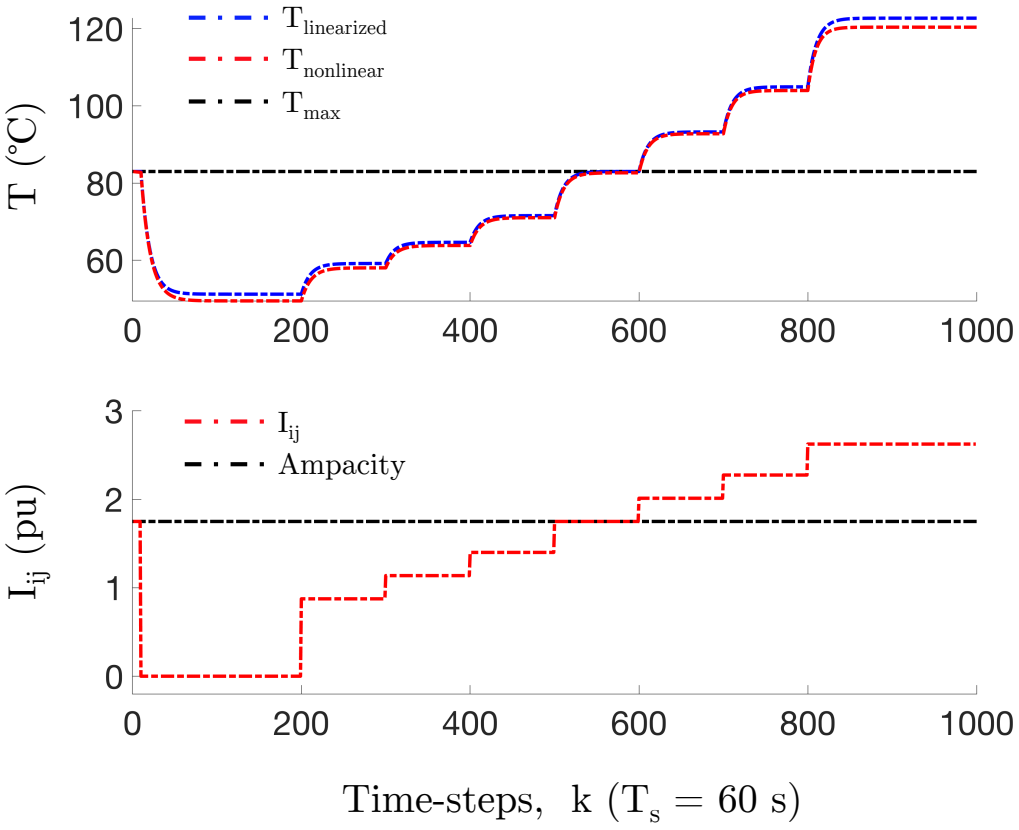


Figure 2.3: Thermodynamical conductor response to step changes in conductor's current

## 2.3 The Optimal power flow problem

The main goal of the power system is to generate and deliver power from generation units to the costumer reliably with the most economical cost. Several tools which can measure, analyze, and control the power system have been invented and developed. In power system literature, there are generally three types of problems such as power flow problem (also known as load flow), economic dispatch problem (ED), and optimal power flow (OPF).

There are various mathematical approaches to solve a power flow problem considering equations related to the power generation, power consumption and power transferred in the power system. However, not all the founded solutions are physically feasible. The Power flow equations do not take into account physical constraints such as transmission lines' power limits or generators' reactive power limit directly, however, these constraint must be included into the power flow solvers.

Economic dispatch is the process of allocating generation between different generation units to meet the electrical demand and required reserve margin in a manner that minimizes the total cost of generation. Each generation unit has its own generation cost curve and the purpose of solving ED problem is to find the economically optimal power output of the generation units. The ED formulations mostly concerns with quality constraints such as active and reactive power demand and simplifies or sometimes even ignores power flow constraints.

The OPF problem aims to minimize the objective function considering physical and operational constraints. The optimal power flow (OPF) was first introduced in 1960's and researchers soon have proven that OPF would be a very difficult problem to solve [48]. Different methods and techniques of solving OPF have been evolved during these years with developments in optimization theory and advancements in computational capabilities. Linear, non-linear, and mixed-integer methods have been utilized for analyzing OPF problems [49]. Power grid operators need to solve the OPF problem (or its approximation) several times in a day (i.e., every 5 minutes). Since non-linear solvers are computationally expensive and can not guarantee a global optimal solution, linear solvers have been employed to solve a linearized version of the OPF problem. OPF problem is mainly focused on operational cost minimization while some researchers have looked at other aspects of the power system such as active power losses [50], generators reactive power minimization [51], voltage stability [52] and using FACT devices [53]. The general form of the optimal power flow problem can be shown as follows:

$$\min_{x,\,u} \quad f(x,u) \tag{2.38a}$$

$$\text{s.t.} \quad g(x,u) = 0, \tag{2.38b}$$

$$h(x,u) \leq L \tag{2.38c}$$

where $f(x,u)$ is the objective function of the optimization problem, $g(x,u)$ are the nonlinear power flow equations and $h(x,u)$ represents the set of linear, and non-linear inequality constraints such as output power of the generation units and power limits of the transmission lines. Moreover, $x$ represents state variables such as voltage magnitude and phase angles. The control variables $u$ are defined based on the objective of the optimization problem such as active and reactive output power of the generation unit, angle of phase shifter or control voltage setting.

For example, for an active power loss minimization, the OPF problem can be modeled as follows:

$$\min \quad \sum_{i\in\mathcal{N}} \sum_{k\in\mathcal{N}} G_{ik}(V_i^2 + V_j^2 - 2V_iV_jcos(\theta_{ik})) \tag{2.39a}$$

$$\text{s.t.} \quad \Delta P = P_i^{sp} - V_i \sum_{k\in\mathcal{N}} V_k(G_{ik}cos(\theta_{ik}) + B_{ik}sin(\theta_{ik})) = 0, \qquad \forall i \in \mathcal{N}, \tag{2.39b}$$

$$\Delta Q = Q_i^{sp} - V_i \sum_{k\in\mathcal{N}} V_k(G_{ik}sin(\theta_{ik}) - B_{ik}cos(\theta_{ik})) = 0, \qquad i \in \mathcal{N}, \tag{2.39c}$$

$$\underline{P_{\mathrm{G}_i}} \leq P_{\mathrm{G},i}[l] \leq \overline{P_{\mathrm{G},i}}, \qquad \forall i \in \mathcal{G}, \tag{2.39d}$$

$$\underline{Q_{\mathrm{G}_i}} \leq Q_{\mathrm{G},i}[l] \leq \overline{Q_{\mathrm{G},i}}, \qquad \forall i \in \mathcal{G}, \tag{2.39e}$$

$$\underline{P_{ij}} \leq P_{ij} \leq \overline{P_{ij}} \qquad \forall ij \in \mathcal{L} \tag{2.39f}$$

In the above OPF problem, the total active power loss in the power system is minimized through a quadratic objective function. The equality constraints are nonlinear real and reactive power mismatch at all node. The inequality constraints represent the operational constraints and limits associated with the generation active and reactive power and power limits of transmission lines where $\mathcal{G}$ is a set of all generators in the power system.

## 2.4 Security constrained optimal power flow problem

Security, reliability and resilience of power systems have been studied extensively over past decades and have been referred to as a system's ability to withstand and recover from contingencies without any undesirable disruption of customer service.

Certain security criteria should always be satisfied by a power system to ensure secure operations for all *credible contingencies* at all times. Among the most fundamental of these criteria is the concept of $N-1$ security. A power system is called "$N-1$ secure" when the system can sustain any one-component outage (e.g., line, generator, load) without incurring a loss of load or overloading any components [54]. Thus, an $N-1$ secure system will not cascade into a major blackout after any single-component outage. To achieve security requires solving a large-scale complex grid optimization problem, which in industry today provides locational marginal prices (LMPs) and is critical for system planning and operations.

The security constrained OPF (SC-OPF) includes additional constraints to satisfy security criteria [54], which means that the SC-OPF cost is always bounded below by the corresponding (unsecure) OPF cost. Table 2.1 illustrates and compares the general OPF and SC-OPF optimization formulations. In general, the SC-OPF problem is a non-linear, non-convex optimization problem with continuous or discrete variables and the main challenge is the large problem size (i.e., scalability). Note that corrective control for contingency $k = 1, \ldots, N_c$ are coupled to the pre-contingency solution through the *corrective* coupling constraint, which could represent ramp-rate limits on controllable energy resources. In this context, the term "corrective" implies that pre-defined post-contingency control actions exist that when applied will bring the system back to a secure state.

In the past, $N-1$ preventive SC-OPF algorithms provided operators with a well-understood deterministic methodology for managing risk/security in power systems. In fact, in many ISO markets (e.g., PJM and ISO-NE), it is a linear preventive SC-OPF algorithm that provides the locational marginal prices (LMPs) that price electricity [55]. However, with the recent emergence of competitive markets and stochastic renewable generation, systems have become more stressed, uncertain, and variable, which makes preventive SC-OPF challenging due to its restrictive nature: *one control, $u_0$, to manage all contingencies.*

Table 2.1: Comparing general OPF and SC-OPF formulations

| **OPF** | | **SC-OPF** |
|---|---|---|
| min $f(x,u)$ | $\leftarrow$ pre-contingency objective $\rightarrow$ | min $f(x,u)$ |
| *subject to:* | | *subject to:* |
| $g(x,u)=0$ | $\leftarrow$ power flow equation $\rightarrow$ | $g(x,u)=0$ |
| $h(x,u)\leq L$ | $\leftarrow$ pre-contingency constraint $\rightarrow$ | $h(x,u)\leq L$ |
| | contingency $k$ equalities $\rightarrow$ | $g_k(x_k,u_k)=0$ |
| | contingency $k$ inequalities $\rightarrow$ | $h_k(x_k,u_k)\leq L_k$ |
| | corrective coupling constraints $\rightarrow$ | $\lvert u_k-u\rvert\leq \Delta u_k$ |

Although the DC Optimal Power Flow (DCOPF) is a relatively simple linear programming problem, a full DC-based SCOPF including all possible line outages as contingencies can become computationally cumbersome, especially for large systems. Therefore, a constraint filter based on Power Transfer Distribution Factor (PTDF) and line outage distribution factors (LODF) is standard baseline against which one can test any other SCOPF approach.

To make the system $N-1$ secure , contingency constraints must be added, which is where the Power Transfer Distribution Factor (PTDF) matrix and Line Outage Distribution Factor (LODF) matrix are used to estimate post-contingency line flows after each possible contingency. LODF is an $N$-by-$N$ matrix where $N$ represents the number of lines in the network. Each entry of LODF matrix, $h_{lm}$ shows the relative change of flow on line $l$ due to removing line $m$.

$$|P_l + h_{lm}P_m| \leq P_{l,max} \tag{2.40}$$

$P_l$, $P_m$ represent the pre-contingency flow variable for line $l$ and $m$, respectively. By adding constraints (2.40) to optimization problem, effect of outage of line $m$ on line $l$ is taken into account.

PTDF is an $N$-by-$M$ matrix where $M$ represent number of buses. Each entry of PTDF matrix, $d_{lk}$ shows the relative change of flow on line $l$ due to change of injecting power on bus $k$.

$$|P_l + d_{lk}\Delta P_g| \leq P_{l,max} \tag{2.41}$$

Also by adding constraint (2.41) to optimization problem, effect of change in bus injection power of each bus (that could because of change in injecting power of generators, wind generation, load and etc) on line $l$ is taken into account.

The power injection at bus $i$, $P^i_{inj}$ can be written as

$$P^i_{inj} = P^i_G + P^i_{\omega_f} - P^i_L \tag{2.42}$$

where $P^i_G$,$P^i_{\omega_f}$ and $P^i_L$ are generating power, forecasted wind power and demand at bus $i$. The injected power at bus $i$ flows on the neighboring buses , (i.e., $\Omega^N_i$) via connected branches.

$$P^i_{inj} = \sum_{k \in \Omega^N_i} P^k_f \tag{2.43}$$

where $P^k_f$ is power flows on line $k$ connecting bus $i$ and $j$.

Total deviation of the wind power at different locations from their forecasted values, leads to generation-load mismatch which is a function of the total difference of the forecasted and actual wind production, $P_m(\sum_i P^i_{\omega_f} - P^i_{\omega})$. Generators shall deviate from their forecasted set-points, $P^i_{Gf}$, relative to their contribution factors, $d_i$ to compensate this power mismatch as follows:

$$P^i_G = (P^i_{Gf} + d_i * P_m(\sum_i P^i_{\omega_f} - P^i_{\omega})) \tag{2.44}$$

The main objective is to design a minimum cost dispatch while satisfying $N-1$ security constraints in probabilistic sense and decision variables are generations dispatch. Let $c_1$ and $c_2$ be cost function of generators. The resulting optimization problem is given by

$$min \quad \Sigma(c_1^T P_G + P_G^T[c_2]P_G) \tag{2.45}$$

subject to:

**Deterministic constraints for DC power flow (hourly):** These constraints correspond to the case where the wind power is equal to its forecasted value.

1. power balance constraint:

$$P_G^i + P_{\omega_f}^i - P_L^i - P_{inj}^i = 0 \tag{2.46}$$

2. line limit:

$$\underline{P}_f^k \leq P_f^k \leq \bar{P}_f^k \tag{2.47}$$

3. generators capacity:

$$\underline{P}_G^i \leq P_G^i + d_i * P_m(\sum_i P_{\omega_f}^i - P_\omega^i) \leq \bar{P}_G^i \tag{2.48}$$

where $\underline{P}_f^k$ and $\bar{P}_f^k$ represent upper and lower limit of line $k$ and $\underline{P}_G^i$ and $\bar{P}_G^i$ are minimum and maximum generating capacity of generator $i$.

**Probabilistic constraint** These constraints involve the uncertainty of the wind power forecast.

$$P(\underline{P}_G^i \leq P_G^i + d_i * P_m(\sum_i P_{\omega_f}^i - P_\omega^i) \leq \overline{P}_G^i) \geq 1 - \epsilon \tag{2.49}$$

The chance constraint encode the fact that the inequalities therein should be satisfied with the probability at least $1 - \epsilon$. There are different methods to satisfy the probabilistic constraint such as scenario approach of analytical reformulation which are explained in chapter 4 and chapter 5.

In our work, we use the output of the SC-OPF as economically optimal reliable reference trajectory and dispatch VESSs such that minimize the deviation of generators from their set-points.

# 3 Chapter 3: Investigating Delays in Frequency-Dependent Load Control


## Abstract

Increased penetration of renewables will require significant regulating reserves, so there is a need to re-think the traditional operating paradigm: *supply follows demand*. Recent work has expanded the role of flexible and controllable energy resources, such as energy storage and dispatchable demand, to regulate power imbalances and stabilize grid frequency. However, as shown in this chapter, the large-scale deployment of dispatchable (i.e., controllable) loads needs to carefully consider the existing regulation schemes in power systems, i.e., generator droop control. That is, this chapter illustrates with a standard linearized model, the complex nature of system-wide frequency stability from time-delays in actuation of dispatchable loads and the effect of different network topologies. Interestingly, we show that delay-induced instability can be stabilized by injecting additional delay into load controller.


## 3.1 Introduction

The quality of delivered electrical power and safety of electrical facilities are related to the nominal system frequency (e.g., 60 Hz in the U.S.). Small frequency deviations from nominal is generally caused by active power imbalances between generation and demand and is regulated through local (proportional) adjustments in the generator's governor (i.e., primary frequency control or PFC). PFC events generally take less than 30 seconds to stabilize the system frequency. However, with energy policy rapidly driving the installation of intermittent and low-inertia renewable generation, e.g., solar PV and wind farms, frequency deviations from nominal power imbalances are increasing [56, 57], which raises concerns over the ability of PFC to operate well in a future power system with significant penetrations of renewable energy [58]. As such, partial automated participation of flexible loads (e.g., energy storage and demand) in response to system frequency represents an alternative.

In operations, load "control" (i.e., *load shedding*) has been employed when severe imbalances threaten system integrity. However, active consumer-side participation has led to some revision on

the former demand side control logic. The concept of active consumer load coordination (i.e., aggregation) of air conditioners, radiators, plug-in electrical vehicles and other home appliances to balance the supply and demand has been discussed widely as means to reduce needed power reserves [59–63]. In fact, grid-scale distributed load frequency control algorithms have been proposed for stabilizing system frequency [64, 65]. However, due to phasor measurement units' (PMUs') communication channels that transmit data to the actuators or load coordinators (i.e., an aggregator), actuators or coordinators processing the PMU data, and the physical characteristics of the actuators and aggregators, significant constant or variable time-delays can be observed in power systems [66]. In [67, 68], the performance of a load aggregation scheme is tested for delays of tens of seconds. Note that the delays considered herein are the combined sensor-to-controller, controller-to-aggregator, aggregator-to-actuator, and physical actuator delays until flexible loads provide expected change in power. That is, we do not only consider the delays associated with PMU communication. Prior work has focused on designing generator control loops (i.e., PFC and AGC) that are robust against uncertain time-delays [69–71], but little (if any) work has considered the effect of time-delays on load coordination algorithms and system-wide effects. Therefore, to maximize the potential of fully automated load aggregation (at the MW-scale), the role of time-delayed load dispatch in power networks and its interaction with PFC schemes must be fully investigated.

To this effect, we present herein preliminary results on the system-wide effects of time-delays in flexible frequency-dependent loads. Specifically, we investigate through simulation-based analysis how different transmission network structures, dispatchable scenarios, and delays affect performance and stability of load coordination schemes.

## 3.2 Dynamic System Model

Consider a graph $\mathcal{G} = (\mathcal{V}, \mathcal{E})$ with a set of buses $\mathcal{V}$ and lines $\mathcal{E}$. Then, the balanced $N$-bus transmission system with $E$ lines will have buses divided into two sets: generator buses and load buses. A bus with a generator is called a generator bus, while all other buses are called load buses (even if the load is zero).

The voltage phase angle of bus $i$ with respect to the rotating framework at nominal frequency is denoted $\theta_i$ and let the angular frequency deviation of bus $i$ from nominal frequency $w_i^{\text{nom}}$ be denoted

$\Delta\omega_i := \omega_i - \omega_i^{\text{nom}}$. Then, their relationship is:

$$\dot{\theta}_i(t) = \Delta\omega_i(t) \quad \forall i \in \mathcal{V} \tag{3.1}$$

From the swing equation, we relate changes in frequency to instantaneous power imbalances:

$$\begin{aligned} M_i\Delta\dot{\omega}_i(t) = \Delta P_i^m(t) - \Delta P_i^e(t) \\ - D_i\Delta\omega_i(t) - \Delta d_i(t) \end{aligned} \tag{3.2}$$

$$\Delta P_i^e(t) = \sum_{j\in\Omega_i^N} \Delta P_{ij}(t) \tag{3.3}$$

$$\Delta P_{ij}(t) = b_{ij}\left(\Delta\theta_i(t) - \Delta\theta_j(t)\right) \tag{3.4}$$

where $\Delta P_i^m, \Delta P_i^e, \Delta d_i, \Delta P_{ij}$ are the changes in injected generator mechanical power, generator electrical power output to neighboring buses of $i$ (i.e., $\Omega_i^N$), controllable net-load, and line flow between buses $i$ and $j$ from nominal steady-state. $M_i$ is the generator inertia constant and $D_i$ is the damping coefficient accounting for mechanical rotational losses (of generators and motors at bus $i$). Also, the generator's droop behavior at bus $i$ is described by the dynamics of the turbine and governor:

$$\Delta\dot{P}_i^m(t) = \frac{1}{\tau_{T_i}}(\Delta P_i^v(t) - \Delta P_i^m(t)) \tag{3.5}$$

$$\Delta\dot{P}_i^v(t) = \frac{1}{\tau_{G_i}}(\Delta P_{\text{ref,i}} - \Delta P_i^v(t) - \frac{1}{r_i}\Delta\omega_i) \tag{3.6}$$

where $\Delta P_i^v$ is the change in turbine output power from nominal, $\Delta P_{\text{ref,i}}$ is the change in reference power of generator $i$, and $\tau_{T_i}, \tau_{G_i}, r_i$ are time-constants of turbine, governor, and speed-regulator, respectively.

In the case when there is no generator at bus $i$ (i.e., $i$ is a load bus), $M_i = 0$ and we have the following algebraic equation describing net-flow into bus $i$:

$$D_i\Delta\omega_i(t) = -\Delta P_i^e(t) - \Delta d_i(t), \tag{3.7}$$

which through differentiation can be re-written as a dynamic state:

$$D_i \Delta\dot{\omega}_i(t) = -\sum_{j\in\Omega_i^N} \Delta\dot{P}_{ij}(t) - \Delta\dot{d}_i(t). \tag{3.8}$$

Finally, (3.4) is transformed into a dynamic equation through differentiation:

$$\Delta\dot{P}_{ij}(t) = b_{ij}\left(\Delta\omega_i(t) - \Delta\omega_j(t)\right). \tag{3.9}$$

An overview of the system model for lines and buses is provided in Table 3.1. The controllable inputs are $\Delta d_i, \Delta\dot{d}_i$ and represent the control of flexible energy resources such as demand and storage. That is, in addition to the governor response of the generators, the controllable loads in the system respond to the imbalances through sensed frequency deviations and is implemented with proportional ($P_i > 0$) control as follows:

$$\Delta d_i(t) = P_i \Delta\omega_i(t - t_d) \qquad \forall i \in \mathcal{V}, \tag{3.10}$$

where $t_d \geq 0$ is the time-delay in load response. Note that the dynamic system model described by Eqs.(3.1)-(3.10) represents a closed-loop system with generator droop and (delayed) load control reacting to changes in sensed local frequencies.

The continuous-time dynamic model is implemented in MATLAB in discrete-time via Modified Euler with sampling time $h = 0.001$s, which has (global) accuracy on the order of $\mathcal{O}(h^2)$ [72].

**Remark 3.1** Since the delay is applied to the (measured) state in the controllable load's closed-loop description in (3.10), the time delay is internal to the closed-loop system, which is more challenging to analyze than the case of external (input/output) delays in the open loop. For example, an internally delayed system with input disturbance $v(t)$ can be described by $\dot{x} = Ax + A_d x(t - t_d) + Wv(t)$ and $y = Cx(t)$. Then, the transfer matrix is given by:

$$H(s) = \frac{Y(s)}{V(s)} = C\left(sI - A - A_d e^{-t_d s}\right)^{-1} W.$$

Table 3.1: Power system model overview

| **Variable Type** | **Variables** |
|---|---|
| Dynamic states | $\Delta\omega_i, \theta_i, \Delta P_i^m, \Delta P_i^v$ |
| Control inputs | $\Delta d_i, \Delta \dot{d}_i$ |
| Constant Parameters | $M_i, D_i, b_{ij}, \tau_{T_i}, \tau_{G_i}, r_i$ |

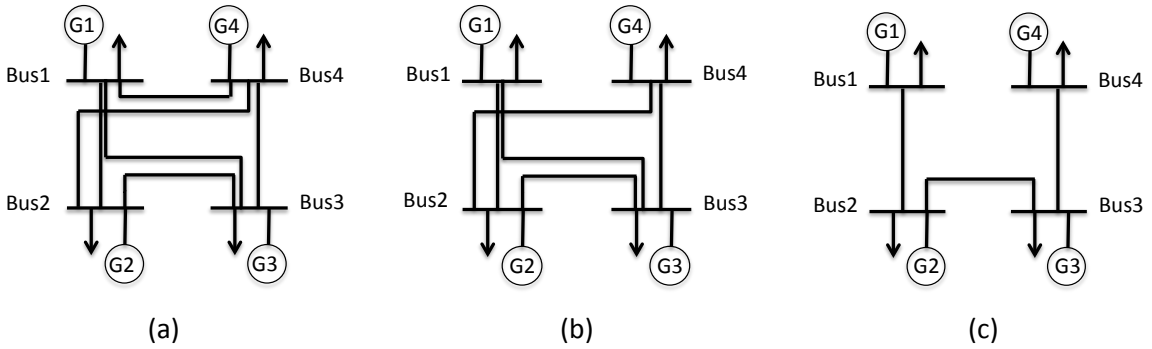


Figure 3.1: Three different 4-bus networks.

The poles of transfer function $[H(s)]_{ij}$ determine stability of output $i$ with respect to disturbance $j$.

## 3.3 Simulation Setup

In this section, we describe the different $N$-bus networks and the controllable load delay scenarios to be investigated.

### 3.3.1 Test networks

We consider three small 4-bus networks (see Fig. 3.1) with different interconnections (e.g., radial and meshed) and two standard IEEE test cases: 9-bus and 30-bus systems. Network parameters for the 4-bus system are based on [73] and provided in Table 3.2. For simplicity, a generator and load is connected to each bus. Note that controllable loads provide regulation at the scale of the damping coefficients, which is an order of magnitude smaller than generator inertias.

Table 3.2: Parameters for 4-bus system

| **Parameter** | **Value** | **Unit** |
|---|---|---|
| $M_1, M_2, M_3, M_4$ | $4, 40, 35, 10$ | $\frac{pu-s^2}{rads}$ |
| $D_1, D_2, D_3, D_4$ | $3.7, 1, 2, 2.7$ | $\frac{pu-s}{rads}$ |
| $\tau_{T_1}, \tau_{T_2}, \tau_{T_3}, \tau_{T_4}$ | 5,10,20,10 | $s$ |
| $\tau_{G_1}, \tau_{G_2}, \tau_{G_3}, \tau_{G_4}$ | 4,25,15,10 | $s$ |
| $r_1, r_2, r_3, r_4$ | 10,15,10,12 | $\frac{rads}{pu-s}$ |
| $b_{12,13,14,23,24,34}$ | $2.5, 2, 2, 1.5, 2.5, 2$ | $pu$ |
| $P_{i=4}$,$P_{i\neq 4}$ | $3, 0$ | $\frac{pu-s}{rads}$ |

### 3.3.2 Determining baseline controller gain

Before investigating the effect of time-delays, we need to design the nominal load controller's gain, $P_i$. The design of stabilizing P-controllers is achieved via closed-loop eigenvalue analysis of the multi-input/multi-output dynamical system and proportional gains are provided in Table 3.2. For example, the sets of closed-loop eigenvalues of the network 3.1(a) is illustrated in Fig. 3.2 for $P_4 \in [1, 100]$. Clearly, for all $P_4$, the poles are stable in the left-hand plane.

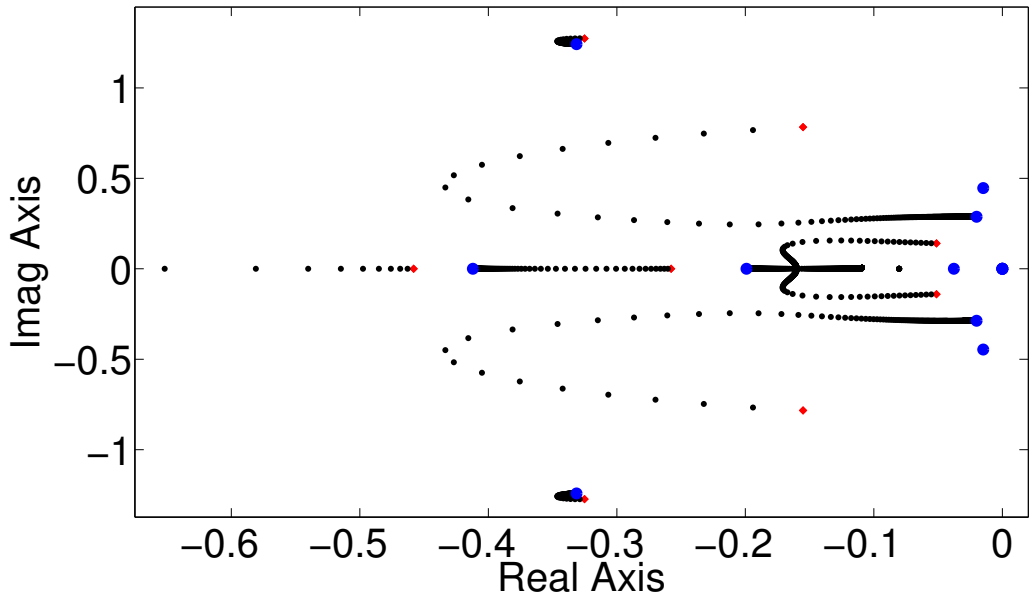


Figure 3.2: Closed-loop poles for network 3.1a as a function of $P_4$. Red dot denotes $P_4 = 1$ and blue dot represents $P_4 = 100$.

### 3.3.3 Time-delay

Since we are interested in the interaction between delays in load control and generator governors, we limit delays to $t_d \leq 30$s. Delay $t_d$ is then applied to the frequency-responsive load at bus $i = 4$ for the 4-bus system, buses $i = 8, 9$ for the 9-bus system, while five loads are controlled (but subjected to identical delays) in the 30-bus system: buses $i = 26 - 30$.

## 3.4 Simulation Results & Analysis

This section illustrates the non-periodic behavior of system stability for increasing delays and the effects of network structure on this stability. Interestingly, we show that delay-induced instability can be re-stabilized by injecting *additional delay* into load controller. The networks described in the previous section are initially in nominal steady-state until a +0.1 pu step-disturbance in the load at bus 1 occurs at $t = 10$ seconds.

For each applied delay $t_d$, the simulations capture performance (and stability conditions) through the settling time $T_{s,i}$ of the nodal frequency at bus $i$ ($\Delta\omega_i$) and is defined as the time after which the frequency enters and remains within specified dead-band, $\epsilon$:

$$T_{s,i} = \min_t \{|\Delta\omega_i(t^*)| < \epsilon,\ \forall t^* \geq t\}.$$

Due to the finite nature of computing, we limit simulations to consider $T_{s,i} \leq 1000$ seconds. That is, the closed-loop response is unstable if $T_{s,i} = 1000s$ for any $i$ (even if $T_{s,i}$ does not exist) and stable if $T_{s,i} < 1000s$.

### 3.4.1 The small 4-bus systems

The 4-bus systems in Fig. 3.1 are simulated according to the setup description. Note that for each $t_d$, we get data pair ($t_d$, $T_{s,i}$). Figure 3.3 illustrates all pairs ($t_d$, $T_{s,i}$) for network 3.1a. Clearly, when $t_d < 2$s, the system is stable and the system frequency settles in less than 15 s. However, by increasing $t_d$ at bus 4, the closed-loop system becomes unstable (e.g., see Fig. 3.6 for $t_d = 5$s) but then additional delay actually recovers stability and further delay again beget instability, etc. These stable-unstable-stable patterns repeat periodically as the load controller delay increases (e.g., see

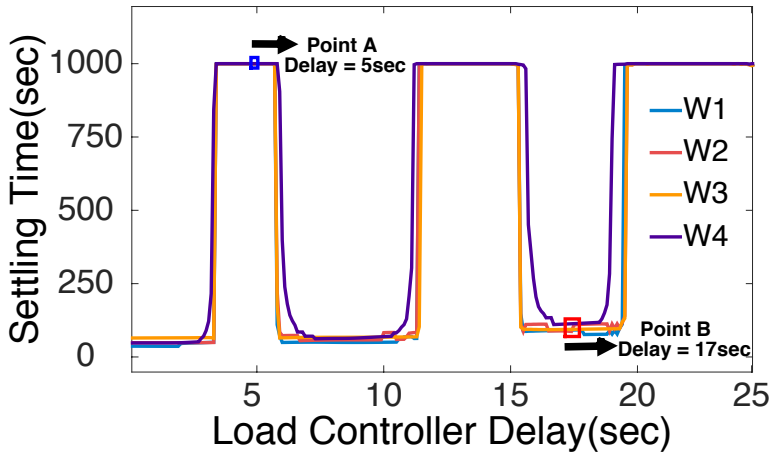


Figure 3.3: Network 3.1a: effects of $t_d$ at bus 4 on stability. System is initially stable ($t_d < 2$s). At Point A ($t_{d,A}$) the system is unstable, yet stable again at Point B, where: $t_{d,B} = 17s > t_{d,A} = 5s$.

Fig. 3.7 for $t_d = 17 > 5$s). To validate the numerical simulations, a 10th-order Padé approximation is applied to the internal delay $e^{t_d s}$ and the resulting poles are computed from the closed-loop transfer function $\Delta\omega_2(s)/d_1(s)$ for each $t_d \leq 25$. The real part of the (complex conjugate) pole-pair traces is illustrated in Fig. 3.8 and confirms the stable/unstable/stable behaviors observed in numerical simulations. For each time delay $t_d$, the poles of the transfer function are given by a vertical slice over all traces. Note that generally $T_{s,i}$ increases with $t_d$. $T_{s,4}$ is most sensitive to $t_d$ due to load controller on bus 4.

Figures 3.4 and 3.5 illustrate all pairs ($t_d$, $T_{s,i}$) for networks 3.1b and 3.1c. As can be seen, the performance of the 4-bus system under delays depends on the interconnection of buses. For example, pairs $(10, T_{s,i})$ illustrate this the across 4-bus networks. Thus, the 4-bus system, while simple to describe, shows the complex manner in which closed-loop stability and instability depends on the nature of delay in actuation of frequency sensitive loads. In the next section, we investigate larger systems, which are shown to exhibit the same type of behavior.

### 3.4.2 The larger 9-bus and 30-bus systems

In this section, the analysis is extended to the 9-bus and 30-bus IEEE standard test cases and considers more than one controllable load to contrast with the results of the simple 4-bus networks.

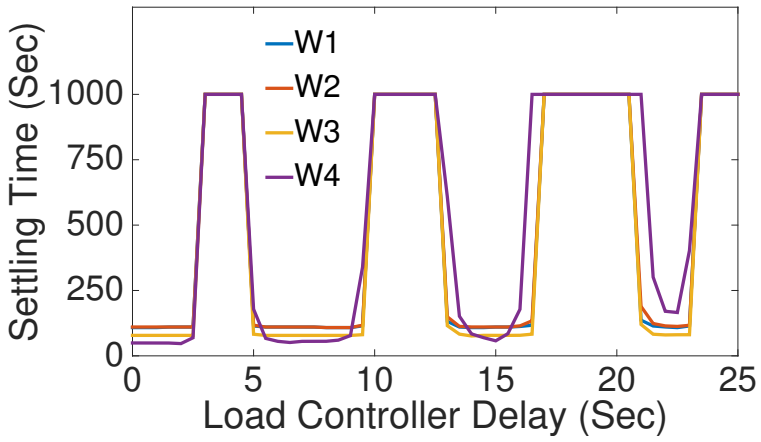


Figure 3.4: Network 3.1b: effects of $t_d$ at bus 4 on stability.

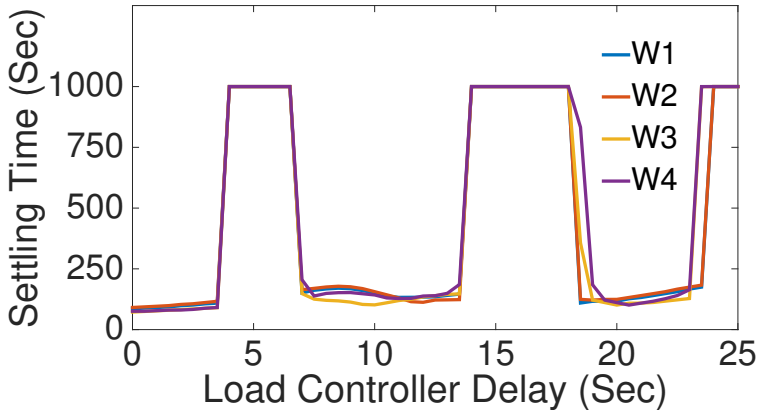


Figure 3.5: Network 3.1c: effects of $t_d$ at bus 4 on stability.

The settling time of the *system* is now defined as the maximum settling time across the $N$ buses:

$$T_s := \max_i \{T_{s,i}\}$$

The IEEE 9-bus test case is simulated with load controllers at bus 8 and bus 9:

$$\Delta d_i(t) = P_i \Delta\omega_i(t - t_d) \qquad \forall i \in \{8, 9\}$$

Figure 3.9 illustrates all pairs of $(t_d, T_s)$ for IEEE 9-bus test case. For $T_s < 1000s$ the system is stable while the system is unstable when $T_s = 1000s$. The stable-unstable behaviors illustrated in

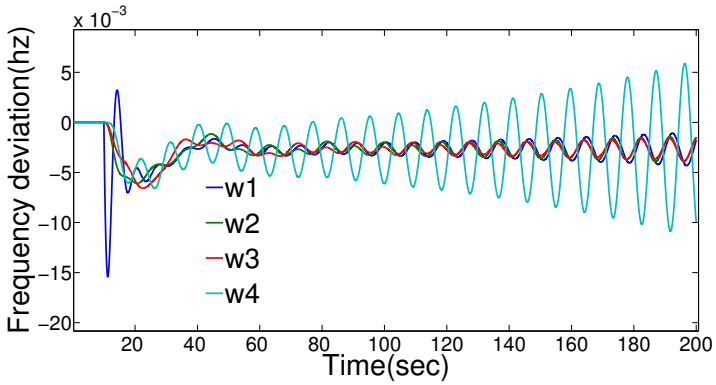


Figure 3.6: Closed-loop response: Point A in Fig. 3.3: $t_d = 5$s.

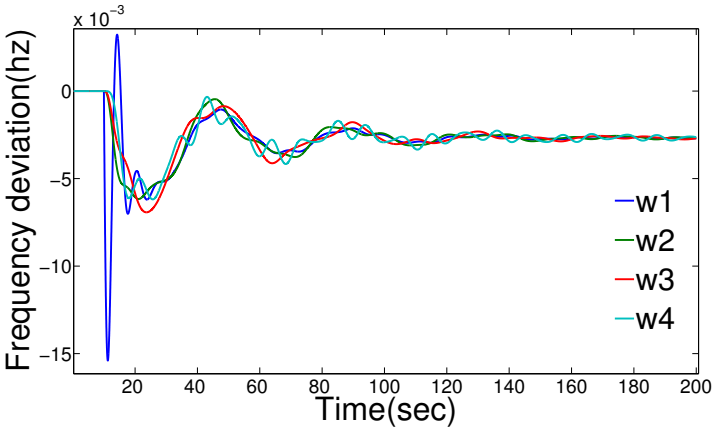


Figure 3.7: Closed-loop response: Point B in Fig. 3.3: $t_d = 17$s.

the 4-bus system occur also in the 9-bus case. That is, with increasing delay on the load controller, the settling time increases.

For the 30-bus network, two load control scenarios are investigated:

(i) a single controllable load at bus 30.

(ii) five controllable loads at buses $\{26 - 30\}$.

Figure 3.10 shows all pairs of $(t_d, T_s)$ for the IEEE 30-bus test system under scenarios (i) and (ii). The stable-unstable behavior is also present in the closed-loop but depends on how many loads are controlled.

**Remark 3.2** As the delay increases, the periods of instability become longer, until a delay, $t_d^*$,

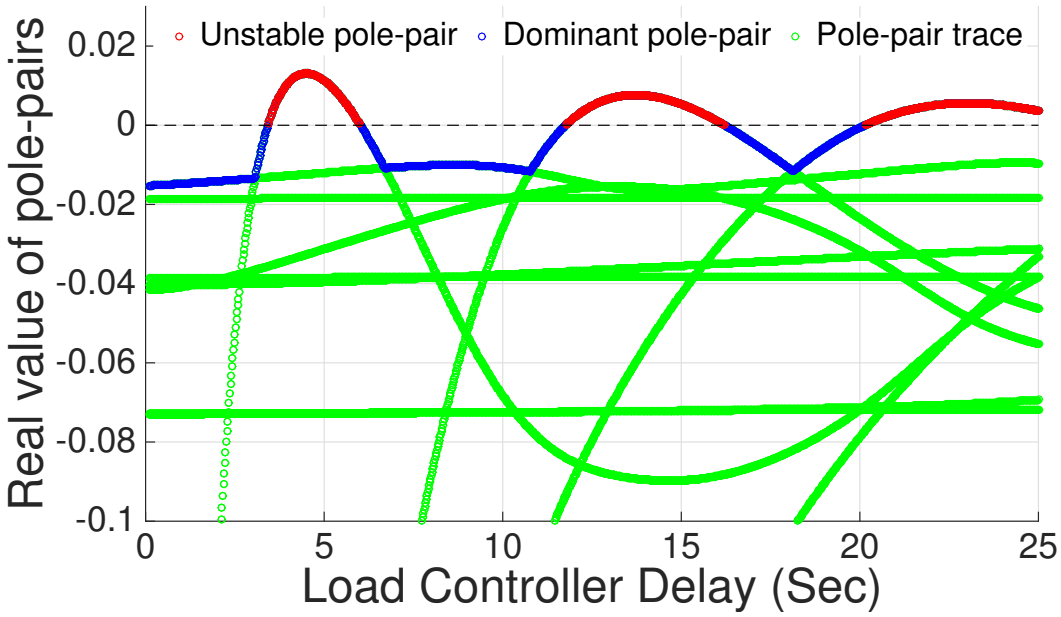


Figure 3.8: The traces of the real parts of the closed-loop (complex conjugate) pole-pairs for increasing time-delays in Fig. 3.1a are approximated with a 10th order Padé approximation. When any pole has positive real part, the system is unstable (in red), which confirms the numerical simulation results from Fig. 3.3. Note that for any given $t_d$, the dominant pole-pair is the trace with the largest real part and is highlighted in blue.

is reached beyond which the system remains unstable for all $t_d > t_d^*$ and the periods of stability exhibit increasing settling times (i.e., the dominant poles move closer to imaginary axis as shown in Fig. 3.8. Furthermore, the stable/unstable/stable patterns illustrated in this chapter are expunged if the generators do not utilize droop control. This indicates that the underlying behaviors are a result of generator and load controllers fighting against each other. Ongoing work is focusing on analytically characterizing this conflict and developing an improved load control scheme.

## 3.5 Conclusion and Future Direction

This chapter presents results on the effects of delay in frequency-dependent load control schemes with droop-controlled generators and investigates how delays affects settling time and stability of the system frequency in transmission networks. It is shown that the closed-loop performance of the system is stable/unstable as delay increases. Specifically, we show that the patterns of sta-

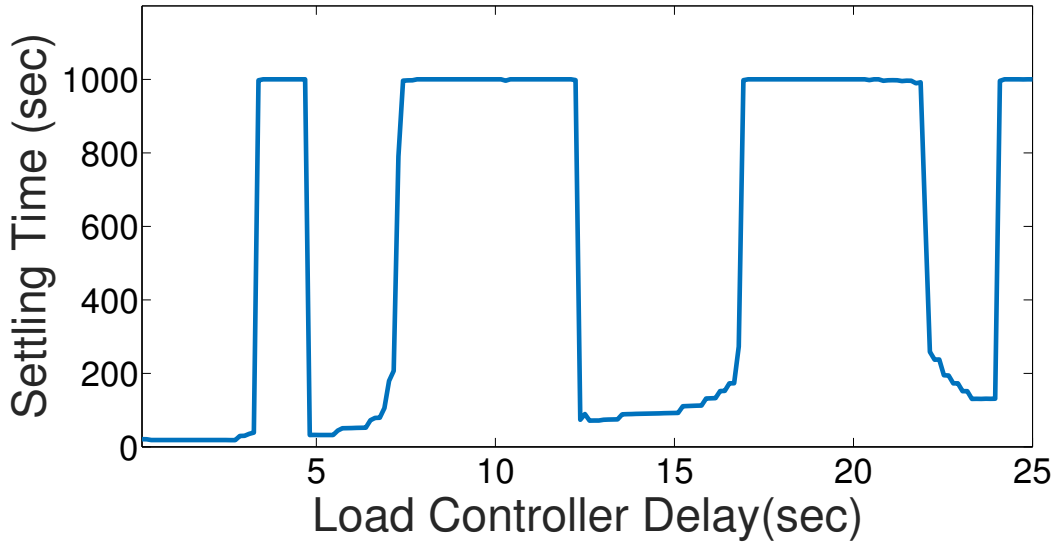


Figure 3.9: Effects of $t_d$ for controllable loads at buses 8 and 9 on closed-loop stability of 9-bus test case.

ble/unstable/stable depends on the network topology and parameters.

Future work will focus on developing analytical expressions for stability and controllability of system frequency as a function of available energy resources and salient network properties. To accomplish this, we seek to leverage recent results from linear delay differential equations where the *Lambert W function* has been utilized in describing stability of linear delay differential equations [74]. Designing controllers that are aware of actuator saturation is also being pursued. The end-goal is to develop load coordination schemes that are robust against a broad class of uncertainties, including unknown time-delays.

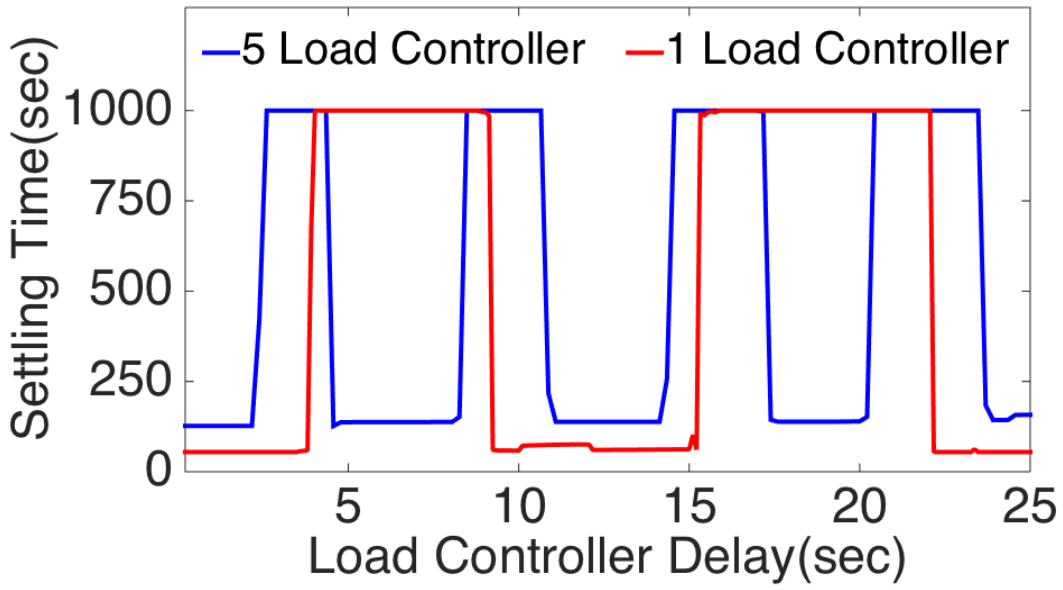


Figure 3.10: The 30-bus system experiences the same stable/unstable/stable patterns for different delayed load control scenarios.

# 4 Chapter 4: Trading off robustness and performance in receding horizon control with uncertain energy resources

## Abstract

Increased utilization of residential and small commercial distributed energy resources (DERs) has led DER aggregators to develop concepts such as the virtual energy storage system (VESS). VESSs aggregate the energy resources and dispatch them akin to a conventional power plant or grid-scale battery to provide flexibility to the system operator. Since the level of flexibility from aggregated DERs is uncertain and time varying, the VESSs' dispatch can be challenging. To improve the system operation, flexible VESSs can be formulated probabilistically and can be realized with chance-constrained model predictive control (CCMPC). This can be solved using scenario-based methodology, which provides a-priori probabilistic guarantees on constraint satisfaction. This chapter focuses on understanding the robustness and performance trade offs in receding horizon control with uncertain energy resources. The CCMPC dispatches robustly the uncertain VESSs and conventional generators while

taking into account economically optimal, secure reference trajectory for generating assets. Closed-loop performance is with respect to minimizing the deviation of conventional generators from their reference trajectory. To evaluate the trade off between robustness and system performance with uncertain energy resources, a simulation-based analysis is carried out on the modified IEEE 30-bus system.

## 4.1 Introduction

In recent years, environmental and energy concerns have led to increased penetration of distributed energy resources (DERs), such as solar photovoltaic and wind generation, which represents both a challenge and opportunity for grid operators. The intermittency of renewable energy sources as well as forecast uncertainties in load, price, and renewable in-feed profiles, call for storage solutions and appropriate control strategies [44]. So far, imbalances between production and load are compensated by fast acting reserves from generators, such as gas turbines or hydro storage power plants. However, due to the on-going increase in intermittent sources, day-ahead planning becomes more demanding. The grid operators can pay high penalties when load forecasts are inaccurate and require generators re-scheduling to balance demand and supply [75]. Furthermore, an increasing number of backup generation units is needed, running on reduced power or even idling, to quickly react to output changes of intermittent sources. Instead of compensating forecast uncertainties with fast acting backup generators, as it is often done in practice, the imbalances can also be compensated by means of coordinating flexible energy resources, i.e., demand dispatch [13, 38].

Recently, the concept of Virtual energy storage system (VESSs) has been proposed as a novel technology for aggregating and coordinating a large fleet of residential flexible energy resources, including electric battery storage, thermostatically controlled loads (TCLs), and deferrable loads. The VESS offers the aggregate flexibility to the system operator as a synthetic reserve to preserve grid stability [15]. When called upon, the VESS can rapidly respond to changes in net-load by quickly coordinating its fleet of assets to provide requested balancing reserves [16]. Since offered flexibility by VESSs to the system operator is limited, to benefit the most from them, careful planning through smart techniques such as MPC is required.

Today, in practice, based on market conditions and load and renewable forecasts, an optimal

power flow problem is solved with a day ahead window prediction horizon (i.e. 24 hours) on an hour by hour time scale to provide an economically optimal schedule for generators and flexible resources [76]. However, due to variable uncertainty in the net-load forecast, there will always be mismatches between scheduled operating set-points and the actual operating points. Therefore, the scheduled operating point may no longer be feasible and balancing reserves are required and can be provided by a set of VESSs by adjusting the aggregate output of DERs [77].

As a VESS derives its flexibility from aggregating thousands of DERs, estimation of the VESS's current energy state, energy limits, and up/down power capabilities are inherently uncertain and time-varying. Therefore, this chapter seeks to formulate the VESS's flexibility in a probabilistic manner with chance constraints. Then, we solve this by a scenario-based approach, which provides a-priori guarantee to the probabilistic constraints [78–80]. The authors in [54, 78] use probabilistically robust optimization method provides a priori guarantees on the probability of constraint violation without needing any knowledge of the uncertainty distribution, however it requires large number of uncertainty scenarios. Other recent studies also solve chance constraint problem using scenario approach as authors do in [81], or by using analytical reformulation, e.g., [82], but these studies do not model the uncertainty on the VESS's capacity.

To take uncertainty of VESS's energy capacity into account, we employ chance constraints to a receding-horizon model predictive controller (MPC) that is similar to the author's prior work in [46, 83]. At each step, net-load forecasts (i.e., load minus renewable generation) and dynamic states (e.g., storage and generators) are updated to provide a prediction of power imbalances. The chance-constrained predictive dispatch operates on minute-by-minute time scale with 20-40 minutes prediction horizon and responds to any mismatches caused by forecasting error, which is denoted as chance-constrained model predictive control (CCMPC). The CCMPC provides an open-loop schedule for the entire horizon yet only implement the first control decision. This procedure is repeated every minute in receding horizon fashion. The objective of the chance constrained MPC optimization problem is to minimize the deviation of conventional generation from the scheduled set points provided by the economic trajectory.

**Contributions of this chapter include the following:**

- Prior works have explored allocating flexible resources in a techno-economic setting to com-

pute optimal economic trajectories as reference signals for a fast timescale dispatch of energy resources. In this chapter, we expand these bilevel frameworks to couple these economic trajectories with a fast timescale stochastic predictive dispatch.

- As far as the authors are aware, prior work on stochastic OPF methods, focuses mainly on the uncertainty of (algebraic) power injections (e.g., wind, demand), which temporally decouples the OPF problem and side-steps the computational challenges of multi-period optimization under uncertainty, e.g., [84, 85]. Unlike those works, this chapter presents a stochastic predictive OPF with uncertain dynamic energy capacity and analyze how robustness (i.e., uncertainty in VESS energy capacities) trades off with system performance (i.e., ability of VESS to supply corrective power balancing). Related work in [81, 82, 86] also investigate uncertain energy storage capacity, however, the authors manage that uncertainty through day-ahead reserve scheduling at a 15-60 minute time-scale rather than the stochastic predictive dispatch presented herein.

- Computing optimized charging/discharging commands for uncertain energy resources deterministically, based on the expected energy capacity estimate may result in saturation of the control action under unexpected energy capacity realization. This saturation phenomena gives rise to the notion of dynamic capacity saturation (DCS), which we present and analyze in this chapter for the first time. We show that DCS is helpful to describe how uncertain resources can participate in corrective power balancing.

The remainder of this chapter is organized as follows. Section 4.2 describes the optimal power flow problem and tracking control framework, and discusses the roles of each, and their interactions. In Section 4.3, we explain role of uncertainty on capacity of storage devices and describe chance constrained model predictive control (CCMPC). In Section 4.4 the results of case studies on the modified IEEE 30-bus power system is presented. Finally the concluding remarks and future work are given in Section 4.5.

## 4.2 Problem Formulation

We consider a transmission system model comprising of $N_b$ buses, $N_l$ lines, $N_G$ generators, $N_L$ loads and $N_B$ VESSs. Given a forecast of demand and expected renewable generation (i.e., net-load) for

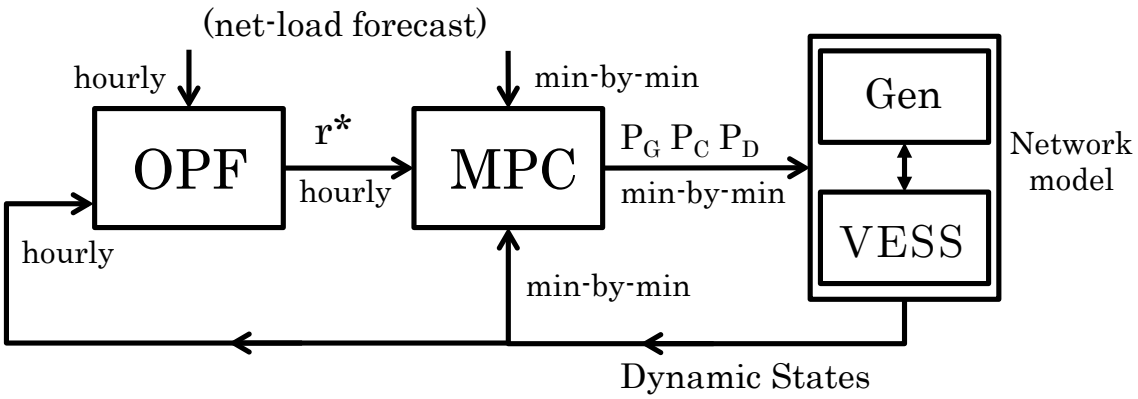


Figure 4.1: Overview of control scheme showing controller including OPF and MPC part and how each part is related to power grid

a number of hours (e.g., day-ahead), an economically optimal trajectory is computed. However, due to forecasting error, it may be necessary for generators to deviate from the predefined trajectory. The controller's objective is to meet the demand while minimizing the tracking error by utilizing the flexibility of VESSs. This suggests a bi-level control strategy for electric power systems. In this work our focus is on predective reference tracking-MPC. Figure. 4.1 provides an overview of the proposed control system.

### 4.2.1 Optimal Economic Trajectory

Like most of related works, e.g., [46, 81, 86], the DC power flow approximation is adopted which gives us a tractable linear representation of the power system while ensuring the convexity of optimization problem.

Based on net-load forecast, the optimal, $N_T$-hour ahead (i.e. $N_T = 24$), schedule is computed as a multi-period, quadratic programming (QP) problem whose objective is to minimize energy (fuel) costs of conventional generators [87]. Let $a$ [\$/h-pu] and $b$ [\$/h-pu$^2$] are linear and quadratic coefficient of generators cost curve, $P_{G_i} \in R^{N_G}$ refers to power set point of generator $i$ corresponding to the forecasted load power. With this definition, the resulting objective of the problem can be

expressed as:

$$\min_{P_{Gi}} \sum_{\forall k \in N_T} \sum_{\forall i \in N_G} a_i^k P_{Gi}[k] + b_i^k P_{Gi}^2[k], \tag{4.1}$$

subject to the physical and operational constraints corresponding to the power flow on the system generator and line limits for all $k \in N_T$ :

$$P_{Li}^f[k] + \sum_{j \in \Omega_i^N} f_{ij}[k] = \sum_{z \in \Omega_i^G} P_{Gz}[k] \qquad \forall i \in N_b \tag{4.2}$$

$$\underline{P_{Gi}} \leq P_{Gi}[k] \leq \overline{P_{Gi}} \qquad \forall i \in N_G \tag{4.3}$$

$$-R_{Gi} \leq P_{Gi}[k+1] - P_{Gi}[k] \leq R_{Gi} \qquad \forall i \in N_G \tag{4.4}$$

$$f_{ij}[k] = b_{ij}(\theta_i[k] - \theta_j[k]) \qquad \forall ij \in N_l \tag{4.5}$$

$$\underline{f_{ij}} \leq f_{ij}[k] \leq \overline{f_{ij}} \qquad \forall ij \in N_l \tag{4.6}$$

where $\Omega_i^N$ and $\Omega_i^G$ refer to set of all buses connected to bus $i$ and set of all generators at bus $i$. Forecasted electrical net-load (i.e., demand minus renewables) is represented by $P_L^f$ while $\overline{P_G}(\underline{P_G}^1)$ and $R_G$ represent, maximum (minimum) generation capacity and ramp rate limit of generator, respectively. Also $\theta_i$ is the voltage bus angles at bus $i$ and $b_{ij}$ denotes the imaginary part of the admittance of the line connecting node $i$ to node $j$ and $f_{ij}$ represent power flows on the corresponding line. By solving this problem every hour, a reference signal over a horizon of $N_T$ is established based on the updated measurements and forecasts.

**Remark 4.1** In this chapter, we assume that the responsive VESSs are available from previously allocated reserves (e.g., akin to [81]) and have baseline consumption. By shifting the controllable loads consumption from its baseline, VESSs can respond to the instantaneous mismatches caused by forecast error quickly. Any decrease/increase in the consumption of the VESSs relative to its baseline consumption can be translated as discharging/charging the VESSs. We assume that market interactions have determined the regulation capability from each VESS [88].

[1]The lower bounds of the generator set-points would be available from unit commitment (UC) problem which is not within the scope of this chapter. In this chapter for simplicity the lower bound is assumed to be zero.

If constraints related to generator ramping is ignored, the multi-period problem becomes temporally decoupled and each time-step can be solved separately as is the case in [89] which solving problem with $N_G$ variables, $N_T$ time rather than solving a problem with $N_G \times N_T$ decision variables. However, by taking into account generators ramp-rate limits, generator set points changes are coupled in time and bounded. Taking intro account coupling yields a smaller feasible region, means more expensive dispatch and coupled problem takes longer to solve. By solving this problem every hour, a reference signal over a horizon of $N_T$ is established based on the updated measurements and forecasts.

### 4.2.2 Trajectory tracking and managing uncertainty

Due to mismatches between forecasted and actual values of net-load, forecasted optimal set points of generator may not be a feasible solution for the power flow problem.

Therefore, in the second level, a model predictive controller (MPC) is in charge of responding to any deviation in load consumption and renewable production from their predicted value in a way to minimizing the deviation from reference optimal trajectory while satisfying all the constraints such as line limits, generators limit, ramp rate limits of generators and dynamic and power ratings of energy storage devices (VESSs). The MPC iteratively, based on initial states, updated net-load forecast and updated reference signal, optimizing over a finite time horizon, $M$, by solving an open-loop optimization problem. This yields a sequence of optimal control action for the next $M$ steps, where only applying the first instance of control sequence.

In general, the outcomes of the first level (optimizing under deterministic condition) are used as our base trajectories which already take care of our primal objectives like cost or security while the VESSs make the aggregated flexibility available to controller as balancing reserve and enhance tracking performance. Since time step of MPC ($\approx$ 1 minute ) is much shorter than OPF ($\approx$ 1 hour), reference trajectory provided by OPF is interpolated by time step of $T_s$.

Control actions will be applied for the whole step-width $T_s$ such that $u(t) = u[k]$ for $t \in [kT_s, kT_s + T_s]$. At each time $k$, the state of the charge (SOC) of VESSs and generator set-points are the dynamic states which are measured and included as initial state of the system for the next step. Based on [46], MPC scheme can be summarized as follows:

1. At time $k$, with initial SOC, $S_k$, updated net-load forecasts and generator set-points from solving OPF, MPC solves a finite-horizon open-loop optimal control problem, over interval $[k,k+M]$. This returns sequence of optimal control action such as charging or discharging VESSs and re-scheduling generator set-points if needed, for the next $M$ steps ($k$ to $k+M$).

2. Apply only the control action corresponding to time $k$

3. Measure the actual system state based on the actual load consumption and renewable generation at time $k+1$.

4. Set $k = k+1$

The open-loop MPC optimization is as follows:

$$J^* = \min_{P_{Gi},P_{Ci},P_{Di}} \quad \sum_{m=k}^{k+M} \sum_{\forall i \in N_g} c_G^i (P_{Gi}[m] - P_{Gi}^r[m])^2 + \sum_{m=k}^{k+M} \sum_{\forall i \in N_B} c_C^i P_{Ci} + c_D^i P_{Di} \tag{4.7a}$$

s.t.

$$P_{Ni}[m] + \sum_{j \in \Omega_i^N} f_{ij}[m] - \sum_{z \in \Omega_i^G} P_{Gz}[m] = 0, \tag{4.7b}$$

$$P_{Ni}[m] = P_{Ci}[m] - P_{Di}[m] + P_{Li}^f[m], \tag{4.7c}$$

$$\underline{f_{ij}} \leq f_{ij}[m] \leq \overline{f_{ij}}, \tag{4.7d}$$

$$f_{ij}[m] = b_{ij}(\theta_i[m] - \theta_j[m]), \tag{4.7e}$$

$$\underline{P_{Gi}} \leq P_{Gi}[m] \leq \overline{P_{Gi}}, \tag{4.7f}$$

$$\underline{P_{Ci}} \leq P_{Ci}[m] \leq \overline{P_{Ci}}, \tag{4.7g}$$

$$\underline{P_{Di}} \leq P_{Di}[m] \leq \overline{P_{Di}}, \tag{4.7h}$$

$$P_{Gi}[m] - P_{Gi}[m-1] \leq R_{Gi}, \tag{4.7i}$$

$$-R_{Gi} \leq P_{Gi}[m-1] - P_{Gi}[m] \leq R_{Gi}, \tag{4.7j}$$

$$S_i[m+1] = S_i[m] + T_s \left( \eta_{ci} P_{Ci}[m] - \frac{1}{\eta_{di}} P_{Ci}[m] \right), \tag{4.7k}$$

$$\underline{S_i} \leq S_i[m] \leq \overline{S_i}, \tag{4.7l}$$

$$S_i[k-1] \leq S_i[k+M], \tag{4.7m}$$

$$P_{Ci}[m] P_{Di}[m] = 0 \tag{4.7n}$$

where (4.7b)-(4.7n) are satisfied, $\forall m = k, k+1, \ldots, k+M$. Note that $c_G$ and $c_C(c_D)$ are positive scalars representing tracking and charging (dis-charging) cost coefficients. Moreover, $P_{Ci}, P_{Di} \in R_+$ are positive scalars representing charging and discharging commands of VESSs and $P^r_{Gi}$ is the reference signal. $\overline{P_{Ci}}$ ($\overline{P_{Di}}$) and $\overline{S_i}$ represent the maximum charging (discharging) power capacity and the maximum energy capacity of VESS located at bus $i$, respectively. Similarly, $\underline{P_{Ci}}$ ($\underline{P_{Di}}$) and $\underline{S_i}$ represent the minimum charging (discharging) power rate and the minimum energy level of the VESSs which in our work assumed to be equal to zero for simplicity. The charging and discharging efficiency of VESS located at bus $i$ are denoted $\eta_{ci}$ and $\eta_{di}$ respectively. The net power injected from VESS $i$ at time $m$ equal to $(P_{Ci}[m] - P_{Di}[m])$ that could be positive (charging the VESS) or negative (discharging) or zero. We impose terminal constraint (4.7m) on SOC of VESSs to ensure sustainablity of VESS resources at the end of each optimization horizon.

**Remark 4.2** To prevent simultaneous charging and discharging which is not physically realizable for most of the storage devices, complementary condition (4.7n) is employed, however since this constraint is non-linear, it makes the problem strongly non-convex and needs applying mixed-integer approach [90]. Authors in [83] employed a heuristic method that enabled them to solve the convex problem while preventing simultaneous charging and discharging. Furthermore, as VESSs aggregate large population of small-scale flexible energy resources, they have the ability to send charging and discharging commands to different devices in their group simultaneously and the aggregated charging and discharging commands are what determine the next time steps overall energy level.

## 4.3 The chance constrained problem

The chance-constrained optimization has been employed to solve the optimization problem under uncertainties. It formulates the optimization problem such that ensures that the a certain constraint should be satisfied with a pre-defined probability.

VESSs can be formed from a large number of different resources including storage devices, wind farms, solar farms as well as different forms of flexible energy resources like plug-in electric vehicles (EVs) and TCLs [91].

The flexibility offered by VESSs can enable renewable integration into the power system and

provide significant balancing reserves to the system operator and prevent frequent rescheduling due to imbalances from weather and load/demand forecasts. However, the level of the flexibility that VESSs can provide to system operator is uncertain itself.

As an example, coordinated aggregation of large population of TCLs is often modeled as virtual storage resources [92]. However, due to stochastic and time-varying human usage of hot-water, the size of the virtual storage resources is time-varying. More specifically, available flexibility offered by aggregated TCL to the system operator, which can be translated to the upper bound of the virtual storage resource, is a function of different stochastic quantities such as weather condition and human behavior.

Flexibility offered by each device is uncertain and considered an independent random variable (i.e. background usage of each device is independent from background usage of other devices). Since, VESSs are formed from a large number of flexible resources, the central limit theorem implies that the VESS's energy capacity is a normally distributed random variable centered on the true mean (i.e $\overline{S} \sim \mathcal{N}(\mu, \sigma^2)$. Thus, the stochastic variable ($\overline{S}$) is present only on the right hand side of (4.7l).

**Definition 4.3 Dynamic capacity saturation (DCS):** Computing optimized control actions, such as charging/discharging commands, for uncertain energy resources that provide balancing reserves can be based on a mean (or average) energy capacity estimate. When using the mean capacity values result in a deterministic optimization problem. However, the underlying uncertain energy capacity may realize itself unexpectedly and saturate (or zero out) the optimized control action. We call this saturation phenomenon *dynamic capacity saturation* (DCS). Under DCS, an energy resource may saturate, which zeros out its control action, leading to unexpected power imbalances in the system. To regulate these DCS-induced imbalances, grid operators must rely on (expensive) generation to supply the difference based on their participation factor $d_i$, as shown in (4.8). In addition, SOC of VESS could be updated to reflect actual capacity as shown in (4.9). Figure 4.2 shows an example of how forecast errors lead to DCS. Plot (a) illustrates the expected and actual capacity of VESS (dotted lines). Also, the state evolution of SOC based on the expected capacity of VESS and needed correction due to forecasting error are shown (dashed lines). Plot (b) and (c) show the optimal schedule for charging/dis-charging of VESS and how DCS causes deviation from optimal solution:

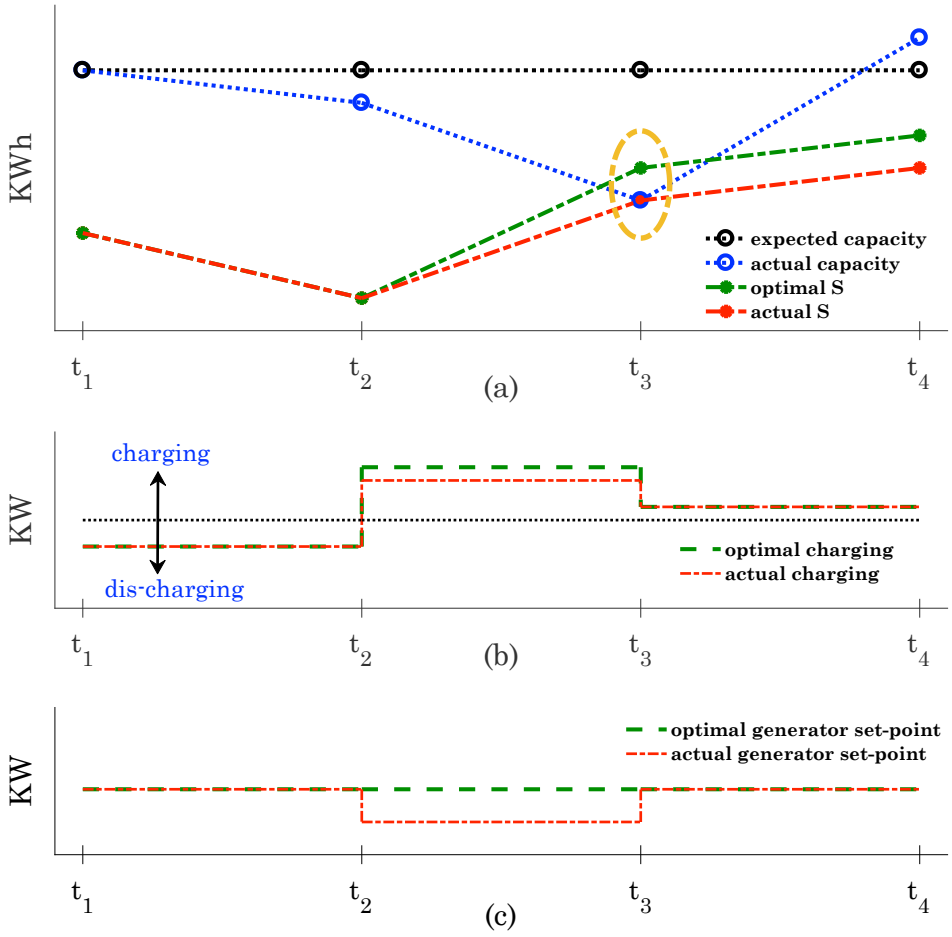


Figure 4.2: An example of how forecast error causes dynamic capacity saturation.

$$\Delta P_{Gi}[k+1] = -d_i \sum_{i \in N_b} T_s^{-1} \max(S_i[k+1] - \overline{S_i}, 0)) \tag{4.8}$$

$$S_i[k+1] = \max(S_i[k+1], \overline{S}) \tag{4.9}$$

Since the capacity of VESS is a stochastic variable, we could approach the problem in a probabilistic manner. The chance constraint is one such option whereby we decide on the probability

level of $1-\epsilon$, where $\epsilon \in (0,1)$, as shown below

$$P(S_i[k+1] \leq \overline{S_i}(\delta)) \geq 1-\epsilon \tag{4.10}$$

In [79], a scenario is introduced, in which the chance constraint is substituted by a finite number of deterministic constraints and provide a-priori guarantees on satisfying the chance constraint with some certain level of confidence $\beta$ , where $\beta \in (0,1)$.

Ref. [78] proposed a two step method based on [79] that results in a lower number of realizations. In the first step, the set $\Delta$, including at least $1-\epsilon$ probability mass of uncertainty, is made with confidence level of at least $1-\beta$. To form this set, we need at least $N$ realizations, where $e$ denotes the Euler number and $N$ is calculated based on the number of uncertain parameters $N_\omega$,

$$N \geq \frac{1}{\epsilon}\frac{e}{e-1}(ln\frac{1}{\beta}+2N_\omega-1) \tag{4.11}$$

Based on the set $\Delta$, the chance constraint is substituted to the robust constrain

$$S_i[k+1] \leq \overline{S_i}(\delta) \qquad \text{for all } \delta \in \Delta \tag{4.12}$$

While only expected value of capacity of VESS is needed to come up with a deterministic solution, $N$ realizations are needed for a probabilistic solution. For example, to ensure a violation probability of maximum $\epsilon = 0.1$ with a confidence level of $\beta = 0.05$, in presence of one VESS with uncertain capacity, we need to consider 64 realizations of VESS capacity as shown in Fig 4.3. The green, dashed line represents expected values and the red, solid line represent the robust bound.

We introduce coefficient $\alpha \in [0, \inf)$, as an average level of robustness to investigate role of robustness on performance of the controller.

$$\overline{S} = \alpha \overline{S}_{\text{expected}} \tag{4.13}$$

By setting $\alpha$ based on the robust bound (e.g, robust bound computed by scenario approach), we can reduce the probability of DCS, but part of the flexibility offered by VESSs will be dismissed.

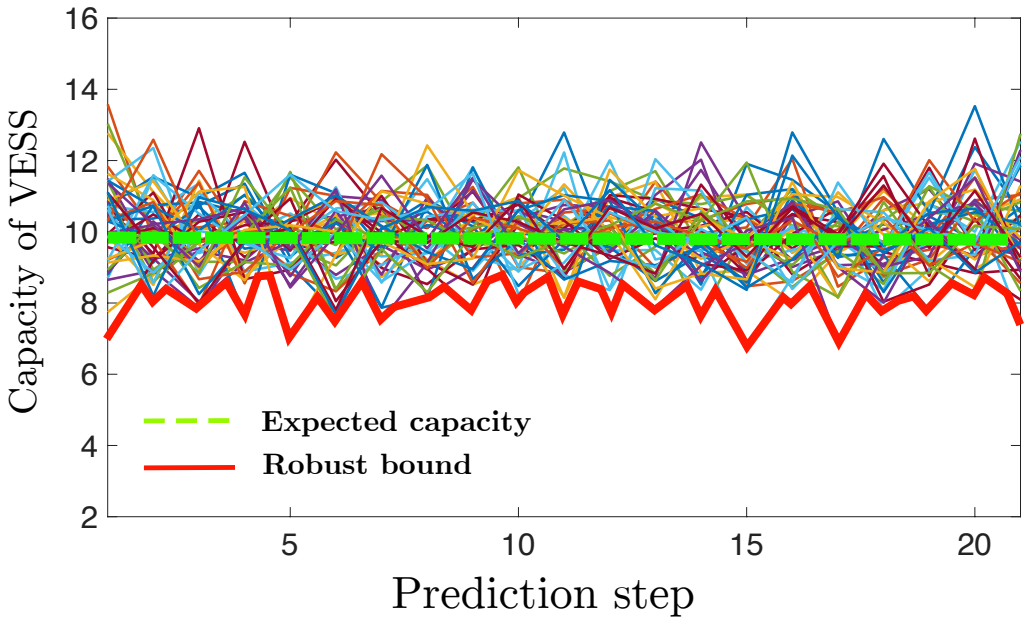


Figure 4.3: Expected value of VESS capacity versus 64 realizations

On the other hand, by selecting $\alpha \geq 1$, the predictive optimizer will have more VESS resources available for balancing, however, DCS will occur more frequently in the system, which can reduce closed-loop performance (i.e., generator having to make up the slack resulting from DCS.) Therefore, there should be a balance between robustness and flexibility. i.e. coefficient $\alpha$ must be chosen in such a way that controller can use the most flexibility offered by VESSs and minimize chances of DCS. The forecasting error occurs almost at all time steps (e.g., see Fig 4.2a for $t > t_1$). However, despite forecast errors, sub-optimal solution happens only when DCS occurs (e.g., see Fig 4.2a at $t = t_3$). If DCS is absent, optimal regulation can be achieved despite forecasting errors.

## 4.4 Simulation result

In this section, the introduced control approach is applied to modified IEEE 30 bus power system, consisting 30 substations, 6 generators, 21 loads, 37 transmission lines and 4 transformers [93] as shown in Fig. 4.4. The power system is modified to include one VESS at bus 5. All optimization problem were solved via the MATLAB and AMPL using the solver GUROBI.

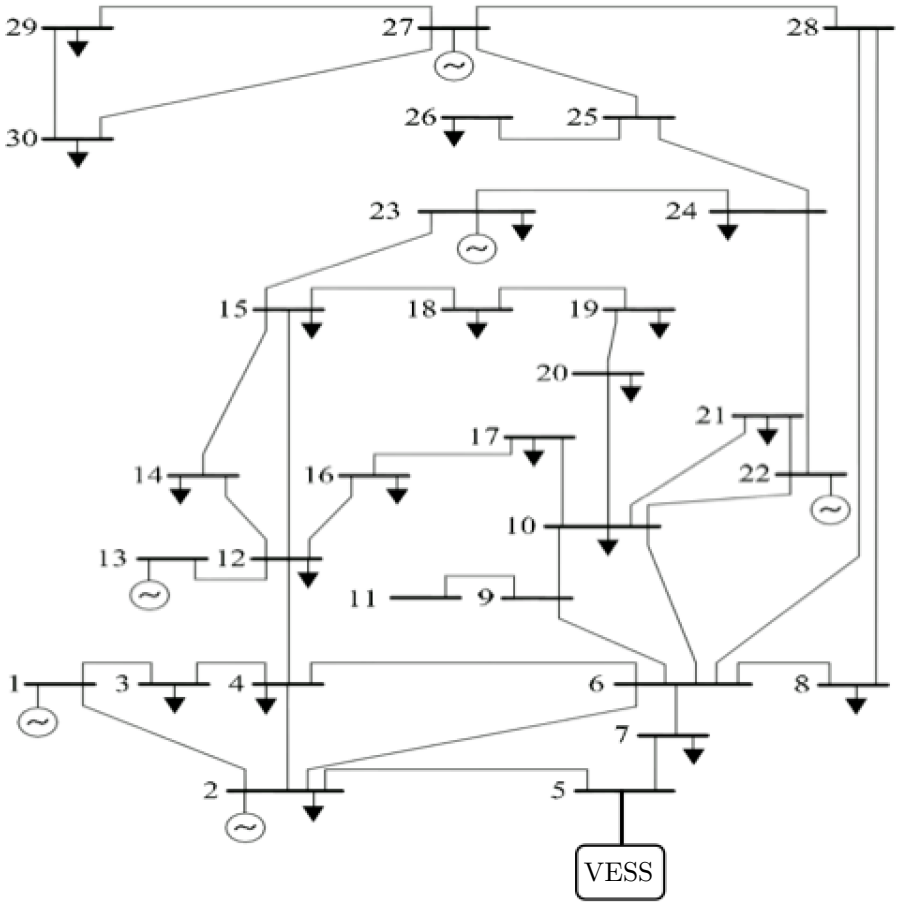


Figure 4.4: Modified IEEE 30 bus system

### 4.4.1 Perfect prediction of VESS capacity

Initially, we assume that the capacity of VESS can be forecasted perfectly. Based on the forecasts of net-load, an optimal schedule for generators is computed. To model net-load forecast error raised from uncertain renewable generation, mean reverting random walk with zero mean is added to the forecasted net-load. Performance and behavior of MPC (with horizon length of $M = 20$) is shown in Fig. 4.5.

Recall that reference signal is the generator set-point, which means high performance implies generators do not respond to imbalances (i.e., do not ramp through reserves). Obviously, in presence

of VESS, tracking performance is improved and the flexibility offered by VESS, make MPC able to effectively limit the ramping up or down of generators. However, the tracking error can not be zero due to limited capacity of VESS.

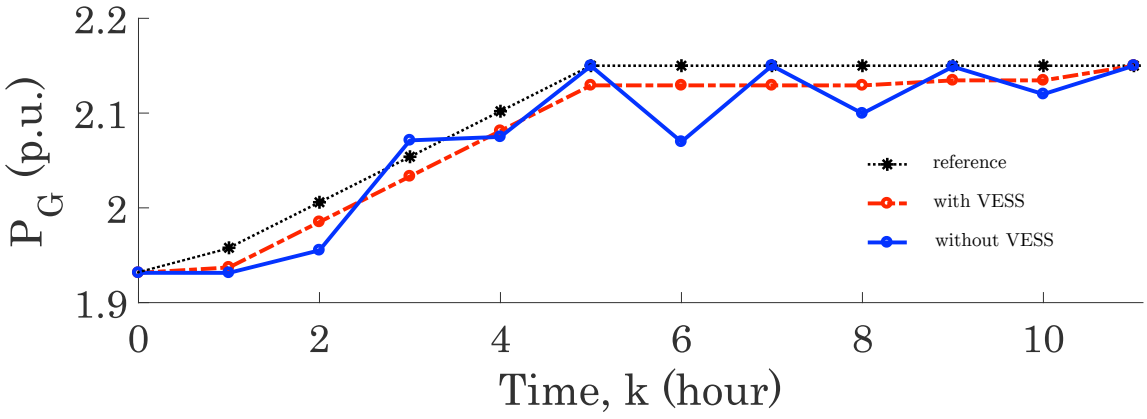


Figure 4.5: Optimal schedule based on the forecasted net-load as a reference trajectory and performance of the MPC scheme for one generator under two cases: without VESS and with VESS.

The role of MPC prediction horizon on reference-tracking MPC performance is investigated and shown in Fig. 4.6a. Longer horizons lead to better performance, as expected, but performance benefit diminishes as a function of VESS capacity. This is because the capacity of VESSs increases long-term flexibility which improves value of predicted information. Figure 4.6b illustrates the role of the VESS capacity on the MPC performance. Using larger VESSs leads to less ramping from generators which reduces MPC objective. Average economic dispatch run time for each hour and average run time of MPC under horizon of 40 steps is shown in Table 4.1. Average economic dispatch run time for each hour is less than one second ($\sim 0.5$ sec) and average run time of MPC under horizon of 40 steps is less than two seconds ($\sim 1.5$ sec) as it shown in Table 4.1.

Table 4.1: Run-time metrics for OPF and MPC

| | Average (s) | Standard deviation (s) |
|---|---|---|
| OPF (hourly) | 0.5045 | 0.0021 |
| MPC ($M = 40$ mins) | 1.8289 | 0.0035 |

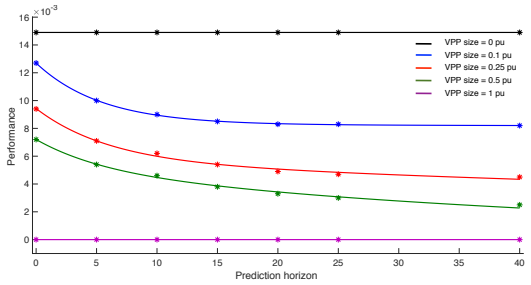


(a) role of prediction horizon on MPC performance

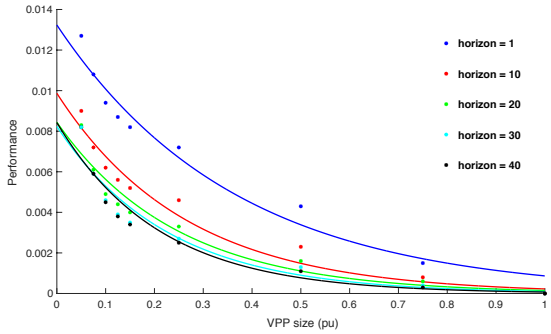


(b) role of the VESS capacity on the MPC performance

Figure 4.6: Investigating the role of MPC prediction horizon and VESS capacity on reference-tracking MPC performance. Note that benefit of prediction horizon and VESS capacity diminish signicantly after 20 minutes and expected VESS capacity of 0.5 p.u., respectively. All trend lines are fitted with an exponentially curve.

### 4.4.2 Uncertain VESS capacity

In this part, we assumed that the expected capacity of VESS is given and the probability distribution of the uncertainty is known. The actual capacity of VESS at each time step is computed as

$$\overline{S}_{\text{act}} = (1 + \zeta/10)\overline{S}_{\text{expected}}, \tag{4.14}$$

where $\zeta$ is normally distributed (i.e $\zeta \sim \mathcal{N}(0, 1)$).

To investigate the role of uncertain capacity of VESS in tracking performance of MPC, a simple forecast of net-load that stays constant over the next 24 hours is created. Actual net-load is created by injecting 20 percent step down and 10 percent step up error while each error persists for 10 minutes, as shown in Fig 4.7. A comparison of the tracking performance of deterministic and robust

approaches, at $\alpha = 0.9$, is provided in Fig. 4.8.

The first plot shows one realization of actual capacity of VESS, $\overline{S}$ (dashed blue line) and state evolution of SOC of VESS under the deterministic and robust approaches. The second plot shows optimal schedule for charging/discharging VESS under the deterministic and robust approaches. And the third plot shows tracking performance of the system under different scenarios. As illustrated, under deterministic approach, DCS occurs twice (i.e. before and after $t = 30$ in the first plot) which cause unscheduled adjustment in generator power (red dashed line in the third plot). Although by using robust approach part of the offered flexibility is dismissed, chance of DCS reduces which leads to less generators adjustment.

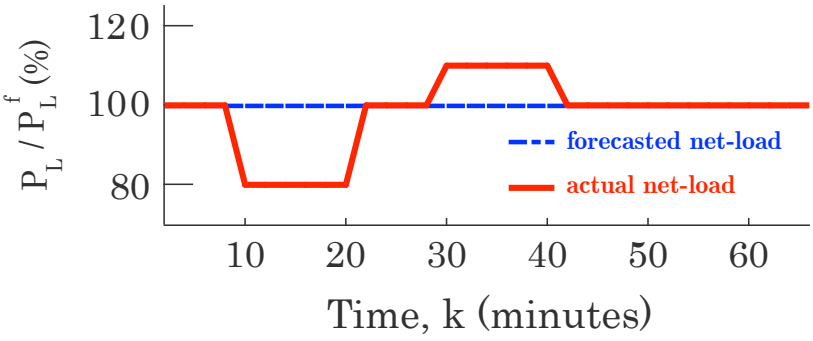


Figure 4.7: The actual net-load is created by injecting 10 minutes long, step down and step up error to the forecasted net-load.

To evaluate the tracking performance of deterministic and robust approaches under stochastic behavior of VESS capacity, $100,000$ repeated trials are performed. Each trial differs in expected capacity of VESS (0.4 p.u. and 0.8 p.u.) and $\alpha$ (from 0 to 2). Objective functions of robust approach $J_R^*$ and deterministic approach $J_D^*$ are used as a metric for the tracking performance. Smaller objective means less average deviation from scheduled set-points and indicates better tacking. Figure 4.9 shows $J_R^*$,$J_D^*$ and their ratio, at $\alpha = 0.9$, where capacity of VESS is 0.8 p.u. for 2000 trials. The results of deterministic and robust approaches where capacity of VESS equals 0.4 p.u. and 0.8 p.u., at $\alpha = 0.9$, is shown in Table 4.2.

Figure 4.10 compares the average tracking performance under deterministic and robust approach for different values of $\alpha$ (i.e. level of robustness). By choosing a small $\alpha$ (conservative choice), DCS

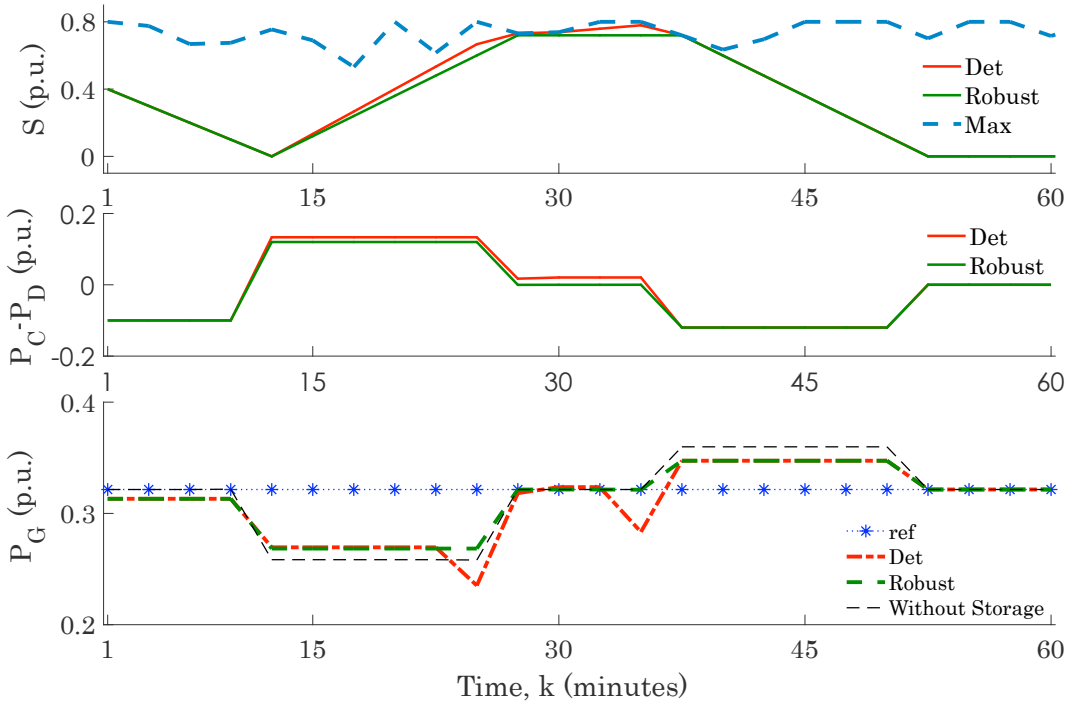


Figure 4.8: The tracking performance of system under three different scenarios: no VESS, deterministic approach and robust approach.

Table 4.2: Comparing the average of $J_D^*$,$J_R^*$ and their ratio as a metric of performance based on 2000 trials

| $\mathrm{E}(\overline{S})$ | $\widetilde{J_D^*}$ | $\widetilde{J_R^*}$ | $\widetilde{J_D^*/J_R^*}$ | $J_D^* > J_R^*$ |
|---|---|---|---|---|
| 0.4 p.u. | 0.1390 | 0.1336 | 1.0402 | 83% |
| 0.8 p.u. | 0.0848 | 0.0756 | 1.1227 | 74.5% |

occurs less frequently, however, larger part of flexible resources are not utilized. By choosing large $\alpha$, the controller benefits from the full flexibility offered by resource. However, by discounting the role of uncertainty, DCS occurs more frequently and consequently generators rescheduling is needed more often. In both of these cases, the deterministic approach outperforms the robust one (i.e. $J_D^* < J_R^*$ ). If $\alpha$ is chosen appropriately, the flexibility offered by the VESSs can be used effectively while limiting occurrence of DCS. In other words, sacrificing some robustness in dispatching the uncertain resource leads to improved tracking performance. It is interesting to note that in the scenario-based approach with typical selection of $\epsilon = 0.1$ and $\beta = 0.05$, 64 realizations are needed based on (4.11)

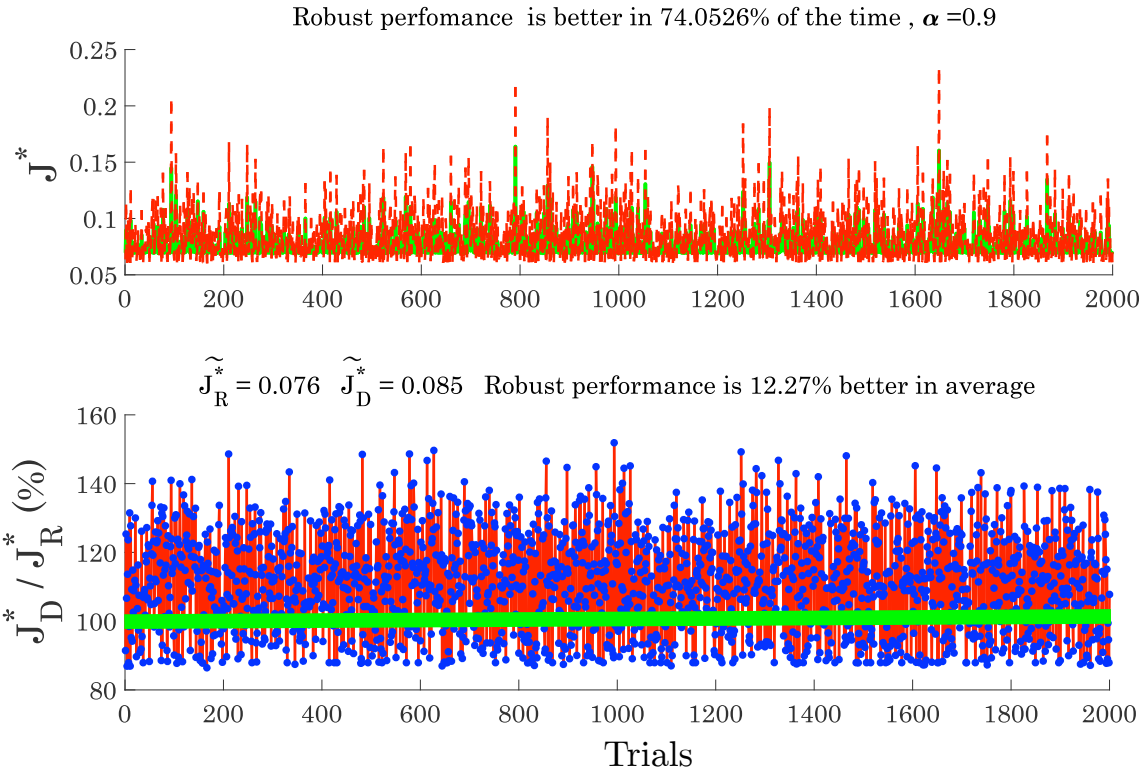


Figure 4.9: The first plot compares $J_D^*$ and $J_R^*$ for 2000 trials (VESS capacity = 0.8 pu) and the second plot illustrates their ratio. Any points above the green line indicates better performance of the robust approach. The robust approach outperformed the deterministic approach on 1480 of the 2000 trials and on average, it is 12% better.

and we would get an equivalent $\alpha = 0.75$, for which the deterministic (average) approach actually outperforms the robust approach (i.e., it is overly conservative). However, equivalent violation probability of $\alpha = 0.85$ in which the robust approach (on average) outperforms the deterministic one by 4.5% is a non-intuitive $\epsilon = 0.6$.

To explore the performance of the robust approach for a more general net-load scenarios, a mean reverting random walk (MRRW) noise is added to the actual load profile shown in Fig. 4.7, and 1000 realizations are created (Fig. 4.11). Table 4.3 provides result of the tracking performance of robust and deterministic approaches regarding the 1000 trials. To better understand the effect of DCS on performance of the controller, the total number of times that DCS occurs $N^{\text{DCS}}$ using each method is calculated. Note that each trial includes 60 time-steps (minutes) and 1000 trials are considered for

each scenario of capacity of VESS. Therefore, $N^{\mathrm{DCS}}$ is computed with respect to 60000 time-steps.

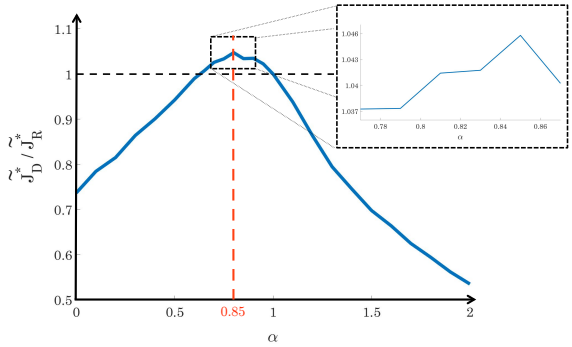


Figure 4.10: Trade-off between robustness and tracking performance (VESS capacity = 0.4 pu). Average ratio of $J_D^*$ and $J_R^*$ is used as a metric for performance of the system regarding to the different levels of the robustness. At $\alpha = 0.85$, on average the robust approach is 4.5% better than the deterministic one.

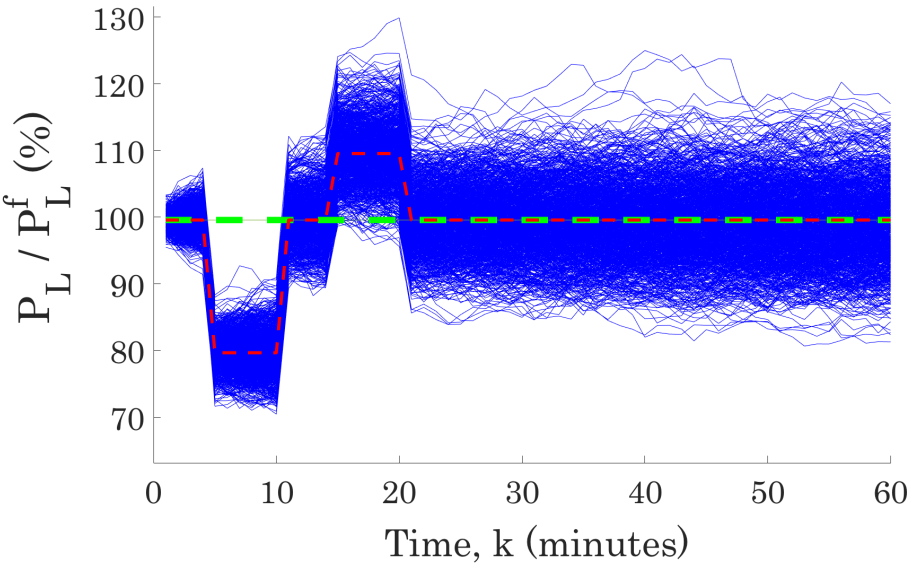


Figure 4.11: One thousands realization of load profiles are created based on the Fig. 4.7 while the green dashed line shows the forecasted load and the red line shows mean of all created load profiles.

Table 4.3: Comparing average performance of the system under deterministic and robust approach with 1000 trials

| $\mathrm{E}(\overline{S})$ | $\widetilde{J_D^*}$ | $\widetilde{J_R^*}$ | $\widetilde{J_D^*/J_R^*}$ | $J_D^* > J_R^*$ | $N_D^{\mathrm{DCS}}$ | $N_R^{\mathrm{DCS}}$ |
|---|---|---|---|---|---|---|
| 0.4 p.u. | 0.1536 | 0.1480 | 1.0376 | 83% | 2867 | 1769 |
| 0.8 p.u. | 0.0947 | 0.0884 | 1.0713 | 69% | 2089 | 1045 |

## 4.5 Conclusion and Future Work

This chapter studies the performance of a bilevel receding-horizon predictive optimal power flow problem for managing short-term variability with grid assets (VESSs) that are uncertain in their energy capacity. This gives rise to the notion of dynamic capacity saturation (DCS) for uncertain energy resources. The numerical studies indicate that there exists a sensitive trade-off between robustness of the optimized dispatch (i.e., severity of DCS) and closed-loop system performance (i.e., VESSs ability to provide regulating reserves). It is shown that sacrificing some robustness in the dispatch of the uncertain energy capacity can significantly improve system performance (up to 4-12%). Interestingly, the popular approach of robustifying chance-constraints with scenario-based sampling may lead to reduced closed-loop system performance. Future work will focus on analytically quantifying the effects of DCS on the closed-loop response and developing tools that optimally manages storage commitment under dynamic uncertainty (i.e., $\alpha$). Additionally, we plan to extend the current work to consider multi-VESSs with uncertain capacity under system constraints such as line flow limits, and address the question of where the VESSs should be placed and how many VESSs are advantageous for a given power network.

# 5 Chapter 5: Corrective dispatch of uncertain energy resources


## Abstract

High penetrations of intermittent renewable energy resources in the power system require large balancing reserves for reliable operations. Aggregated and coordinated loads can provide these fast reserves, but represent energy-constrained and uncertain reserves (in their energy state and capacity). To optimally dispatch uncertain, energy-constrained reserves, optimization-based techniques allow one to develop an appropriate trade-off between closed-loop performance and robustness of the dispatch. Therefore, this chapter investigates the uncertainty associated with energy-constrained aggregations of flexible distributed energy resources (DERs). The uncertainty studied herein is associated with estimating the state of charge and the capacity of an aggregation of DERs (i.e., a virtual energy storage system or VESS). To that effect, a risk-based chance constrained control strategy is developed that optimizes the operational risk of unexpectedly saturating the VESS against deviating generators from their scheduled set-point. The controller coordinates energy-constrained VESSs to minimize unscheduled participation of and overcome ramp-rate limited generators for balancing variability from renewable generation, while taking into account grid conditions. To illustrate the effectiveness of the proposed method, simulation-based analysis is carried out on an augmented IEEE RTS-96 network with uncertain energy resources.


## 5.1 Introduction

The rest of this chapter is organized as follow. In Section 5.2, we summarize the proposed control framework and discuss the role and interactions of the OPF problem within a reference-tracking predictive controller. Section 5.3 details the system models while Section 5.4 describes the nature and management of uncertainty in a chance-constrained formulation. Via a simulation-based case-study on the IEEE RTS 96 test system augmented with black VSSEs. In Section 5.5 the risk-based approach is introduced. Section 5.6 illustrates the analytical results and compares the proposed method against deterministic and robust approaches. Section 5.7 summarizes the key results and

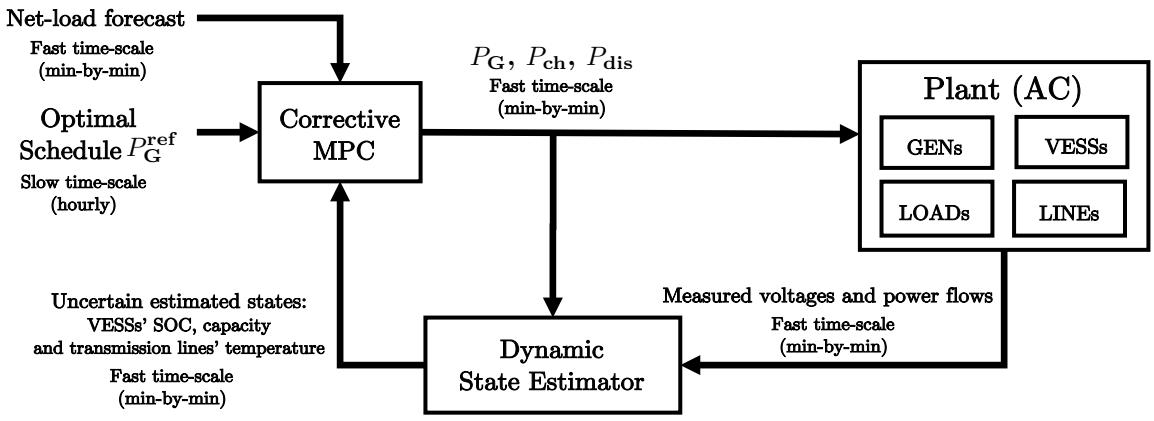


Figure 5.1: Overview of control scheme showing controller including economic dispatch (slow) and corrective MPC (fast) part and how each part is related to the power grid.

describes future work directions.

The rest of this chapter is organized as follow. In Section 5.2, we summarize the proposed control framework and discuss the role and interactions of the OPF problem within a reference-tracking predictive controller. Section 5.3 details the system models while Section 5.4 describes the nature and management of uncertainty in a chance-constrained formulation. Via a simulation-based case-study on the IEEE RTS 96 test system augmented with black VSSEs, Section 5.5 illustrates the analytical results and compares the proposed method against deterministic and standard robust approaches. Section 5.6 summarizes the key results and describes future work directions.

## 5.2 System Operation and Control

Based on updated forecasts of demand and renewable generation, economic dispatch computes a secure and economically optimal schedule for the available generators. However, the uncertainty inherent to solar PV and wind forecasts, as well as uncertainty in electrical demand, results in power imbalances that make previously computed set-points sub-optimal. Rescheduling the generators frequently and significantly accumulates cycling costs and economic penalties to the system operator [75, 94]. With responsive VESS resources and temperature-based ratings, corrective power system operations that leverage feedback represents a valuable and inherently robust and dynamic alternative to conventional spinning reserve. Corrective control refers to the coordination of re-

sponsive grid resources immediately *after* a disturbance occurs to drive the system back from an economically sub-optimal or stressed system state to an economically optimal normal operating state [46]. An overview of the proposed uncertainty-aware control strategy is provided in in Fig. 5.1.

While the focus of this chapter is on the corrective part of the controller, the details of the standard ED can be found in [87] and are beyond the scope of this chapter. Thus, the output of the market layer ($P_{\mathrm{G}}^{\mathrm{ref}}$ in Fig. 5.1) satisfies techno-economic objectives such as cost and security. Since the proposed corrective controller's time-step $T_s$ ($\approx$ 1 minute) is much shorter than the updated of the market-based reference signals coming from ED ($\approx 15 - 60$ minutes), linear interpolation is employed to form the reference trajectory.

In the faster control layer, the VESSs represent aggregated DERs and provide flexibility in the form of synthetic balancing reserves. Therefore, based on the dynamic states (i.e., power and energy states of VESSs, power states of generators and thermal states of the transmission lines) and forecasts of the system and available resources, the trajectory-tracking MPC produces a corrective dispatch every minute to respond to forecast errors and other disturbances. The MPC minimizes the deviation of generators and flexible loads from the economic reference trajectory while satisfying physical and operational grid constraints.

## 5.3 Corrective Controller Model Overview

The timescale of the corrective MPC ($\approx$ 1 minute) is much faster than ED ($\approx 15 - 60$ minutes). Thus, linear interpolation is employed between reference trajectory value computed by ED. The corrective MPC scheme can be summarized by the following process:

1. At time $k$, with estimates of initial state of the charge (SOC), line temperatures, generators' operating point, updated net-load forecasts and updated generator trajectory from SC-OPF, the MPC solves a finite-horizon open-loop optimal control problem, over interval $[k,\, k+M]$. This produces a schedule of control actions that describe charging (discharging) rates for VESS and re-dispatch signals for generators.

2. Apply only the control actions corresponding to time $k$

3. Measure/estimate the system's dynamic states based on the realized demand and renewable

generation at time $k+1$.

4. Go to 1)

The open-loop MPC optimization problem is defined below for a power system network $\mathcal{E} = (\mathcal{N}, \mathcal{L})$ with bus $i \in \mathcal{N}$ and line $ij \in \mathcal{L}$. The sets $\mathcal{G}$ and $\mathcal{V}$ represent conventional generators and VESSs, respectively. The objective function seeks to minimize the deviation of generator outputs from the scheduled set-points while penalizing line temperature overloads as follows:

$$\min_{P_{\mathrm{G}},\, P_{\mathrm{ch}},\, P_{\mathrm{dis}}} \quad \sum_{l=k}^{k+M} \left( \sum_{\forall i \in N_{\mathrm{g}}} c_{\mathrm{G},i} \left( P_{\mathrm{G},i}[l] - P_{\mathrm{G},i}^{\mathrm{ref}}[l] \right)^2 + \sum_{\forall ij \in \mathcal{E}} c_{\mathrm{T},ij} \Delta \hat{\mathrm{T}}_{ij}{}^2 \right) \tag{5.1a}$$

s.t.

**Power balance:** $\forall i \in \mathcal{N}$,

$$\sum_{n \in \Omega_i^G} P_{\mathrm{G},n}[l] = \sum_{n \in \Omega_i^L} P_{\mathrm{L},n}[l] + \sum_{n \in \Omega_i^B} P_{\mathrm{ch},n}[l] - P_{\mathrm{dis},n}[l] + \sum_{j \in \Omega_i^N} p_{ij}[l], \tag{5.1b}$$

**Conventional generators:** $\forall i \in \mathcal{G}$,

$$\underline{P_{\mathrm{G}_i}} \leq P_{\mathrm{G},i}[l] \leq \overline{P_{\mathrm{G},i}}, \tag{5.1c}$$

$$-T_s R_{\mathrm{G},i} \leq P_{\mathrm{G},i}[l+1] - P_{\mathrm{G},i}[l] \leq T_s R_{\mathrm{G},i}, \tag{5.1d}$$

**Temperature-based line rating:** $\forall ij \in \mathcal{L}$,

$$p_{ij}^{\mathrm{loss}}[l] = R_{ij} \left( b_{ij} \left( \theta_i[l] - \theta_j[l] \right) \right)^2, \tag{5.1e}$$

$$\Delta p_{ij}^{\mathrm{loss}}[l] = p_{ij}^{\mathrm{loss}}[l] - p_{ij,*}^{\mathrm{loss}}, \tag{5.1f}$$

$$\Delta T_{ij}[l+1] = \tau_{ij} \Delta T_{ij}[l] + \rho_{ij} \Delta p_{ij}^{\mathrm{loss}}[l], \tag{5.1g}$$

$$\Delta \hat{T}_{ij}[l] = \max(0, \Delta T_{ij}) \qquad , \tag{5.1h}$$

**VESSs:** $\forall i \in \mathcal{V}$,

$$0 \leq P_{\mathrm{ch},i}[l] \leq \overline{P_{\mathrm{ch},i}}, \tag{5.1i}$$

$$0 \leq P_{\mathrm{dis},i}[l] \leq \overline{P_{\mathrm{dis},i}}, \tag{5.1j}$$

$$-T_s R_{\mathrm{ch},i} \leq P_{\mathrm{ch},i}[l+1] - P_{\mathrm{ch},i}[l] \leq T_s R_{\mathrm{ch},i}, \tag{5.1k}$$

$$-T_s R_{\mathrm{dis},i} \leq P_{\mathrm{dis},i}[l+1] - P_{\mathrm{dis},i}[l] \leq T_s R_{\mathrm{dis},i}, \tag{5.1l}$$

$$\underline{S_i} \leq S_i[l+1] = S_i[l] + T_s \left( \eta_{\mathrm{ch},i} P_{\mathrm{ch},i}[l] - \frac{1}{\eta_{\mathrm{dis},i}} P_{\mathrm{dis},i}[l] \right) \leq \overline{S_i}, \tag{5.1m}$$

$$S_i[k] = S_{i,k}^{\mathrm{est}} \tag{5.1n}$$

where $\Omega_i^G$, $\Omega_i^L$, $\Omega_i^B$ and $\Omega_i^N$ represent set of generators, demands, energy storage devices (VESSs), and neighboring nodes connected to node $i$, respectively. Constraints (5.1b) to (5.1n) must be satisfied for $\forall l \in [k,\ k+M-1]$ where the four groups of constraints in the MPC formulation are described below. Next, we discuss each type of constraints.

### 5.3.1 Power balance in (5.1b)

Based on Kirchhoff's laws, the net power flow into any node must equal the net power flow out. Generators may inject power, $P_G$ and loads may consume power $P_L$ at each node $i$. If VESSs are available at a node, then positive (negative), $P_{\text{ch}} - P_{\text{dis}}$, corresponds to additional consumption (generation).

### 5.3.2 Conventional generators in (5.1c) to (5.1d):

Each conventional generator is described by its production state, $P_{\text{G}}$, which must be within generator limits, as shown in (5.1c). Furthermore, due to the thermal nature of the generators, the ramp rate of generators are limited to their ramp-rate limit, $R_G$, as shown in (5.1d). VESSs are particularly helpful to overcome limitations imposed by the ramp-rate limits.

### 5.3.3 Transmission lines in (5.1e) to (5.1h)

The temperature-based line ratings provide a mechanism through which the uncertain power injections from renewable generation can be absorbed and directed via MPC's feedback and the optimized VESSs dispatch. The heat gain of transmission line $(i, j)$ is a function of ohmic losses (i.e. $I_{ij}^2 r_{ij}$). Thus, it is necessary to include line losses in the power flow model. Since all values are per-unit (p.u.), and the voltage magnitudes of all buses are close to 1 p.u., the magnitudes of the current and power flows on the respective lines are approximately equal (i.e., $|I| \approx |S|$ ). Therefore, line losses can be effectively approximated in proportion to the square of the power flow [46, 95].

In general, the AC power flow between bus $i$ and $j$, $p_{ij}$, is the solution to a set of nonlinear, algebraic equations. To ensure a tractable approach at the timescale of interest, a suitable convex relaxation of the AC power flow equation has been adopted from [83]. Since the MPC executes on a fast timescale relative to the VESSs and line temperature time constant and the linearized model is updated via feedback for estimating line losses, temperatures, and VESS states, the model is accurate for control.

IEEE Standard 738 [47] defines the current-temperature relationship of bare overhead conductors and has been employed herein to calculate the conductor temperature. To allow for a tractable

implementation of MPC scheme, temperature dynamics of transmission lines are linearized around the equilibrium point $T^* = T^{\text{lim}}$, where $T^{\text{lim}}$ is computed from steady-state conditions with line current at ampacity (i.e., set $p_{ij}^{\text{loss}^*} = (I^{\text{lim}})^2 r_{ij}$, where $r_{ij}$ is the per-unit resistance of line $ij$). The linearized temperature dynamics of the transmission lines are given by (5.1g).

Since line losses are approximated in proportion to the square of the power flow (5.1e), its respective constraint is non-convex in $\theta_{ij}$. Therefore, a convex relaxation is employed (i.e., $p_{ij}^{\text{loss}} \geq R_{ij} b_{ij}^2 (\theta_i - \theta_j)^2$) that is provably binding at optimality for lines that are overloaded since $\Delta \hat{T}_{ij}$ is in the objective function that is similar to [46]. This achieves the desired measure of control over the line flows.

The MPC scheme computes control actions that drive line temperatures below limits, and as long as they are below limits, there is no benefit in further reducing line temperatures. The following set of constraint achieve this purpose as shown by (5.1h). This non-convex constraint can be relaxed with the equivalent linear formulation $0 \leq \Delta \hat{T}_{ij}$ and $\Delta T_{ij} \leq \Delta \hat{T}_{ij}$.

### 5.3.4 Virtual energy storage system in (5.1i) to (5.1n)

In this chapter, responsive VESSs, which are available throughout the network, have a baseline consumption (i.e., aggregated baseline consumption of individual flexible loads in a VESS), and are allocated as balancing reserves (e.g., via [81]). Note also that the models used in this work are agnostic to the specifics of the coordination scheme. By shifting the VESS's controllable load in time, the VESS can respond to the mismatches caused by forecast errors. Any decrease (increase) in the consumption of the VESS relative to the baseline can be translated as discharging (charging) the VESS. Each VESS is described by an estimated SOC and the amount of power it provides to (consumes from) the grid. At time $k$, the initial SOC of a VESS is given by a dynamic state estimator (5.1n) and the SOC of a VESS over the prediction horizon is defined by the discrete integrator dynamics as shown in (5.1m) . Non-negative scalar $P_{\text{ch}}$ ($P_{\text{dis}}$) represents charging (discharging) power of a VESS and the charging (discharging) efficiency is denoted by $\eta_{\text{ch}}$ ($\eta_{\text{dis}}$).

Charging (discharging) power and SOC of the VESSs are subject to constraints (5.1i), (5.1j) and (5.1m) where $\overline{P_{\text{ch}}}$ ($\overline{P_{\text{dis}}}$) and $\overline{S}$ ($\underline{S}$), respectively, represent maximum charging (discharging) power and the maximum (minimum) energy capacity of VESS.

Since VESSs represent the aggregate effects of coordinated DERs, they inherit the characteristic timescales of the coordination schemes that underpin them. That is, in general, coordination schemes do not offer instant control over all DERs in a fleet, but are subject to separate internal control, actuation, and communication loops [96, 97]. These cyber-physical control considerations generalize themselves as ramp-rate limits on the charging ($R_{\text{ch}}$) and discharging ($R_{\text{dis}}$) of VESSs as shown in (5.1k) and (5.1l). At high levels of renewable penetration, since the VESS's are responsive, they represent a valuable resource to overcome demand-supply imbalances. However, unlike a conventional generator, the VESS's energy-constrained characteristics necessitate careful management of its state of charge.

**Remark 5.1 (Simultaneous charging/discharging)** For most physical ESSs, simultaneous charging and discharging is not physically realizable. To model this phenomenon generally requires complementary constraints (i.e., $P_{\text{ch},i}[l]P_{\text{dis},i}[l] = 0$) which are non-linear and makes the problem non-convex [83, 90]. However, Since a VESS coordinates large populations of flexible loads (via an underlying control scheme), a VESS can indeed realize simultaneous charging and discharging commands across the population [97]. Thus, it is reasonable to assume, in this work, that it is just the net charging commands that determine a VESS's energy evolution. Furthermore, unlike grid-tied batteries, the amount of flexibility available to the system operator is time-varying and uncertain.

That is, the flexibility available to the system operator from a VESS can be translated into upper and lower bounds on the VESS's energy state. These upper and lower bounds are functions of different stochastic quantities, such as human behavior and weather. To capture these considerations, VESSs herein are formulated probabilistically and are modeled with chance constraints.

## 5.4 Uncertainty management

Individual flexible loads are subject to device-specific background effects (such as hot water usage or EV driving patterns), however, a VESS represents a macro-level object. These time-varying and stochastic background processes realize themselves as uncertainty in the VESS's energy bounds and states. For example, the upper energy capacity limit of the VESS is uncertain and must be estimated and predicted from a separate model. Considering the central limit theorem, the flexibility

offered by each device is uncertain and represents an independent random variable (i.e., background usage of each device is independent). Therefore, a VESS's energy capacity can be approximated as a normally distributed random variable centered on the true mean (i.e., $\overline{S}_{\text{est}} \sim \mathcal{N}(\overline{S}_{\text{act}}, \sigma_c^2)$). Moreover, in contrast with the grid-scale batteries, the actual SOC of the VESSs can not be measured directly and a dynamic state estimation method (e.g. an Extended Kalman Filter [98]) should be employed to estimate the SOC of a VESS at each time step. State estimation of a VESS's SOC is subject to uncertainty inherent in any state estimation method. In addition, due to the nature of Kalman filters, the noise process can be assumed normally distributed and centered on the true mean (i.e., $S_k^{\text{est}} \sim \mathcal{N}(S_k^{\text{act}}, \sigma_s^2)$ ). An illustration of the uncertain estimation of a VESS's energy capacity and SOC is illustrated in Fig. 5.2.

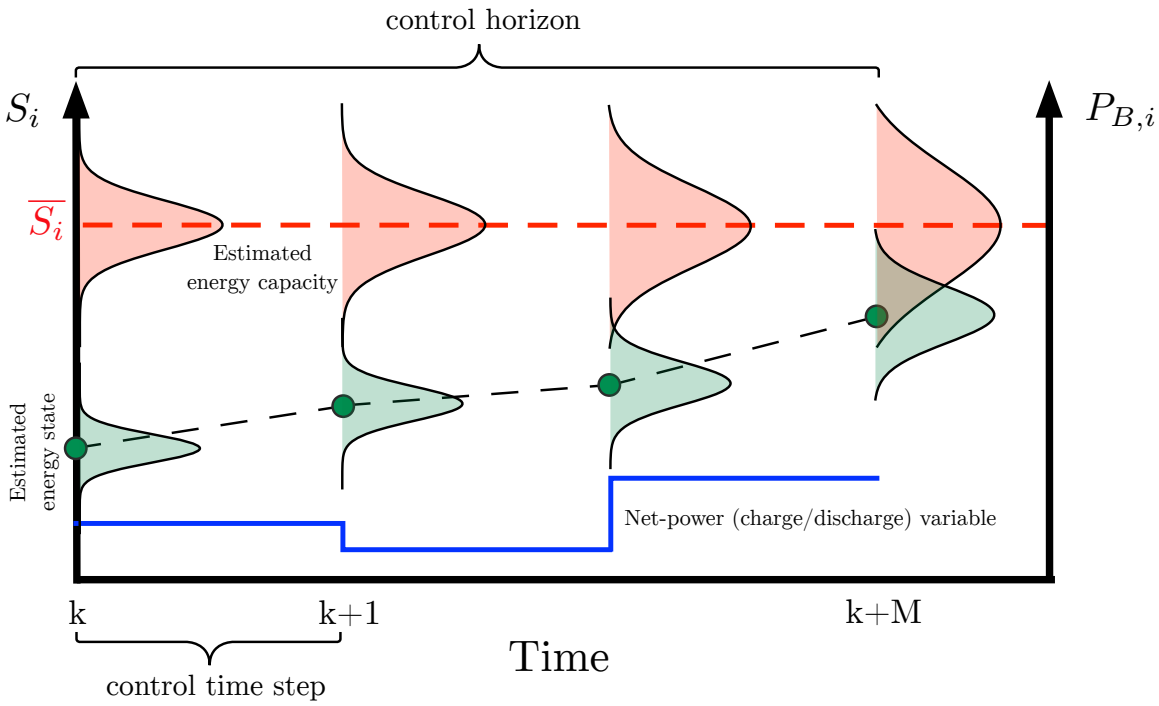


Figure 5.2: Uncertainty in estimation of VESSs energy capacity (Red) and initial SOC (Green). The variance of uncertainties grow over time as the distance from current time step increases.

**Definition 5.2 (Dynamic capacity saturation (DCS))** Charging and discharging commands of the uncertain VESSs can be optimized based on a mean (or average) energy capacity estimate alone (i.e., only consider the first moment and ignore higher-order moments), which is known as a

deterministic optimization problem. However, the underlying, uncertain VESS energy capacity may realize itself unexpectedly and saturate in the energy state, which zeros out the charging rate of the optimized control (power) action. We call this saturation phenomenon dynamic capacity saturation (DCS) [99]. DCS may lead to unexpected power imbalances in the power system. To regulate these unexpected DCS-induced power imbalances, grid operators must rely on (expensive) generation to supply the difference based on their participation factor $d_i$, as shown below:

$$\Delta P_{Gi}[k+1] = -d_i \sum_{i \in N_b} \max \left\{ \frac{S_i[l+1] - \overline{S_i}}{T_s}, 0 \right\}. \tag{5.2}$$

### 5.4.1 Chance constrained formulation

Chance constrained optimization is employed to reduce the risk of DCS and to solve an optimization problem with uncertain parameters. The chance constraints should be satisfied with a predefined probability level $1 - \epsilon$, where $\epsilon \in (0, 1)$ is the acceptable-worst-case violation level. Reducing risk increases system reliability and operational cost, which implies a clear trade-off. Within the context of pay-for-performance ancillary services, the operational costs are defined herein by the generators' reference-tracking errors [100].

Chance constrained optimization problems can be solved with a probabilistically robust scheme, inspired by the so-called scenario approach. In the scenario approach, the chance constraint is substituted with a finite but large number of deterministic constraints corresponding to different realizations of the underlying uncertainty space [101]. By employing an adequate number of scenarios from this set (i.e. $N >> 1$), the approach is able to provide a-priori guarantees of satisfying the chance constraint.The scenario-based approach is useful in offline planning studies when the uncertainty is complex and captured via historical data sets, as it makes no assumption on the underlying distribution of the uncertainty. However, the number of scenarios required is a function of $\epsilon$ and the number of uncertain parameters can grow very large. If the underlying problem is convex, there exists techniques to reduce the number of scenarios and mitigate computation costs by reformulating the problem into a robust optimization problem [78].

Indeed, if an accurate analytical model of the uncertainty distribution is known, the method

*analytical reformulation* can be employed to transform the chance constraint into a robust, deterministic constraint [102, 103]. In contrast to the scenario approach, the analytical reformulation does not require sampling complex distributions or large data-set. This means that only a single reformulation for each chance constraint is needed, which makes implementation tractable at the timescale of interest [104]. Due to the aggregation of many stochastic background processes it is reasonable to assume that the estimation error are normally distributed random variables and the chance constraint can be reformulated analytically.

Next, we introduce the chance constraints related to the uncertain variables of the VESS (i.e., energy capacity and SOC) and briefly describe the analytical reformulation to derive a convex program. The formulation is presented with respect to the upper energy capacity limit of the VESS, but the lower limit can be handled in a similar manner. Note also that while much of the literature of analytical reformulation, the work herein focuses on uncertain energy states rather than power.

### 5.4.2 Analytical reformulation of chance constrained problem

Recall, the evolution of the SOC of the $i^{\text{th}}$ VESS over the prediction horizon (i.e., $l \in [1, M]$), is related to the estimated SOC of the $i^{th}$ VESS at time $k$ (i.e., $S^{\text{est}}_{k,i}$) and charging (discharging) control actions as follows

$$S_i[l] = S_{k,i} + \sum_{m=1}^{l} \Delta S_i[m] \tag{5.3}$$

where $\Delta S_i[l] = T_s(\eta_{\text{ch},i} P_{\text{ch},i}[l] - \eta^{-1}_{\text{dis},i} P_{\text{dis},i}[l])$.

The estimated SOC of VESS is assumed to be a normally distributed random variable centered on the true mean (i.e., $S^{\text{est}}_{k,i} = S^{\text{act}}_{k,i} + \xi_{s,i}$), where the SOC estimation error is denoted by $\xi_s \in R^{N_B}$, with $\mu_s \in R^{N_B}$ as its mean, $\delta_s \in R^{N_B}$ as its standard deviation and $\Sigma_s \in R^{N_B \times N_B}$ as its covariance matrix.

Any VESS technology that does not directly measure each DER's energy state regularly requires a dynamic state estimator that is specific to the model and information exchanges that underpin a specific VESS. However, this work makes no assumption on specific state estimation methods. It is only assumed that the state estimation methods are uncertain and errors are normally distributed

and managing this uncertainty is desirable.

In addition, due to the i.i.d. nature of DERs' end usage, estimation of the energy capacity of the $i^{\text{th}}$ VESSs can be modeled as a normally distributed random variable around its true mean (i.e., $\overline{S}_{\text{est},i} = \overline{S}_{\text{act},i} + \xi_{c,i}$), where $\xi_c \in R^{N_B}$ denotes the VESSs' capacity estimation error, with $\mu_c \in R^{N_B}$ as its mean, $\delta_c \in R^{N_B}$ the standard deviation and $\Sigma_c \in R^{N_B \times N_B}$ the covariance matrix.

Then, for $\forall i = 1, \ldots, \mathrm{N_B}$ the following constraints are equivalent:

$$P\left(S_{k,i}^{\text{act}} + \sum_{m=1}^{l} \Delta S_i[m] - \overline{S}_{\text{act},i} \leq 0\right) \geq 1 - \epsilon \tag{5.4}$$

$$P\left(S_{k,i}^{\text{est}} - \xi_{s,i} + \sum_{m=1}^{l} \Delta S_i[m] - \overline{S}_{\text{est},i} + \xi_{c,i} \leq 0\right) \geq 1 - \epsilon \tag{5.5}$$

$$S_k^{\text{est}} + \sum_{m=1}^{l} \Delta S_i[m] \leq \overline{S}_{\text{est},i} - \alpha_c \sqrt{\delta_{s,i}^2 + \delta_{c,i}^2 + \rho_{cs,i}\delta_{c,i}\delta_{s,i}} \tag{5.6}$$

where $\alpha_c := \Phi^{-1}(1-\epsilon)$ and $\Phi^{-1}$ denotes the inverse cumulative distribution function (cdf) of the standard normal distribution and $\rho_{cs}$ is the correlation coefficient of capacity and initial SOC estimation error. Considering uncertainty introduces an ***uncertainty margin*** which is the amount that the constraint should be tightened in order to secure the system against the prescribed, uncertainty . Thus, the risk associated with each source of uncertainty is captured in a computationally tractable framework via the covariances of the estimation errors, $\delta_{s,i}$ and $\delta_{c,i}$. It is now intuitive to understand the role of uncertainty on the conservativeness of the VESS dispatch.

**Remark 5.3** A VESS's initial SOC and capacity are estimated with an independent state estimator dedicated to that specific VESS. Therefore, even with correlated estimation errors in capacity or correlated estimation errors in initial SOC estimation, dynamic of each VESS only depends on that VESS's capacity and initial SOC estimation.

## 5.5 Risk-based Approach

For a given chance constraint $P(f(x,\xi) \leq b) \geq 1 - \epsilon$, where $x$ and $\xi$ are decision and uncertain variables, the magnitude of constraint violation is a function of $\xi$ and is given by $y(\xi) = f(x,\xi) - b$. Negative $y$ indicates constraint satisfaction while positive $y$ implies constraint violation. The

standard chance constraint limits the probability of violation ($y > 0$) to a predefined risk limit, $\epsilon$. Since chance-constrained approaches ignore the severity of the constraint violation, the approaches are generally conservative and a closed-loop chance constrained MPC (CC-MPC) implementation may lead to reduced performance of the system (by reducing the available flexibility). Authors in [105, 106], consider the severity of a constraint violation, by weighting the probability of the constraint violation by magnitude of the constraint violation.

In applying chance constraints, there is a clear trade-off between high reliability (i.e., conservative uncertainty margin for VESSs) and low nominal cost (i.e., use as much VESS as possible), which depends on how risk limits are chosen. Risk limits are generally chosen as a predefined parameters (e.g. $\epsilon \in (0.90 \quad 0.99)$) based on the importance of the constraint.

Unlike the robust approach that limits the SOC of VESSs to a predefined robust limit $\overline{S}_{\text{rob}}$, we propose a novel risk-based approach that allows the solution to exceed the robust limit at each point in time. This is possible by introducing the operating risk, $\mathcal{R}$, which is a new decision variable. Thus, performance and risks can be co-optimized, which leads to the following multi-objective optimization problem:

$$\min_{P_G, P_{\text{ch}}, P_{\text{dis}}, \mathcal{R}} \quad \sum_{l=k}^{k+M} J_1[l] + J_2[l] \tag{5.7a}$$

s.t.

(5.1b) to (5.1n),

$$\mathcal{R}_i[l] = \max(0, S_i[l] - \overline{S}_{\text{rob},i}), \tag{5.7b}$$

$$\mathcal{R}_i[l] \leq \overline{\mathcal{R}_i}, \tag{5.7c}$$

$$\overline{\mathcal{R}_i} = \overline{S}_{\text{est},i} - \overline{S}_{\text{rob},i} \tag{5.7d}$$

where

$$J_1[l] := \sum_{\forall i \in N_g} c_{G,i}(P_{G,i}[l] - P^{\text{ref}}_{G,i}[l])^2 + \sum_{\forall ij \in \mathcal{E}} c_{T,ij}(\Delta \hat{T}_{ij}[l])^2$$

and

$$J_2[l] := \sum_{\forall i \in N_B} c_{\mathcal{R},i}(\mathcal{R}_i[l])^2$$

The robust limit can be computed by analytical reformulation or scenario based approach or determined by using expert knowledge. As the risk-based MPC receives updated estimates at each time step, the cost of risk, $c_{\mathcal{R}}$, can be designed such that it penalizes risk early in the horizon and lowers the penalty later in the horizon. Larger $c_{\mathcal{R}}$ indicates higher cost and higher security and it is necessary to reach a good balance between risk of violation and nominal cost. To relate the value of improving tracking performance and the associated increase in operational risk, an efficient frontier for the tracking performance versus operational risk was computed by applying the weighting method in [107].

The MPC seeks to drive the SOC of VESSs below the robust limit, and once below the robust limit, there is no risk-induced incentive to lower SOC further as shown in (5.7b). This constraint can be relaxed to the linear formulation equivalent of $0 \leq \mathcal{R}_i[l]$ and $S_i[l] - \overline{S}_{\text{rob},i} \leq \mathcal{R}_i[l]$. Figure 5.3 illustrates an example of the SOC of the VESS with respect to the estimated capacity of the VESS and its robust limit.

Thus, deterministic, robust, and risk-based methods can be summarized as follow

I. The deterministic method dispatches VESSs with respect to the estimated SOC and energy capacity of VESSs.

II. The robust method dispatches VESSs with respect to the robust limit calculated with analytic reformulation.

III. The risk-based chance constrained (RB-CC) method co-optimizes reference-tracking performance and operational risk of DCS. Note that by sweeping $c_{\mathcal{R}}$ from $0 \to \infty$, the performance of the controller changes from the deterministic approach to the standard robust approach.

Recall that unlike the existing literature on chance constrained optimization in power systems, this work considers the uncertainty of **time-coupled energy variables** on a fast time scale for corrective control.

## 5.6 Simulation and result

In this section, the proposed control scheme in Fig. 5.1 is demonstrated on an augmented version of the IEEE RTS-96 power system test case, which includes three interconnected systems. The system

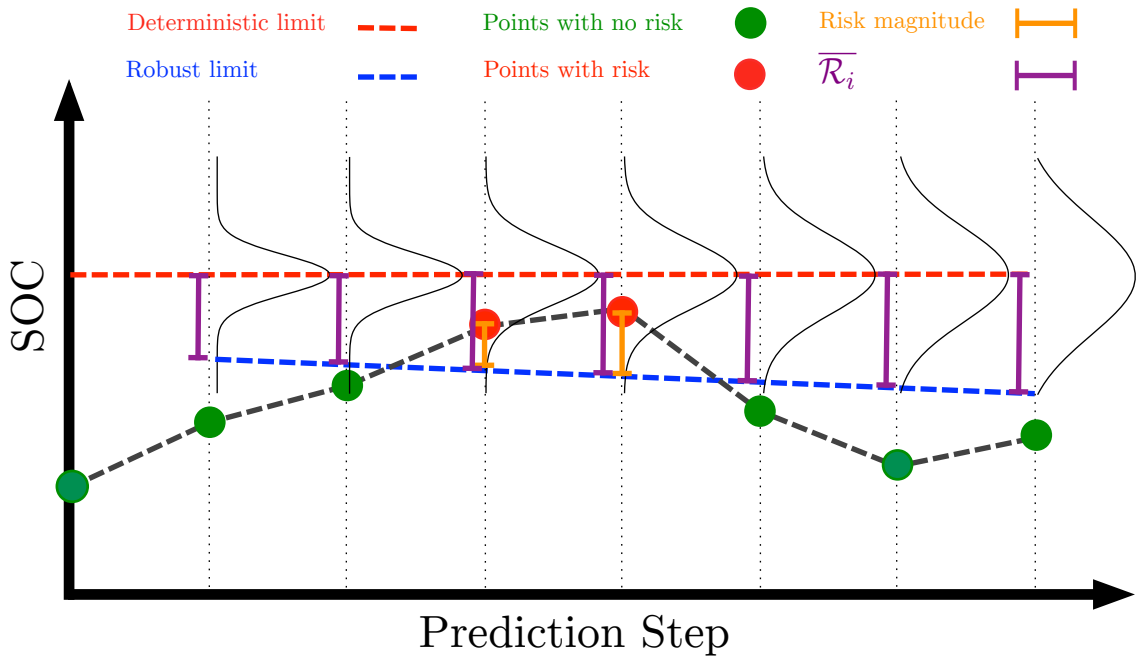


Figure 5.3: Illustrating the evolution of the SOC of a VESS with respect to the estimated capacity and robust bound and the corresponding risk imposed on the system performance.The variance of uncertainties grow over time as the distance from current time step increases. The green circles highlight the points with zero added risk. On the other hand, the red circles demonstrate when the VESSs' SOC is greater than the robust limit and takes on an increased, but weighted risk of DCS.

is fully described in [108]. All optimization problems are solved in MATLAB and AMPL using the solver GUROBI. MPC employs the simplified linear model to compute all optimal control actions. However, the actual plant model is the non-linear AC system, with line temperature computed based on the non-linear thermodynamic IEEE Standard 738 conductor temperature model to accurately capture the effects of implementing MPC. The aim of this case study is to demonstrate generator reference-tracking performance with uncertain VESSs while considering physical constraints of the power system. Since the IEEE RTS-96 system is designed as a highly reliable system with high thermal ratings for lines, to push the system towards its limit and induce more congested scenarios, nominal thermal ratings are reduced by 40%, bringing line temperature limits in the range of $60 - 70°C$. The network parameters are shown in Table 5.1.

Initially, the system is at steady-state (i.e., generators following exactly an economic trajectory and VESS resources being available for balancing reserves), but at time $t = 5$ mins, the system

Table 5.1: Three large VESSs Simulation Parameters

| Description | Value |
|---|---|
| Number of buses | 73 |
| Number of branches | 120 |
| Number of generators | 96 |
| Total load | 8550 MW |
| Number of VESSs | 3 |
| Total capacity of VESSs | 855 MWh |
| VESSS bus ID (location) | $11, 35, 59$ |
| VESS energy capacity | 285 MWh |
| VESS initial SOC | 50% |
| Maximum VESS power | 285 MW |
| VESSs ramp rate limit | 60 MW/min |
| Sampling time | 60 s |
| MPC prediction horizon | 20 mins |
| Avg. MPC solve time | 3.19 sec |

Table 5.2: VESS Uncertainty parameters

| Case | $\sigma_1$ (%) | $\sigma_2$ (%) |
|---|---|---|
| Low uncertainty | 2 | 3 |
| High uncertainty | 5 | 10 |

experiences a net-load disturbance (e.g., forecasted net-load) that requires VESS balancing reserves to provide 10% decrease in the net-load (i.e., 855 MW) to minimize unnecessary generators ramping. The disturbance last for 60 minutes, and therefore, VESSs are designed such that they can provide reserve for 60 minutes.To compare the performance of the proposed RB-CC method aginst deterministic and standard robust approaches, 200 trials (i.e., realizations) are performed ($N_T = 200$) for two different scenarios of uncertainty as shown in Table 5.2. Since the baseline consumption and consequently the capacity of VESSs are dependent on the same types of uncertain parameters, capacity estimation errors of VESSs are assumed to be correlated. The sum of squared error (SSE) of reference tracking of generators over the entire simulation time

$$J_{\text{Gen}} := \sum_{l=1}^{N} \sum_{i \in N_g} (P_{G,i}[l] - P_{G,i}^{\text{ref}}[l])^2 \tag{5.8}$$

is used as the tracking MPC performance metric.

Mean and standard deviation of SSE of reference tracking of generators, for deterministic, robust, and RB-CC approaches under the different scenarios of uncertainty are shown in Table5.3. The robust approach is used as a benchmark to evaluate the proficiency of the proposed RB-CC approach. Smaller SSE, implies better tracking performance. Poor performance of the deterministic approach is due to dispatching VESSs without considering the second-order moment of uncertainties which increase the risk of DCS. By applying the robust approach, chances of DCS is low, but since this method is conservative, the flexibility offered by VESSs are not fully utilized. However, under the proposed RB-CC, the controller uses the available flexibility while considering the uncertainty and exceeds the robust limit (i.e., accepting the risk) only when it is most valuable to do so.

Table 5.3: Comparing mean and standard deviation of tracking performance of the MPC (i.e., $J_{\text{Gen}}$) under deterministic, robust, and RB-CC approaches

| | Low uncertainty | | | High uncertainty | | |
|---|---|---|---|---|---|---|
| | $\mu$ | $\sigma$ | $\mu/\mu_{\text{Rob}}(\%)$ | $\mu$ | $\sigma$ | $\mu/\mu_{\text{Rob}}(\%)$ |
| Deterministic | 403.65 | 404.25 | 307.07 | 1118.90 | 1301.20 | 384.69 |
| Robust | 131.45 | 15.82 | 100 | 290.86 | 18.67 | 100 |
| RB-CC | 103.23 | 28.61 | 78.53 | 212.55 | 34.75 | 73.08 |

Note that for different duration of disturbances, as long as the capacity of VESSs are designed to provide reserve for the desired duration, same behaviour are observed.

Fig. 5.4 shows the cumulative squared error and evolution of the SOC of VESSs over simulation time for one trial (out of 200 trials). The robust approach dispatches VESSs considering the robust limit which results in higher tracking error at the beginning compare to the deterministic approach. However, as time goes on and the SOC of VESSs get closer to their limits, chance of DCS and consequently need to corrective actions increases which results in poor tracking performance of deterministic approach. Since the RB-CC approach considers the the risk-performance trade-off, it optimizes the risk of dispatching VESSs beyond their limits, while preventing DCS reaches the better tracking performance .

consider the the risk-performance trade-off

Histograms of the sum of the squared tracking error ($J_{\text{Gen}}$) of the deterministic, robust and RB-CC approaches are shown in Fig 5.5. Note that as expected, increasing the level of uncertainty

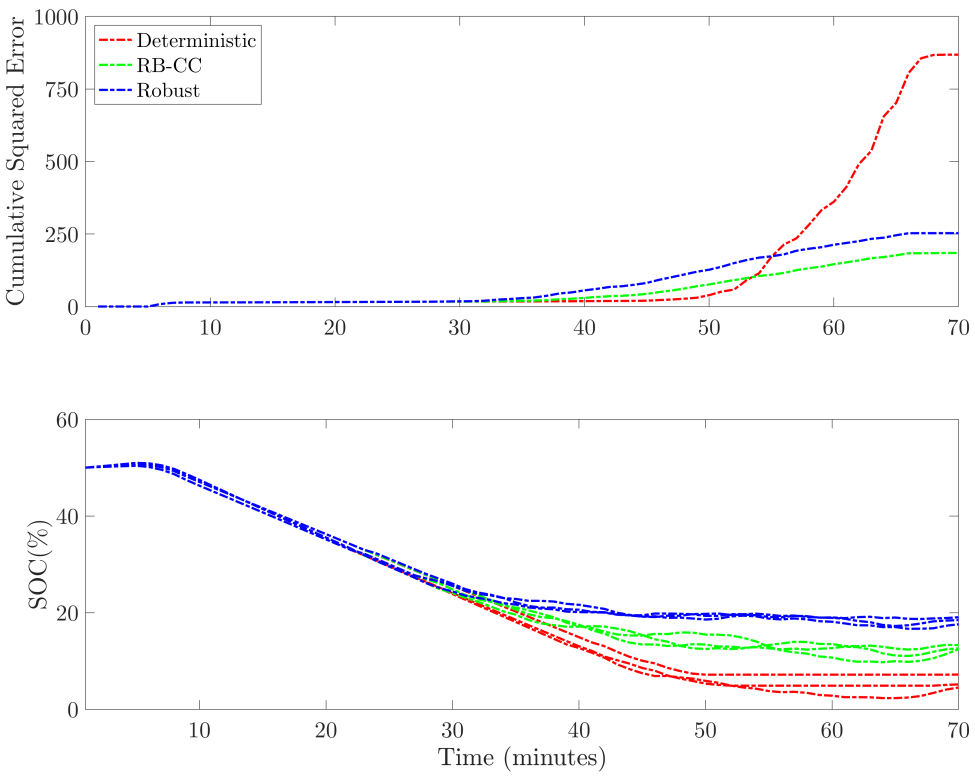


Figure 5.4: Cumulative squared error (top plot) and evolution of the energy state of the charge of the VESSs (bottom plot) under deterministic, robust, and RB-CC approaches for one trial.

makes the deterministic formulation susceptible to poor average performance while the robust and RB-CC formulations achieve similar performance.

To illustrate the role of risk cost, $c_{\mathcal{R}}$, on the tracking performance and total risk imposed to the power system, we scale the risk cost, $c_{\mathcal{R}}$ between 0 and 60 for one trial (out of 200 trials) where 0 resembles the deterministic and 60 approximates the robust approach. The resulting curves in Fig. 5.6 show the optimal trade-off between the tracking performance $J_{\text{Gen}}$, total operational risk that MPC accepts and risk cost. As expected, for small risk cost, controller dispatches VESSs with respect to the expected energy capacity limit, disregarding the robust limit and operational cost. This results in larger total risk, more DCS and poor tracking performance. For large risk cost, VESSs are dispatched conservatively and while the VSEEs are dispatch at a very low risk level, parts of the flexibility offered by VSEEs are declined.

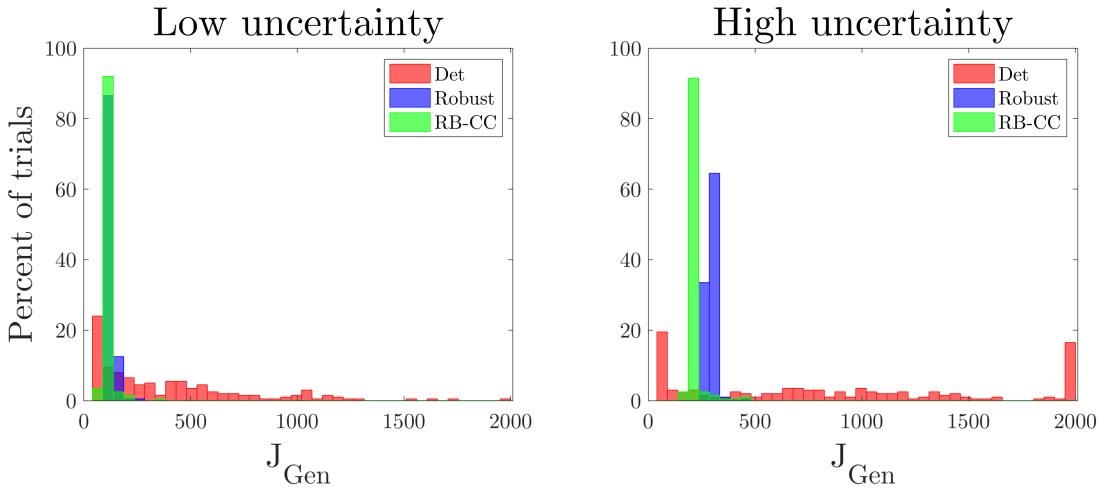


Figure 5.5: Histogram of the squared tracking error under deterministic, robust and RB-CC approaches. For visualization purposes, trials with squared tracking error of greater than 2000 are categorized in the last bin.

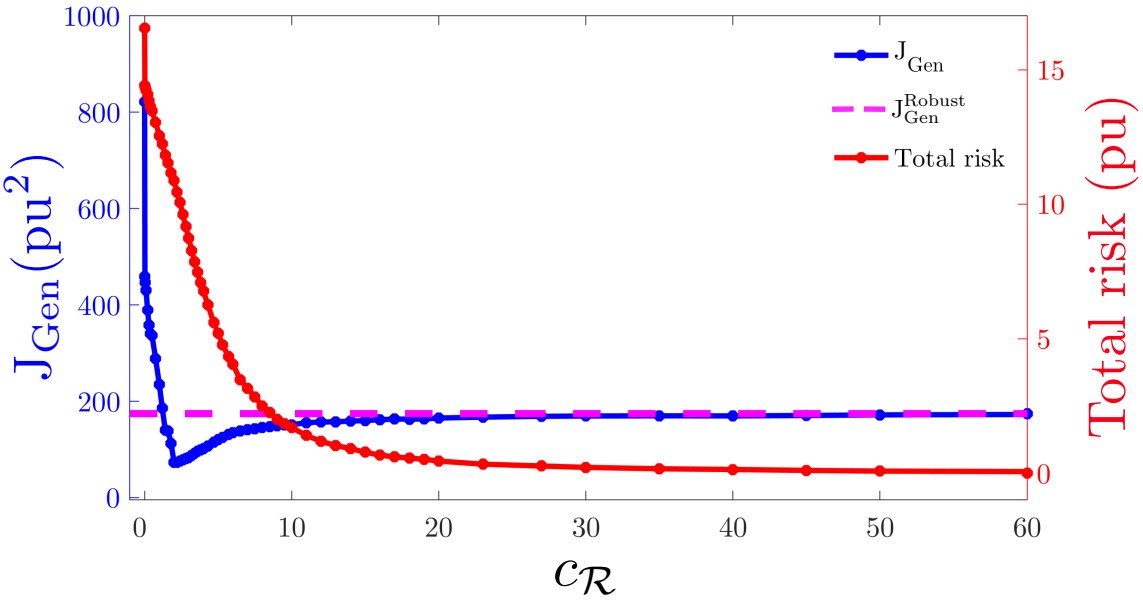


Figure 5.6: Role of the risk cost, $c_{\mathcal{R}}$ on the tracking performance and the total risk imposed to the power system.

To further investigate the effectiveness of the proposed method, the three large VESSs (one located in each region), are replaced by nine smaller VESSs (three located in each region) and

Table 5.4: Parameters of nine small VESSs

| Description | Value |
|---|---|
| Number of VESSs | 9 |
| Total energy capacity of VESSs | 855 MWh |
| Bus ID (location) of VESSs | $11, 17, 24, 35, 41, 48, , 59, 65, 72$ |
| VESS energy capacity | 95 MWh |
| Initial VESS state of charge | 50% |
| Maximum VESS power output | 95 MW |
| VESSs ramp rate limit | 20 MW/min |

location and parameters of small VESSs are shown in Table 5.4. Intuitively, smaller VESSs should reduce the severity of DCS events, but increase their frequency. The same analysis has been carried out on the system with the small VESSs under high uncertainty scenario anad results are shown in Fig. 5.7. The RB-CC outperforms the standard robust method.

Table 5.5: Performances of the deterministic, robust and ACT method are analyzed in presence of nine VESSs (three in each region).

| | $\mu$ | $\sigma$ | $\mu/\mu_{\text{Rob}}(\%)$ |
|---|---|---|---|
| Deterministic | 403.65 | 404.25 | 307.07 |
| Robust | 131.45 | 15.82 | 100 |
| RB-CC | 103.23 | 28.61 | 78.53 |

## 5.7 CONCLUSIONS AND FUTURE WORKS

This chapter studies the performance of a bi-level receding horizon predictive optimal power flow problem for managing variability with uncertain, flexible grid assets, such as VESSs. Since the SOC and capacity of VESSs can not be measured directly, a dynamic state estimator and simplified VESS aggregate model must be employed, which introduce uncertainty. This uncertainty in energy-constrained resources gives rise to the notion of dynamic capacity saturation (DCS). To overcome DCS, uncertainty can be managed by employing robust approaches. However, there is a sensitive trade-off between robustness of the optimized dispatch and closed-loop performance of the system. Indeed, robust approaches may lead to a conservative (high-cost) solution. Therefore, we introduced a RB-CC approach under which the operational risk is optimized with respect to the dynamic states of the VESSs over a receding horizon. The numerical studies indicate that RB-CC outperforms

other methods and significantly reduces DCS while maintaining good tracking performance.

Future work focuses on quantifying how well uncertain VESSs can regulate line temperatures under large disturbances. Furthermore, we are investigating stability guarantees for the MPC scheme and how uncertainty in the temperature estimates affects performance.

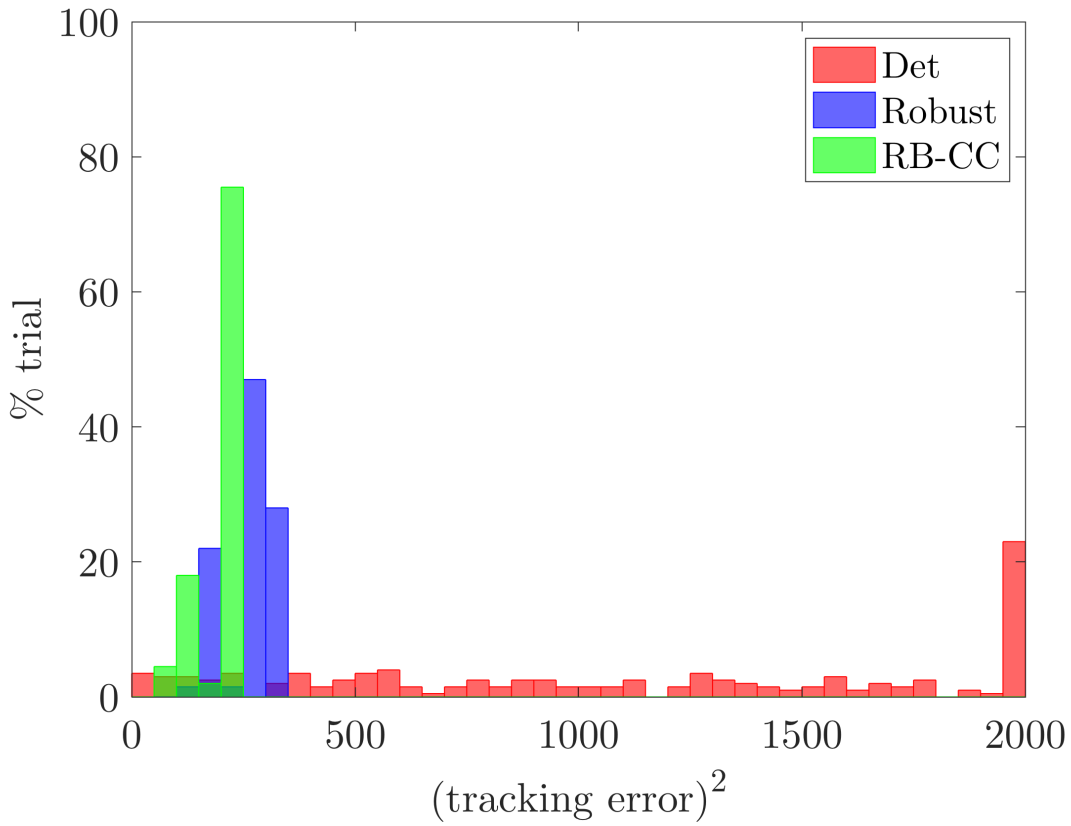


Figure 5.7: Histogram of the squared tracking error under deterministic, robust and RB-CC approaches in presence of nine VESSs (three in each region). For visualization purposes, trials with squared tracking error of greater than 2000 are categorized in the last bin.

# 6 Chapter 6: A Model-Predictive Control Method for Coordinating Virtual Power Plants and Packetized Resources, with Hardware-in-the-Loop Validation

**Abstract**

In this chapter, we employ a bi-level control system to react to disturbances and balance power mismatch by coordinating distributed energy resources (DERs) under packetized energy management. Packetized energy management (PEM) is a novel bottom-up asynchronous and randomizing coordination paradigm for DERs that guarantees quality of service, autonomy, and privacy to the end-user. A hardware-in-the-loop (HIL) simulation of a cyber-physical system consisting of PEM enabled DERs, flexible virtual power plants (VPPs) and transmission grid is developed in this work. A predictive, energy-constrained dispatch of aggregated PEM-enabled DERs is formulated, implemented, and validated on the HIL cyber-physical platform. The energy state of VPPs, composed of a fleet of diverse DERs distributed in the grid, depend upon the distinct real-time usage of these devices. The experimental results demonstrate that the existing control schemes, such as AGC, dispatch VPPs without regard to their energy state, which leads to unexpected capacity saturation. By accounting for the energy states of VPPs, model-predictive control (MPC) can optimally dispatch conventional generators and VPPs to overcome disturbances while avoiding undesired capacity saturation. The results show the improvement in dynamics by using MPC over conventional AGC and droop for a system with energy-constrained resources.

## 6.1 Introduction

The drive to reduce greenhouse gas emissions and declining capital costs are precipitating rapid increases in wind and solar generation capacity. Despite their low emissions profile, wind and solar power supplies vary rapidly in time, motivating the need for additional balancing resources [109, 110].

Since some peaking power plants may take more than an hour to bring online, during times of extensive peak usage, direct load control (i.e., load shedding) has been employed to ensure the security

of the power system [111]. However, the internet-connected distributed energy resources (DERs) are flexible in power demand and can be coordinated to provide ancillary services to the grid [13]. Although the main idea underlying modern demand coordination has existed for decades [11], the infrastructure required for load coordination is still in early stages, but developing rapidly [12–14]. Packetized energy managment (PEM) introduced previously by the authors [12, 112], is one such load coordination scheme. PEM leverages protocols used to manage data packets in communication networks to regulate the aggregate power consumption of DERs. More specifically, as in digital communication systems that break data into packets before transmission, PEM enables load control devices to consume energy in the form of "energy packets" which devices request periodically using a carefully designed randomized control policy. In PEM, the load coordinator only needs to know the aggregate power consumption and aggregate requests from the packetized-load to provide ancillary services to the grid. The energy-packet mechanism of PEM, therefore, provides a significant advantage in terms of communication overhead, over state-estimation based approaches, that require an entire histogram of states, which is addressed through observer design. Furthermore, controller complexity decreases in PEM, since the load coordinator only responds to individual requests depending upon the available flexibility as compared to more complex controllers. By leveraging protocols that are similar to TCP/IP, PEM inherits certain properties with regard to providing statistically uniform access to the grid. PEM guarantees the quality of service (QoS) for individual DERs in the entire population through its unique opt-out mechanism. The mean-field approaches, on the other hand, ensure QoS in the mean sense of the population where individual DERs might violate the QoS [13]. This work describes how aggregated PEM resources can be coordinated in real-time and demonstrates the applicability of the method to practical power systems applications and the role of cyber-physical systems (CPS).

Historically, balancing authorities maintain real-time supply/demand balance through automatic generation control (AGC) and load-frequency control (LFC) by implementing PI controllers in steam turbine generator systems to ensure power system operation at nominal frequency [113]. As the amount and distribution of controllable resources increases, determining an appropriate response to unscheduled events (e.g. power imbalances due to prediction error) is more challenging for the grid operators who need new tools for decision making.

An increasing number of researchers [114, 115] and industry groups [116] are employing virtual power plants (VPPs) to aggregate groups of DERs and then dispatch those resources into energy markets, such as frequency regulation/AGC. VPPs are formed from aggregation of flexible resources which are limited in power and energy. Since PI-control-based AGC does not take energy state estimation of VPPs into account, it may overuse the offered flexibility in short period of time (greedy) which leads to the sudden saturation of VPPs (i.e. cannot provide any more flexibility). To overcome this phenomenon, model-predictive control (MPC) can be employed. MPC is a multi-input, multi-output (MIMO), optimization-based, predictive control technique that considers system constraints explicitly [117]. MPC strategies have previously been applied in power systems for optimal coordination of controllable loads, load shedding, capacity switching, tap-changer operation, etc. The main purpose of those strategies is contingency management, voltage stability, thermal control of transmission lines, and energy management [99, 118, 119]. In this work, an MPC scheme is employed to track a secure, economically-optimal reference trajectory of generators and VPPs while responding to power imbalances and satisfying physical constraints of the power system. For frequency regulation in the power system under high penetration of renewables, MPC has several advantages over PI controllers including robustness of the system against disturbance and uncertainty [120].

This chapter demonstrates the benefit that MPC has on dispatching resources with limited energy supply. An HIL platform is developed that consists of a transmission grid, MPC corrective dispatch scheme and PEM-enabled DERs emulated on a high-performance PC that requests packets of energy from the aggregator. The VPPs are physically realized in a micro-controller that connects the DERs to the grid via analog signals. The experimental results demonstrate the effectiveness of the MPC in a real-time CPS, thereby validating the ability of a VPP to track challenging signals under such control.

The remainder of the chapter is organized as follows. Section 6.2 details Packetized Energy Management of DERs. In Section 6.3, we demonstrate our cyber-physical validation platform. Section 6.4 gives an overview of the system operation and control. Implementation results are provided in Section 6.5 and Section 6.6 concludes the chapter.

## 6.2 Packetized energy management of DERs

Packetized energy management is a bottom-up DER coordination scheme in which the DERs submit randomized requests of energy packets. The VPP accepts or rejects these requests based on the available flexibility. The DERs considered in this work are thermostatically controlled loads (TCLs) and energy storage systems (ESS).

The PEM-enabled DERs are designed to operate in one of the four following logical states: (i) charge (ii) discharge (iii) off (iv) opt-out. The first three states (charge, discharge, off) are associated with the normal PEM operation whereas the fourth OPT-OUT state ensures quality of service (QoS). A DER in OFF stochastically requests a charge packet or a discharge packet. If a charge packet is accepted, the DER changes state from OFF to CHARGE and consumes power for a specific time interval $\delta_c$. If a discharge packet is requested and consequently accepted, the DER transitions from OFF to DISCHARGE state and discharges power into the system for a fixed time $\delta_d$. After completing a charge or discharge packet, the device automatically transitions to OFF mode and this process of stochastically requesting charge/discharge packets repeats. PEM aims to maintain the DER's state within minimum and maximum operating bounds. PEM provides QoS guarantees by enabling the devices to opt out of the *packetizing* behavior when the energy state goes outside of allowable upper and lower limits.

## 6.3 Cyber-Physical Layout

The smart grid paradigm [121] is largely about the transformation of power systems into full cyber-physical systems that enable bidirectional flows of energy and communications. CPS are of vital importance to the grid, especially when increasing the presence of renewable generation and smart devices, improving control [122, 123], and adding resiliency to the system [124, 125]. The validation of CPS require accurate models of both cyber and physical sub-systems (e.g. HIL systems communicating with one another over realistic communication protocols). In order to validate the proposed demand-side CPS scheme, a real-time HIL platform is developed consisting of a transmission system and packetized load. The OP5600 real-time digital simulator from OPAL-RT is used to simulate the HIL cyber-physical system. The OP5600 has a multi-core processor along with digital and ana-

log I/O with the capability of interfacing to a network of PCs in order to simulate large models in real-time while real-time refers to timescales on the order of tens of milliseconds. The RT-Lab software allows the communication between a host PC and the target (OP5600) simulator such that a real-time physical model can run on the simulator while the controller would run on the PC where an operator could make adjustments when necessary.

"ePHASORSIM" is a tool developed by OPAL-RT to offer dynamic simulation of power systems in order to conduct power system studies and test control schemes. A grid is modeled with a standard positive-sequence equivalent single-phase constant-power AC model in ePHASORSIM, based on the Vermont Electric Power Company (VELCO) transmission system to be run in real time on the OP5600. RT-LAB and ePHASORSIM can be interfaced extremely easily with MathWorks' Simulink, which is used to develop the controls for the power system. The OPAL-RT blockset for Simulink allows a section of the Simulink block diagram to be run in real time on the OP5600 and the controls can be run asynchronously on the PC with the ability to accept user inputs when necessary. ESP8266 microchips were used to emulate VPP interconnections to the grid in real time. ESP8266 communicate with the cloud server over WIFI, while the server is being hosted on a Linux machine. Fig. 6.1 shows an overview of the cyber-physical platform used in this study.

## 6.4 Energy aware dispatch of diverse energy resources

Security constrained optimal power flow (SCOPF) enables grid operators to implement economic schedules for generators, flexible loads and importing power into the area for a number of hours. However, the volatility and intermittent characteristic of net-loads (i.e., demand minus renewables) results in forecast error and power imbalances. Since grid operators may pay high penalties for rescheduling generators or importing power through tie lines to balance supply and demand [75], power mismatches can be balanced by controlling flexible resources. This suggests a bi-level control strategy where the first level is in charge of economic scheduling and its outputs are used as a reference input to the second level which is in charge of dispatching generators and VPPs to balance the system against any disturbance. An overview of the proposed control system is provided in Fig. 6.2.

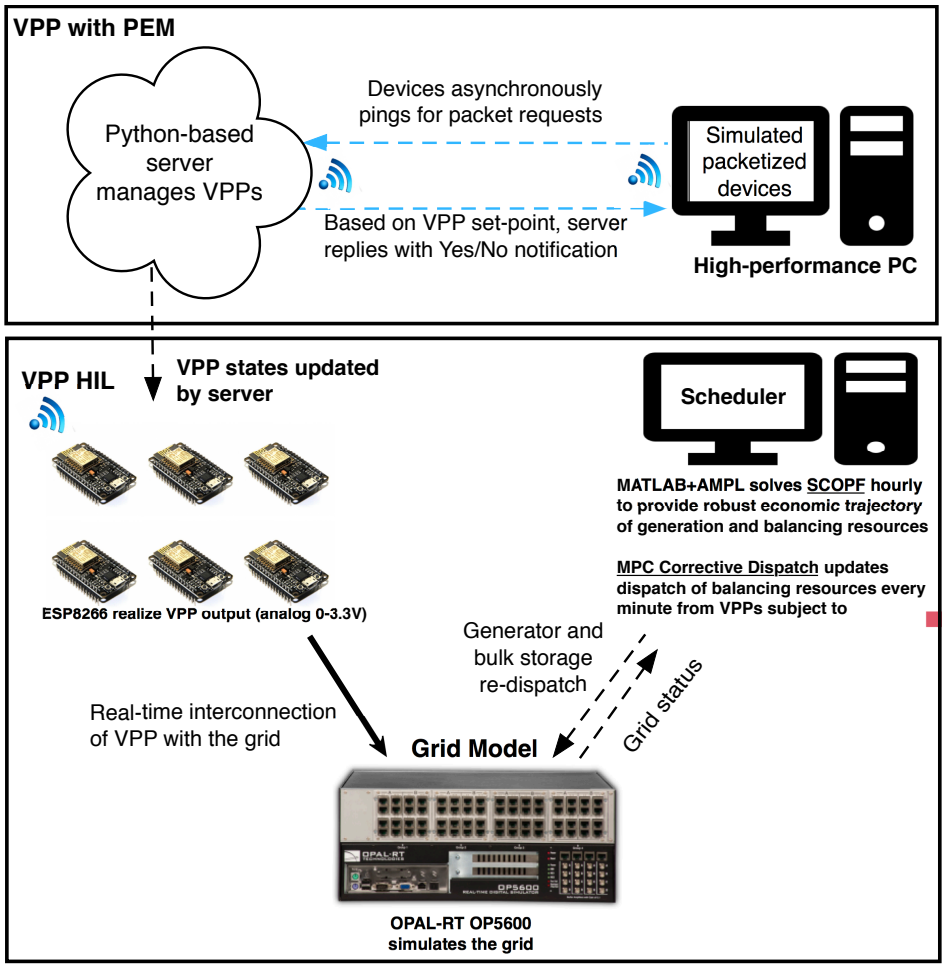


Figure 6.1: Cyber-physical platform overview: The transmission grid is simulated on the OP5600 and MPC-corrective dispatch is realized on a host PC and generates balancing signals. ESP8266 devices are connected to a python-based server via WiFi and transmit the VPPs' states through the analog interface. The packetized load is emulated on a high performance PC and requests energy packets from the VPP through WiFi communication.

### 6.4.1 AGC

In the power system, safety of the electrical equipment and quality of delivered power is dependant on nominal system frequency. Therefore, the frequency should be controlled and monitored regularly and any mismatches in generation and consumption shall be corrected through load frequency control (LFC) [15]. Traditionally, the primary frequency regulation (speed-droop) on each gener-

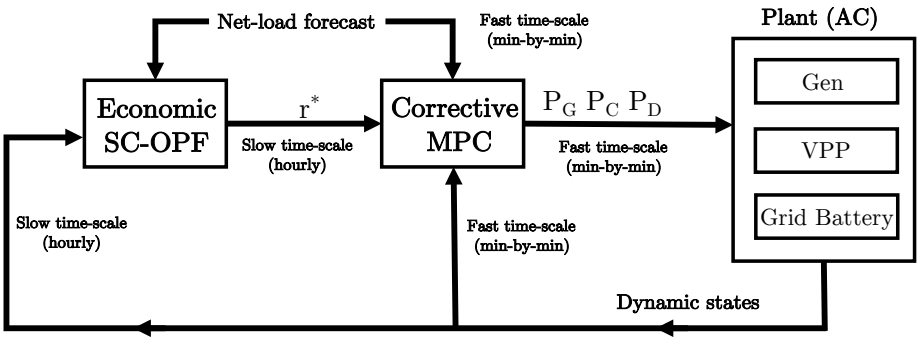


Figure 6.2: Overview of control scheme showing controller including OPF and MPC part and how each part is related to the power grid.

ator stabilizes the power system with a steady-state frequency deviation from the desired system frequency depending on the droop characteristic and frequency sensitivity. A linear combination of frequency errors and change in imported power through tie lines from their scheduled contract basis is used as an error signal called area control error (ACE). AGC acts as a secondary control using an integral controller that sends out control signals to generators and VPPs to reduce ACE to zero in steady state. For the purposes of this work, only two areas are used for simplicity, while being effective enough to demonstrate the flow of power between different areas. The first area represents a small balancing authority (control area), and the second represents the aggregate dynamics of the external system. One machine exists in the external area and has a large inertia and capacity to emulate the properties of the rest of the interconnected power system.

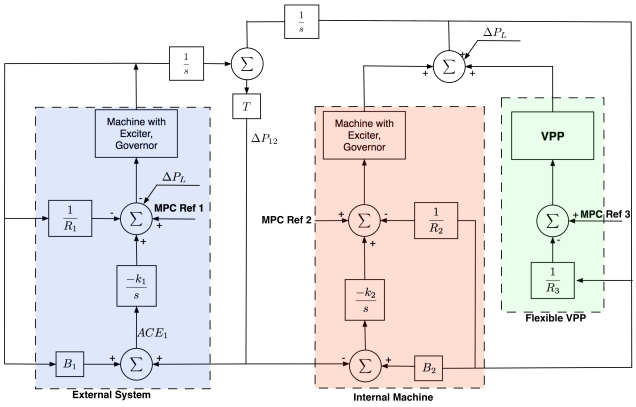


Figure 6.3: Diagram showing a control schematic for the test system including all of the generation in the internal and external areas.

Fig. 6.3 shows the control diagram for the system modeled in this chapter, which is an adapted version of the diagram from [113]. The interaction between the internal and external areas involved are shown. The external machine, one of the internal machines, and the VPPs assist in AGC/ACE, while all of these generation sources are equipped for primary frequency regulation.

### 6.4.2 Model predictive control for power system

Unlike conventional generators, VPPs (synthetic reserves) are energy-constrained and should be utilized considering their available flexibility. Aforementioned primary and secondary frequency controllers do not take energy states of the VPPs into account. Therefore, VPPs may reach their energy capacity limits (saturate) unexpectedly and cannot provide balancing power anymore. As a result, conventional generators must be rescheduled to provide the required balancing services, which can be expensive, or even infeasible leading to a reliability risk.

As an advanced control technique, MPC forms an alternative to the PI controllers in frequency regulation which uses a mathematical model of the power system based on the current and future information and constraints to find the optimal control actions with respect to the defined objective. Unlike a PI controller, MPC dispatches resources (generators and VPPs) at each time step considering current states and forecasted conditions while handling the energy constraints of the flexible resources. The results of this work show that the MPC is more suitable for frequency regulation and dispatching energy-constrained resources compared to the PI controllers [126, 127]. The MPC scheme can be summarized as follows:

1. Controller uses measured/estimated initial states to solve an open-loop optimal control problem for $M$ steps, which is known as prediction horizon, taking into account current and future constraints. This gives a sequence of optimal open loop control actions and predict output.

2. Apply receding horizon control so that only the first instance of the control sequence is given as the input to the plant.

3. Measure the actual system state after applying the first control action.

4. Go to step 1.

We consider a transmission system model comprising of $N_b$ buses, $N_l$ lines, $N_G$ generators, $N_L$ loads and $N_B$ VPPs. Parameters $\Omega_i^N$ and $\Omega_i^G$ refer to a set of all buses connected to bus $i$ and set of all generators at bus $i$ respectively. Since MPC relies on a linear model of the actual system, the dynamic model of the system is discretized by forward Euler method with sample time $T_s$. The MPC optimization is defined to minimize the cost of the deviation of generator outputs from the scheduled set-points $P_{G,i}^r$ considering deviation cost $c_{G,i}$

$$J^* = \min_{P_G, P_{\text{ch}}, P_{\text{dis}}} \quad \sum_{l=k}^{k+M} \sum_{\forall i \in N_g} c_{G,i}(P_{G,i}[l] - P_{G,i}^r[l])^2 \tag{6.1a}$$

s.t.

$$P_{\text{ch},i}[l] - P_{\text{dis},i}[l] + P_{L,i}^f[l] + \sum_{j \in \Omega_i^N} f_{ij}[l] = \sum_{z \in \Omega_i^G} P_{G,z}[l], \tag{6.1b}$$

$$f_{ij}[l] = b_{ij}(\theta_i[l] - \theta_j[l]), \tag{6.1c}$$

$$-\overline{f_{ij}} \leq f_{ij}[l] \leq \overline{f_{ij}}, \tag{6.1d}$$

$$\underline{P_{G,i}} \leq P_{G,i}[l] \leq \overline{P_{G,i}}, \tag{6.1e}$$

$$-T_s R_{G,i} \leq P_{G,i}[l+1] - P_{G,i}[l] \leq T_s R_{G,i}, \tag{6.1f}$$

$$0 \leq P_{\text{ch},i}[l] \leq \overline{P_{\text{ch},i}}, \tag{6.1g}$$

$$0 \leq P_{\text{dis},i}[l] \leq \overline{P_{\text{dis},i}}, \tag{6.1h}$$

$$-T_s R_{\text{ch},i} \leq P_{\text{ch},i}[l+1] - P_{\text{ch},i}[l] \leq T_s R_{\text{ch},i}, \tag{6.1i}$$

$$-T_s R_{\text{dis},i} \leq P_{\text{dis},i}[l+1] - P_{\text{dis},i}[l] \leq T_s R_{\text{dis},i}, \tag{6.1j}$$

$$S_i[l+1] = S_i[l] + T_s\left(\eta_{\text{ch},i} P_{\text{ch},i}[l] - \eta_{\text{dis},i}^{-1} P_{\text{dis},i}[l]\right), \tag{6.1k}$$

$$\underline{S_i} \leq S_i[l] \leq \overline{S_i} \tag{6.1l}$$

where (6.1b) imposes Kirchhoff's laws, implying that the net flow into a bus must equal the net flow out of that bus. Power flows on the line connecting bus $i$ and $j$ that are determined by (6.1c) must be within the power carrying capacity of the transmission line $\overline{f_{ij}}$ as shown in (6.1d). Generators may inject power, $P_G$ and loads may consume power $P_L$ at each node $i$. Each conventional generator is described by its production state, which must be within generator upper and lower limits, $\overline{P_G}$ and $\underline{P_G}$, as shown in (6.1e). Furthermore, due to the thermal nature of the generators, their ramp rates

are limited to up and down limits, $R_G$, as shown in (6.1f). The responsive VPPs overcome limitations of generator ramping rates. Non-negative scalar $P_{\text{ch}}$ and $P_{\text{dis}}$ represent charging and discharging power of a VPP. The charging and discharging efficiencies are denoted by $\eta_{\text{ch}}$ and $\eta_{\text{dis}}$. Charging and discharging power and SOC of the VPPs are subject to constraints (6.1g), (6.1h) and (6.1l) where $\overline{P_{\text{ch}}}$, $\overline{P_{\text{dis}}}$, $\overline{S}$, and $\underline{S}$ represent maximum charging and discharging power and the maximum and minimum energy capacity of VPP, respectively. In general, coordination schemes do not offer instant control over all DERs in a fleet, but are subject to separate internal control, actuation, and communication loops [97]. These cyber-physical control considerations manifest themselves as ramp-rate limits on the charging ($R_{\text{ch}}$) and discharging ($R_{\text{dis}}$) of VPPs as shown in (6.1i) and (6.1j). The dynamic of the VPP's SOC is shown in (6.1k).

## 6.5 Results

This section experimentally demonstrates that energy-aware dispatch of flexible VPPs enhances the AGC performance. The details of the test-setup are as follows. The transmission system consisting of 161 buses, 223 transmission lines and three generating units, is set up in ePHASORSIM and supplies a total load of 609 MW consisting of approximately 50% renewable generation and remaining load is supplied from one external and two internal machines and generators. The flexibility is provided by two VPPs consisting of one bulk battery and one HIL VPP. The HIL VPP consists of real packetized-enabled DERs emulated on a high-performance PC, that requests the VPP (server) for packets of energy through web-sockets. The VPP obtains balancing signals from the grid operator and accepts/rejects the packets based on the available flexibility. ESP8266 is the physical realization of VPP that obtains the VPP's state from the server and sends it to the grid through an analog interface.

### 6.5.1 Capacity saturation of VPP

The HIL VPP and grid scale battery providing grid services are energy-limited and ignoring their energy capacity results in inferior AGC performance. The effect of their capacity on the ancillary services provided to the grid is demonstrated in Fig. 6.4. The capacity of the battery is 45 MWh. Fig. 6.4 shows that the load reduces by 50 MW resulting in excess generation and both battery and

VPP take up 45 MW and 5 MW respectively, of this excess generation. The battery is initially 50% charged, as shown in Fig. 6.4 (b). After $t \approx 36$ mins, in Fig. 6.4 (b), the battery saturates and can no longer provide ancillary services to the grid. The power output of Gen. 2 is therefore reduced to account for the loss of 45 MW and the system deviates from its scheduled generation (Fig. 6.4 (c)) in order to keep the system stable (Fig. 6.4 (d)).

### 6.5.2 MPC with capacity saturation

The proposed *energy aware* scheme improves the performance by explicitly accounting for the energy limits of the flexible resources. Fig. 6.5 shows a load change $\Delta P_L = 50$ MW that results in the HIL VPP and the battery providing the remaining slack. MPC keeps track of the current state of charge of the HIL VPP and the battery (Fig. 6.5 (a) and (b)) and after $t \approx 13$ mins, gradually reduces the set-points of the battery to avoid saturation as shown in Fig. 6.5 (b). The HIL VPP and the battery can therefore supply ancillary services to the grid for over 60 mins.

## 6.6 Discussion/Conclusion

This chapter presents a hardware-in-the-loop implementation of PEM-based cyber-physical platform and demonstrates that aggregated PEM-enabled DERs can provide ancillary services to the grid. The system consists of emulated DERs, an aggregator realized as real live webserver, and a transmission system developed from the real data provided by VELCO. The experimental studies carried out in this work show that conventional control schemes (i.e. AGC and droop) do not take into account the state of charge of VPPs while providing ancillary services to the grid that leads to capacity saturation of the VPPs. As a result, the VPP can no longer support the requested flexibility and cause a disturbance in the grid because the generators have to ramp-up quickly to ensure stability. Conventional schemes are therefore greedy in managing flexible resources and leads to capacity saturation and unwanted disturbances. Model predictive control (MPC) responds to the unexpected disturbances by dispatching resources depending upon the hourly load forecast as well as minute-by-minute dispatch in a receding horizon. MPC is shown to proactively vary the consumption of flexible resources depending upon the SOC, which utilizes these resources for a longer time than the base case with AGC. The generators therefore operate as close as possible to their optimal limits

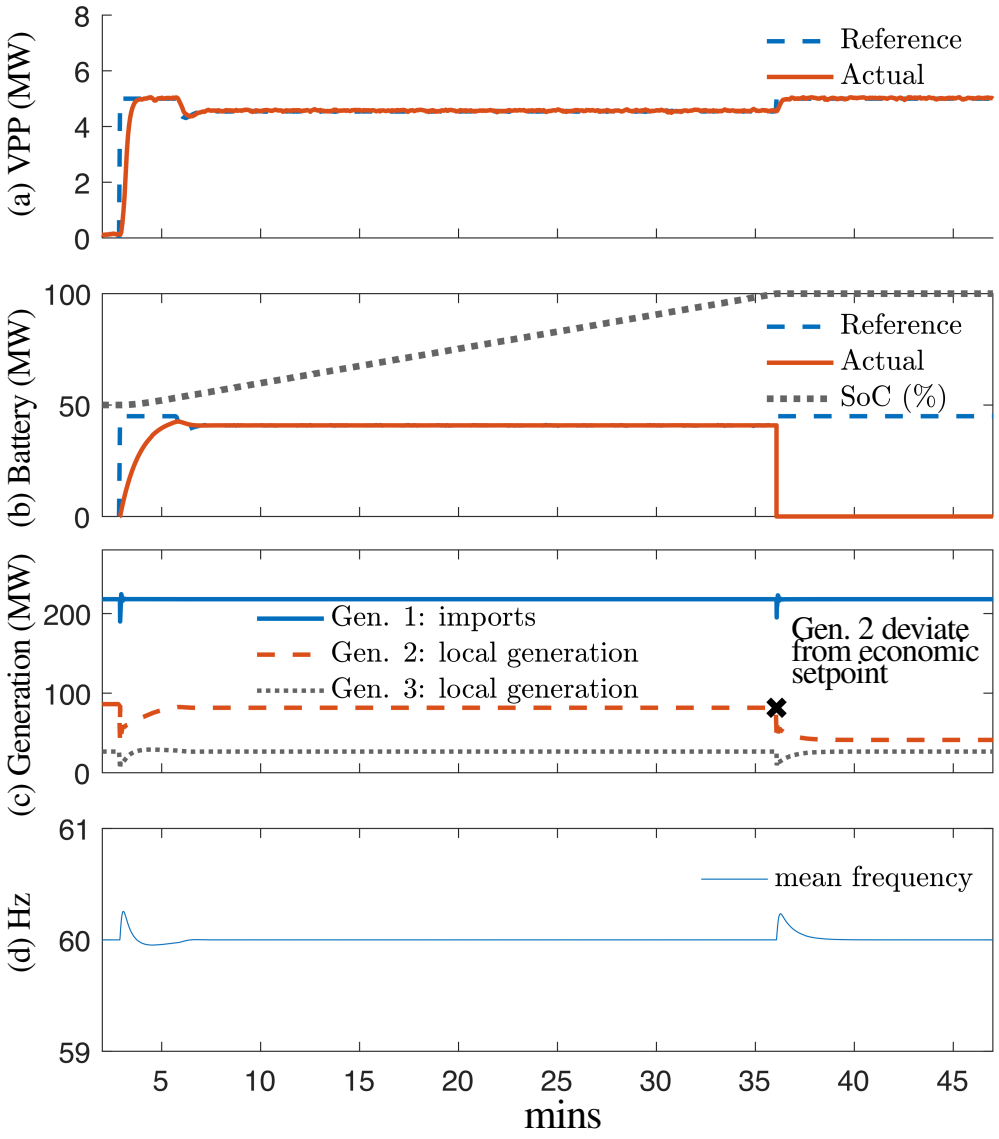


Figure 6.4: (a) The HIL VPP's actual and reference power (MW) (b) Grid scale battery's actual power (MW), reference power (MW) and state of charge (SOC %) during charge/discharge events (c) Generators' power output (MW) (d) Generators' mean frequency (Hz). The saturation of the VPP to a step decrease in load is shown in this figure. For the change in load, the HIL VPP and the battery charges at a continuous rate. The battery saturates at about t = 36 mins, after which their output goes to zero and cannot support the requested flexibility.

for a much longer time.

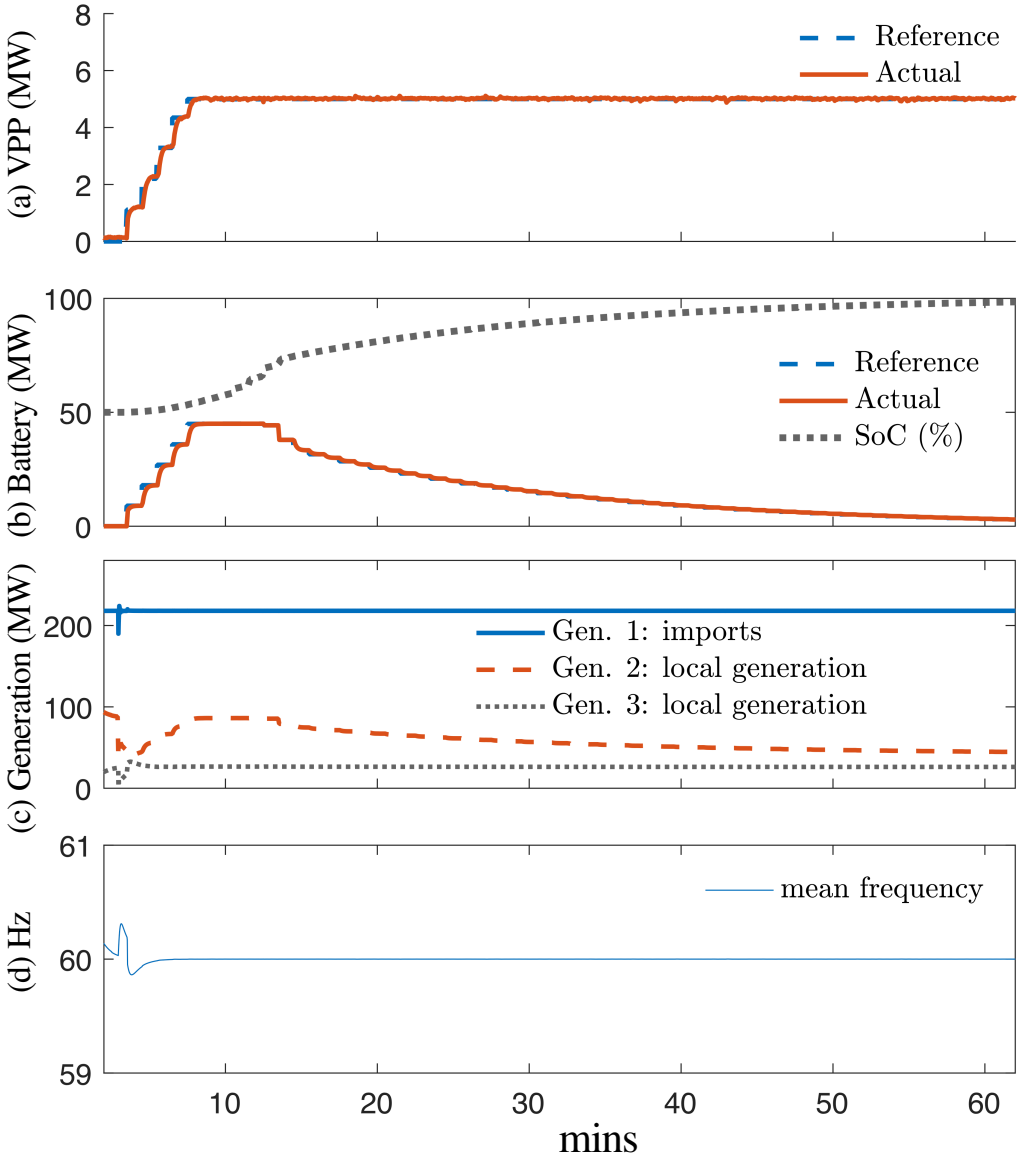


Figure 6.5: (a) The HIL VPP's actual power (MW) and reference power (MW) (b) Grid scale battery's actual power (MW), reference power (MW) and state of charge (SOC %) during charge/discharge events (c) Generators' power output (MW) (d) Generators' mean frequency (Hz). MPC with capacity saturation takes into consideration the current state of charge of the VPP and initially ramps up to the requested 50 MW. However, at t = 13 mins, MPC lowers the setpoint in steps to avoid VPP saturation and provide support to the system for a longer time.

# 7 Chapter 7: Conclusion and Future Work

## 7.1 Summary

The global increasing of electrical demands and environmental concerns, prioritize investments in integrating renewable energy sources which results in a significant reduction in air pollution and fossil fuel consumption. Decreases in cost of renewable generation technologies, advance metering technologies developments, and efficiency incentives make renewable generation a growing trend in the world and especially in the United States. For decades, conventional fast ramping generators enable reliable operation of the power system by providing required operational reserve. However, integrating more uncertain, intermittent RES, has brought more uncertainties and challenges to the power system that may have a significant impact on the power system reliability. Therefore, appropriate control technologies are needed to be employed in order to facilitate integration of the these renewable energy sources.

Chapter 1 presents an introduction to this thesis and motivation behind the research I have done during my PhD is laid out. A review of the literature focusing on the demand response and how virtual energy storage system are formed by aggregating flexible loads is presented. Moreover, the existed challenges and the main research objectives are outlined.

In chapter 2 the formulation of the power system operations including power flow analysis problem, optimal power flow problem, ensuring security under optimal power flow and dynamic line rating of transmission lines are presented.

VESS can provide similar functions of the grid scale battery to support the power grid. However, due to the physical characteristics of the VESS, significant constant or variable delays can be observed in the power system. Moreover, the VESSs' energy capacity and state of the charge can not be measured directly and should be estimated. These estimates both contains uncertainty and should be carefully considered.

Chapter 3 investigates how inevitable delays in implementing frequency-dependent load control in a power system with droop-controlled affects settling time and stability of the power system. It is shown that the closed-loop performance of the power system follows a stable-unstable-stable

patterns which directly depends on the network topology.

In chapter 4, a bi-level receding horizon optimal power flow framework has been introduced and developed. The first level of the controller was in charge of the security constrained optimal power flow and produce a reference trajectory for generator outputs while the second level manages the net-load variability by VPP with uncertain energy capacity. If a VPP reached its actual (but unknown) bound, it can not supply the desired set-point anymore and we say that it saturates. The AC load-flow then allocates any remaining mismatch between demand and supply with a slack bus mechanism, which, in the physical system, distributes the slack among available generators (e.g., via secondary frequency control or AGC). Reducing occurrence and severity of these saturation is, therefore, key to avoid calling upon generator spinning reserves (via AGC). We showed there is a sensitive trade-off between robustness and closed-loop performance of the system and the popular robust approaches may lead to too conservative solutions that reduce the closed-loop performance of the system. The numerical studies illustrates that the closed-loop performance of the system can be improved significantly (up to 12%) by sacrificing some robustness.

Chapter 5 extends the results of the chapter 4 and propose a risk-based chance constrained model predictive control approach that co-optimizes the delivery of the VESSs against operational risk inherent to the VESSs' uncertainty energy capacities and state of the charge. This approach is compared with the deterministic and robust approach and it is shown that the proposed approach outperforms the robust and deterministic approaches and significantly prevent VESSs saturation while maintain good tracking performance.

Chapter 6 develops a hardware-in-the-loop cyber-physical platform and demonstrates that the flexible resources can be aggregated to provide ancillary service to the grid. The system consits of emulated DERs, and aggreagtor realized as webserver and transmission systsem inspired from the real data provided by VELCO. The simulation studies carried out in this work shows that conventional control schemes (i.e. AGC and droop) do not use the state of charge of VPPs while providing ancillary services to the grid and leads to capacity saturation of the VPPs. As a result, the VPP can no longer support the requested flexibility and cause a disturbance in the grid because the generators have to ramp-up fast to ensure stability. Conventional schemes are therefore greedy in managing flexible resources and leads to capacity saturation and unwanted disturbances. Model

predictive control (MPC) dispatches resources depending upon the hourly load forecast as well as minute-by-minute dispatch in a receding horizon. MPC is shown to proactively vary the consumption of flexible resources depending upon the SOC and utilized these resources for a longer time than dynamic AGC. The generators therefore operate as close as possible to optimal limits for as long as possible.

## 7.2 Future Work

There are a number of different ways that the work in this dissertation could be extended. These proposed paths for future research can be classified as: i) developing analytical expressions for stability and controllability of system frequency as a function of available energy resources and salient network properties. Recent results from linear delay differential equations where the *Lambert W function* has been utilized in describing stability of linear delay differential equations can be leveraged to accomplish this. Designing controllers that are aware of actuator saturation also can be pursued. The end-goal should be developing load coordination schemes that are robust against a broad class of uncertainties, including unknown time-delays; ii) by incorporating transmission line temperature limits, value of the dispatchable VESSs increases significantly as it allows for congestion management. Future work can address the question of how much flexible loads should be provided for a given power system and where they should be placed; iii) generalizing the VESS models to include non-Gaussian errors and analyze how the uncertainty affects the regulation of line temperatures in the presence of disturbances; iv) the hardware-in-loop platform developed for the emulation of packetized DERs enables the validation and testing of real-time control schemes for dispatch of flexible resources (demand dispatch). Quantifying the flexibility of packetized DERs is crucial in demand dispatch as it provides the aggregator with an estimate of the "current state" of the DERs. This information is crucial for the aggregator to provide ancillary services to the grid. This platform can be used to develop and validate virtual battery models that estimate the current state of the charge of a fleet of packetized DERs. Furthermore, it can be used to develop and validate optimal dispatch algorithms of DERs under real-time grid constraints.

# References


[1] E. Delarue and J. Morris, "Renewables intermittency: operational limits and implications for long-term energy system models," 2015.

[2] J. Matevosyan, S. Sharma, S. . Huang, D. Woodfin, K. Ragsdale, S. Moorty, P. Wattles, and W. Li, "Proposed future ancillary services in electric reliability council of texas," in *2015 IEEE Eindhoven PowerTech*, June 2015, pp. 1–6.

[3] M. H. Albadi and E. F. El-Saadany, "Demand response in electricity markets: An overview," in *2007 IEEE power engineering society general meeting*. IEEE, 2007, pp. 1–5.

[4] K. Ponds, A. Arefi, A. Sayigh, and G. Ledwich, "Aggregator of demand response for renewable integration and customer engagement: Strengths, weaknesses, opportunities, and threats," *Energies*, vol. 11, no. 9, p. 2391, 2018.

[5] X. Luo, J. Wang, M. Dooner, and J. Clarke, "Overview of current development in electrical energy storage technologies and the application potential in power system operation," *Applied energy*, vol. 137, pp. 511–536, 2015.

[6] E. I. A. (US), *Annual energy review 2011*. Government Printing Office, 2012.

[7] E. Kabir, P. Kumar, S. Kumar, A. A. Adelodun, and K.-H. Kim, "Solar energy: Potential and future prospects," *Renewable and Sustainable Energy Reviews*, vol. 82, pp. 894–900, 2018.

[8] S. Sharma, S.-H. Huang, and N. Sarma, "System inertial frequency response estimation and impact of renewable resources in ercot interconnection," in *2011 IEEE power and energy society general meeting*. IEEE, 2011, pp. 1–6.

[9] M. Mahmoudi, A. Fatehi, H. Jafari, and E. Karimi, "Multi-objective micro-grid design by nsga-ii considering both islanded and grid-connected modes," in *2018 IEEE Texas Power and Energy Conference (TPEC)*, Feb 2018, pp. 1–6.

[10] M. G. Morgan and S. N. Talukdar, "Electric power load management: Some technical, economic, regulatory and social issues," *Proceedings of the IEEE*, vol. 67, no. 2, pp. 241–312, 1979.

[11] F. C. Schweppe, R. D. Tabors, J. L. Kirtley, H. R. Outhred, F. H. Pickel, and A. J. Cox, "Homeostatic utility control," *IEEE Transactions on Power Apparatus and Systems*, no. 3, pp. 1151–1163, 1980.

[12] M. Almassalkhi, L. D. Espinosa, P. D. Hines, J. Frolik, S. Paudyal, and M. Amini, "Asynchronous coordination of distributed energy resources with packetized energy management," in *Energy Markets and Responsive Grids*. Springer, 2018, pp. 333–361.

[13] S. P. Meyn, P. Barooah, A. Bušić, Y. Chen, and J. Ehren, "Ancillary service to the grid using intelligent deferrable loads," *IEEE Transactions on Automatic Control*, vol. 60, no. 11, pp. 2847–2862, 2015.

[14] J. L. Mathieu, S. Koch, and D. S. Callaway, "State estimation and control of electric loads to manage real-time energy imbalance," *IEEE Transactions on Power Systems*, vol. 28, no. 1, pp. 430–440, 2013.

[15] M. Amini and M. Almassalkhi, "Investigating delays in frequency-dependent load control," in *2016 IEEE Innovative Smart Grid Technologies - Asia*, Nov 2016, pp. 448–453.

[16] M. Almassalkhi, J. Frolik, and P. Hines, "Packetized energy management: Asynchronous and anonymous coordination of thermostatically controlled loads," in *2017 American Control Conference (ACC)*, May 2017, pp. 1431–1437.

[17] M. Amini, A. Khurram, A. Klem, M. Almassalkhi, and P. Hines, "A model-predictive control method for coordinating virtual power plants and packetized resources, with hardware-in-the-loop validation," in *2019 IEEE Power and Energy Society General Meeting (PESGM)*. IEEE, 2019, pp. 1–5.

[18] J. Torriti, "A review of time use models of residential electricity demand," *Renewable and Sustainable Energy Reviews*, vol. 37, pp. 265–272, 2014.

[19] U.S. Energy Information Administration. (2017) How many smart meters are installed in the united states, and who has them? [Online]. Available: https://www.eia.gov/tools/faqs/faq.php?id=108&t=3t=_blank

[20] Digital Journal. (2017) Growth seen in advanced metering infrastructure in u.s. [Online]. Available: http://www.digitaljournal.com/tech-and-science/technology/growth-seen-in-advanced-metering-infrastructure-in-usa/article/504413#ixzz5hV8V5Vmu

[21] F. Shariatzadeh, P. Mandal, and A. K. Srivastava, "Demand response for sustainable energy systems: A review, application and implementation strategy," *Renewable and Sustainable Energy Reviews*, vol. 45, pp. 343–350, 2015.

[22] A. Rabiee, A. Soroudi, B. Mohammadi-Ivatloo, and M. Parniani, "Corrective voltage control scheme considering demand response and stochastic wind power," *IEEE Transactions on Power Systems*, vol. 29, no. 6, pp. 2965–2973, 2014.

[23] S. Annala *et al.*, "Households willingness to engage in demand response in the finnish retail electricity market: an empirical study," 2015.

[24] P. Cappers, "Mass market demand response and variable generation integration issues: a scoping study," 2011.

[25] P. Bertoldi, P. Zancanella, and B. Boza-Kiss, "Demand response status in eu member states," *Europa. eu: Brussels, Belgium*, 2016.

[26] Z. Zhao, C. Yu, M. Yew, and M. Liu, "Demand side management: A green way to power beijing," *Journal of Renewable and Sustainable Energy*, vol. 7, no. 4, p. 041505, 2015.

[27] M. S. Modarresi, L. Xie, , and C. Singh, "Reserves from controllable swimming pool pumps: Reliability assessment and operational planning," in *2018 51st Hawaii International Conference on System Sciences (HICSS)*, Jan 2018.

[28] M. Braun and P. Strauss, "A review on aggregation approaches of controllable distributed energy units in electrical power systems," *International Journal of Distributed Energy Resources*, vol. 4, no. 4, pp. 297–319, 2008.

[29] S. Burger, J. P. Chaves-Ávila, C. Batlle, and I. J. Pérez-Arriaga, "A review of the value of aggregators in electricity systems," *Renewable and Sustainable Energy Reviews*, vol. 77, pp. 395–405, 2017.

[30] T. Samad, E. Koch, and P. Stluka, "Automated demand response for smart buildings and microgrids: The state of the practice and research challenges," *Proceedings of the IEEE*, vol. 104, no. 4, pp. 726–744, 2016.

[31] S. Braithwait and K. Eakin, "The role of demand response in electric power market design," *Edison Electric Institute*, 2002.

[32] H. Chen, T. N. Cong, W. Yang, C. Tan, Y. Li, and Y. Ding, "Progress in electrical energy storage system: A critical review," *Progress in natural science*, vol. 19, no. 3, pp. 291–312, 2009.

[33] O. Palizban and K. Kauhaniemi, "Energy storage systems in modern gridsmatrix of technologies and applications," *Journal of Energy Storage*, vol. 6, pp. 248–259, 2016.

[34] M. Avendano-Mora and E. H. Camm, "Financial assessment of battery energy storage systems for frequency regulation service," in *2015 IEEE power & energy society general meeting*. IEEE, 2015, pp. 1–5.

[35] P. Fairley, "Flywheels keep the grid in tune," *IEEE Spectrum*, vol. 48, no. 7, pp. 16–18, 2011.

[36] S. A. Pourmousavi, M. H. Nehrir, and R. K. Sharma, "Multi-timescale power management for islanded microgrids including storage and demand response," *IEEE Transactions on Smart Grid*, vol. 6, no. 3, pp. 1185–1195, 2015.

[37] D. Wang, S. Ge, H. Jia, C. Wang, Y. Zhou, N. Lu, and X. Kong, "A demand response and battery storage coordination algorithm for providing microgrid tie-line smoothing services," *IEEE Transactions on Sustainable Energy*, vol. 5, no. 2, pp. 476–486, 2014.

[38] D. S. Callaway and I. A. Hiskens, "Achieving controllability of electric loads," *Proceedings of the IEEE*, vol. 99, no. 1, pp. 184–199, 2011.

[39] N. Lu, "An evaluation of the hvac load potential for providing load balancing service," *IEEE Transactions on Smart Grid*, vol. 3, no. 3, pp. 1263–1270, 2012.

[40] G. Strbac, M. Aunedi, D. Pudjianto, P. Djapic, F. Teng, A. Sturt, D. Jackravut, R. Sansom, V. Yufit, and N. Brandon, "Strategic assessment of the role and value of energy storage systems in the uk low carbon energy future," *Report for Carbon Trust*, no. 2012, 2012.

[41] M. Cheng, S. S. Sami, and J. Wu, "Benefits of using virtual energy storage system for power system frequency response," *Applied energy*, vol. 194, pp. 376–385, 2017.

[42] H.-J. Bullinger, C. Doetsch, and P. Bretschneider, "Smart grids-the answer to the new challenges of energy logistics?" *CESifo DICE Report*, vol. 10, no. 3, pp. 29–35, 2012.

[43] J. Eyer and G. Corey, "Energy storage for the electricity grid: Benefits and market potential assessment guide," *Sandia National Laboratories*, vol. 20, no. 10, p. 5, 2010.

[44] G. Strbac, "Demand side management: Benefits and challenges," *Energy policy*, vol. 36, no. 12, pp. 4419–4426, 2008.

[45] N. I. Commission *et al.*, "Smart power," *UK Gov*, 2016.

[46] M. R. Almassalkhi and I. A. Hiskens, "Model-predictive cascade mitigation in electric power systems with storage and renewables-Part II: Case-study," *IEEE Transactions on Power Systems*, vol. 30, no. 1, pp. 78–87, 2015.

[47] "IEEE standard for calculating the current-temperature relationship of bare overhead conductors," *IEEE Std 738-2012*, pp. 1–72, Dec 2013.

[48] H. W. Dommel and W. F. Tinney, "Optimal Power Flow Solutions," *IEEE Transactions on Power Apparatus and Systems*, vol. PAS-87, no. 10, pp. 1866–1876, 1968.

[49] J. Carpentier and A. Merlin, "Optimization methods in planning and operation," *International Journal of Electrical Power & Energy Systems*, vol. 4, no. 1, pp. 11–18, 1982.

[50] G. Chen and J. Yang, "A new particle swarm optimization solution to optimal reactive power flow problems," in *2009 Asia-Pacific Power and Energy Engineering Conference*. IEEE, 2009, pp. 1–4.

[51] Y. Li, Y. Wang, and B. Li, "A hybrid artificial bee colony assisted differential evolution algorithm for optimal reactive power flow," *International Journal of Electrical Power & Energy Systems*, vol. 52, pp. 25–33, 2013.

[52] T. Niknam, M. Narimani, J. Aghaei, and R. Azizipanah-Abarghooee, "Improved particle swarm optimisation for multi-objective optimal power flow considering the cost, loss, emission and voltage stability index," *IET generation, transmission & distribution*, vol. 6, no. 6, pp. 515–527, 2012.

[53] I. M. Malik and D. Srinivasan, "Optimum power flow using flexible genetic algorithm model in practical power systems," in *2010 Conference Proceedings IPEC*. IEEE, 2010, pp. 1146–1151.

[54] X. Zhang, K. Margellos, P. Goulart, and J. Lygeros, "Stochastic model predictive control using a combination of randomized and robust optimization," in *Decision and Control (CDC), 2013 IEEE 52nd Annual Conference on*. IEEE, 2013, pp. 7740–7745.

[55] F. Capitanescu, J. L. M. Ramos, P. Panciatici, D. Kirschen, A. M. Marcolini, L. Platbrood, and L. Wehenkel, "Electric Power Systems Research," *Electric Power Systems Research*, vol. 81, no. 8, pp. 1731–1741, Aug. 2011.

[56] N. Miller, M. Shao, S. Pajic, and R. DAquila, "Eastern frequency response study," *Contract*, vol. 303, pp. 275–3000, 2013.

[57] H. Jafari, M. Mahmoudi, A. Fatehi, M. H. Naderi, and E. Kaya, "Improved power sharing with a back-to-back converter and state-feedback control in a utility-connected microgrid," in *2018 IEEE Texas Power and Energy Conference (TPEC)*, Feb 2018, pp. 1–6.

[58] M. Mousavi, Y. Sangsefidi, A. Mehrizi-Sani, and R. Beiranvand, "Generalized step-down switched-capacitor converter under zcs for photovoltaic applications," *IEEE Transactions on Energy Conversion*, vol. 33, no. 3, pp. 1321–1329, Sep. 2018.

[59] M. G. Morgan and S. N. Talukdar, "Electric power load management: some technical, economic, regulatory and social issues," in *Proceedings of the IEEE*, 1979.

[60] F. C. Schweppe, R. D. Tabors, J. L. Kirtley Jr, H. R. Outhred, F. H. Pickel, and A. J. Cox, "Homeostatic utility control," *Power Apparatus and Systems, IEEE Transactions on*, no. 3, pp. 1151–1163, 1980.

[61] J. H. Eto, J. Nelson-Hoffman, C. Torres, S. Hirth, B. Yinger, J. Kueck, B. Kirby, C. Bernier, R. Wright, and A. Barat, "Demand response spinning reserve demonstration," *Lawrence Berkeley National Laboratory*, 2007.

[62] A. Molina-García, F. Bouffard, and D. S. Kirschen, "Decentralized demand-side contribution to primary frequency control," *IEEE Transactions on Power Systems*, vol. 26, no. 1, pp. 411–419, 2011.

[63] D. Callaway and I. Hiskens, "Achieving Controllability of Electric Loads," *Proceedings of the IEEE*, vol. 99, no. 1, pp. 184–199, 2011.

[64] C. Zhao, U. Topcu, N. Li, and S. Low, "Design and Stability of Load-Side Primary Frequency Control in Power Systems," *IEEE Transactions on Automatic Control*, vol. 59, no. 5, pp. 1177–1189, 2014.

[65] C. Zhao, E. Mallada, and F. Dörfler, "Distributed frequency control for stability and economic dispatch in power networks," in *Proceedings of IEEE American Control Conference*, 2015.

[66] S. Wang, X. Meng, and T. Chen, "Wide-area control of power systems through delayed network communication," *IEEE Transactions on Control Systems Technology*, vol. 20, no. 2, pp. 495–503, 2012.

[67] H. Hao, B. M. Sanandaji, K. Poolla, and T. L. Vincent, "Frequency regulation from flexible loads: Potential, economics, and implementation," in *2014 American Control Conference*. IEEE, 2014, pp. 65–72.

[68] ——, "Aggregate flexibility of thermostatically controlled loads," *IEEE Transactions on Power Systems*, vol. 30, no. 1, pp. 189–198, Jan 2015.

[69] L. Jiang, W. Yao, Q. H. Wu, J. Y. Wen, and S. J. Cheng, "Delay-dependent stability for load frequency control with constant and time-varying delays," *IEEE Transactions on Power Systems*, vol. 27, no. 2, pp. 932–941, 2012.

[70] C. K. Zhang, L. Jiang, Q. H. Wu, Y. He, and M. Wu, "Further results on delay-dependent stability of multi-area load frequency control," *IEEE Transactions on Power Systems*, vol. 28, no. 4, pp. 4465–4474, 2013.

[71] K. Ramakrishnan and G. Ray, "Stability Criteria for Nonlinearly Perturbed Load Frequency Systems With Time-Delay," *IEEE Journal on Emerging and Selected Topics in Circuits and Systems*, vol. 5, no. 3, pp. 383–392, 2015.

[72] T. I. Lakoba, "Lecture notes in numerical differential equations higher-order odes and systems of odes," May 2016.

[73] R. M. Hermans, A. Jokić, M. Lazar, A. Alessio, P. P. J. van den Bosch, I. A. Hiskens, and A. Bemporad, "Assessment of non-centralised model predictive control techniques for electrical power networks," *International Journal of Control*, vol. 85, no. 8, pp. 1162–1177, Aug. 2012.

[74] S. Yi, P. Nelson, and A. Ulsoy, "Survey on analysis of time delayed systems via the Lambert W function," *Advances in Dynamical Systems*, vol. 14, pp. 296–301, 2007.

[75] M. Arnold and G. Andersson, "Model predictive control of energy storage including uncertain forecasts," in *Power Systems Computation Conference, Stockholm, Sweden*, vol. 23, 2011, pp. 24–29.

[76] M. Almassalkhi, Y. Dvorkin, J. Marley, R. Fernández-Blanco, I. Hiskens, D. Kirschen, J. Martin, H. Pandžič, T. Qiu, M. Sarker *et al.*, "Incorporating storage as a flexible transmission asset in power system operation procedure," in *Power Systems Computation Conference (PSCC), 2016*. IEEE, 2016, pp. 1–7.

[77] J. L. Mathieu, M. G. Vayá, and G. Andersson, "Uncertainty in the flexibility of aggregations of demand response resources," in *Industrial Electronics Society, IECON 2013-39th Annual Conference of the IEEE*. IEEE, 2013, pp. 8052–8057.

[78] K. Margellos, P. Goulart, and J. Lygeros, "On the road between robust optimization and the scenario approach for chance constrained optimization problems," *IEEE Transactions on Automatic Control*, vol. 59, no. 8, pp. 2258–2263, 2014.

[79] G. C. Calafiore and M. C. Campi, "The scenario approach to robust control design," *IEEE Transactions on Automatic Control*, vol. 51, no. 5, pp. 742–753, 2006.

[80] M. S. Modarresi, L. Xie, M. Campi, S. Garatti, A. Carè, A. Thatte, and P. R. Kumar, "Scenario-based economic dispatch with tunable risk levels in high-renewable power systems," *IEEE Transactions on Power Systems*, pp. 1–1, 2018.

[81] M. Vrakopoulou, B. Li, and J. L. Mathieu, "Chance constrained reserve scheduling using uncertain controllable loads Part I: Formulation and scenario-based analysis," *IEEE Transactions on Smart Grid*, 2017.

[82] B. Li, M. Vrakopoulou, and J. L. Mathieu, "Chance constrained reserve scheduling using uncertain controllable loads Part II: Analytical reformulation," *IEEE Transactions on Smart Grid*, 2017.

[83] M. R. Almassalkhi and I. A. Hiskens, "Model-predictive cascade mitigation in electric power systems with storage and renewables-Part I: Theory and implementation," *IEEE Transactions on Power Systems*, vol. 30, no. 1, pp. 67–77, 2015.

[84] B. Li, S. D. Maroukis, Y. Lin, and J. L. Mathieu, "Impact of uncertainty from load-based reserves and renewables on dispatch costs and emissions," in *2016 North American Power Symposium*, Sept 2016, pp. 1–6.

[85] Y. Zhang and J. L. Mathieu, "Two-stage Distributionally Robust Optimal Power Flow with Flexible Loads," *PowerTech 2017*, 2017.

[86] K. Baker, G. Hug, and X. Li, "Energy storage sizing taking into account forecast uncertainties and receding horizon operation," *IEEE Transactions on Sustainable Energy*, vol. 8, no. 1, pp. 331–340, Jan 2017.

[87] A. J. Wood and B. F. Wollenberg, *Power generation, operation, and control*. John Wiley & Sons, 2012.

[88] B. Henson. Regulation performance monitor. [Online]. Available: https://www.iso-ne.com/static-assets/documents/support/training/courses/energy_mkt_ancil_serv_top/regulation_performanc_monitor_rollout.pdf

[89] M. Vrakopoulou and S. Chatzivasileiadis, "Probabilistic security-constrained optimal power flow including the controllability of HVDC lines," pp. 1–5, 2013.

[90] L. Bai, J. E. Mitchell, and J.-S. Pang, "On convex quadratic programs with linear complementarity constraints," *Computational Optimization and Applications*, vol. 54, no. 3, pp. 517–554, 2013.

[91] S. M. Nosratabadi, R.-A. Hooshmand, and E. Gholipour, "A comprehensive review on microgrid and virtual power plant concepts employed for distributed energy resources scheduling in power systems," *Renewable and Sustainable Energy Reviews*, no. Supplement C, pp. 341–363.

[92] M. Almassalkhi, J. Frolik, and P. Hines, "Packetized energy management: asynchronous and anonymous coordination of thermostatically controlled loads," in *American Control Conference, 2017*. IEEE, 2017, pp. 1431–1437.

[93] R. D. Zimmerman, C. E. Murillo-Sánchez, and R. J. Thomas, "Matpower: Steady-state operations, planning, and analysis tools for power systems research and education," *IEEE Transactions on power systems*, vol. 26, no. 1, pp. 12–19, 2011.

[94] California Independent System Operator. Revised update to CAISO draft final proposal on uneconomic adjustments policy and parameter values. [Online]. Available: http://caiso.com/documents/update-draftfinalproposalonuneconomicAdjustments.html

[95] H. Banakar, N. Alguacil, and F. D. Galiana, "Electrothermal coordination part i: theory and implementation schemes," *IEEE Transactions on Power Systems*, vol. 20, no. 2, pp. 798–805, May 2005.

[96] L. Duffaut Espinosa and M. Almassalkhi, "A Packetized Energy Management Macro-model, Part I: Deferrable loads and Quality of Service," Submitted to the IEEE Transactions on Power Systems.

[97] L. Duffaut Espinosa, M. Almassalkhi, and A. Khurram, "A Packetized Energy Management Macro-model, Part II: Tracking with Diverse DER Populations," Submitted to the IEEE Transactions on Power Systems.

[98] L. A. D. Espinosa, M. Almassalkhi, P. Hines, and J. Frolik, "Aggregate modeling and coordination of diverse energy resources under packetized energy management."

[99] M. Amini and M. Almassalkhi, "Trading off robustness and performance in receding horizon control with uncertain energy resources," in *Power Systems Computation Conference (PSCC), 2018 IEEE*. IEEE, 2018.

[100] S. Peralta. FCM pay for performance evaluations. [Online]. Available: https://www.iso-ne.com/static-assets/documents/2017/11/20171023-14-fcm101-pfp.pdf

[101] M. Vrakopoulou, K. Margellos, J. Lygeros, and G. Andersson, "A probabilistic framework for reserve scheduling and $n-1$ security assessment of systems with high wind power penetration," *IEEE Transactions on Power Systems*, vol. 28, no. 4, pp. 3885–3896, Nov 2013.

[102] L. Roald, F. Oldewurtel, T. Krause, and G. Andersson, "Analytical reformulation of security constrained optimal power flow with probabilistic constraints," in *2013 IEEE Grenoble Conference*, June 2013, pp. 1–6.

[103] L. Roald, S. Misra, T. Krause, and G. Andersson, "Corrective control to handle forecast uncertainty: A chance constrained optimal power flow," *IEEE Transactions on Power Systems*, vol. 32, no. 2, pp. 1626–1637, 2017.

[104] B. Li and J. L. Mathieu, "Analytical reformulation of chance-constrained optimal power flow with uncertain load control," in *2015 IEEE Eindhoven PowerTech*, June 2015, pp. 1–6.

[105] L. Roald, S. Misra, A. Morrison, and G. Andersson, "Optimized risk limits for stochastic optimal power flow," in *Decision and Control (CDC), 2017 IEEE 56th Annual Conference on*. IEEE, 2017, pp. 4476–4483.

[106] L. Roald, S. Misra, M. Chertkov, and G. Andersson, "Optimal power flow with weighted chance constraints and general policies for generation control," in *Decision and Control (CDC), 2015 IEEE 54th Annual Conference on*. IEEE, 2015, pp. 6927–6933.

[107] K. Deb, K. Sindhya, and J. Hakanen, "Multi-objective optimization," in *Decision Sciences: Theory and Practice*. CRC Press Boca Raton, FL, 2016, pp. 145–184.

[108] C. Grigg, P. Wong, P. Albrecht, R. Allan, M. Bhavaraju, R. Billinton, Q. Chen, C. Fong, S. Haddad, S. Kuruganty *et al.*, "The ieee reliability test system-1996. a report prepared by the reliability test system task force of the application of probability methods subcommittee," *IEEE Transactions on power systems*, vol. 14, no. 3, pp. 1010–1020, 1999.

[109] C. Budischak, D. Sewell, H. Thomson, L. Mach, D. E. Veron, and W. Kempton, "Cost-minimized combinations of wind power, solar power and electrochemical storage, powering the grid up to 99.9% of the time," *Journal of Power Sources*, vol. 225, pp. 60–74, 2013.

[110] M. Mousavi, P. M. Shabestari, and A. Mehrizi-Sani, "Analysis and output voltage control of a high-efficiency converter for dc microgrids," in *IECON 2018 - 44th Annual Conference of the IEEE Industrial Electronics Society*, Oct 2018, pp. 1029–1034.

[111] A. Molina-Garcia, F. Bouffard, and D. S. Kirschen, "Decentralized demand-side contribution to primary frequency control," *IEEE Transactions on Power Systems*, vol. 26, no. 1, pp. 411–419, Feb 2011.

[112] K. Desrochers, V. Hines, F. Wallace, J. Slinkman, A. Giroux, A. Khurram, M. Amini, M. Almassalkhi, and P. Hines, "Real-world, full-scale validation of power balancing services from packetized virtual batteries," in *Proceedings of the 10th Conference on Innovative Smart Grid Technologies (ISGT 2019)*, 2019.

[113] P. Kundur, N. J. Balu, and M. G. Lauby, *Power system stability and control*. McGraw-hill New York, 1994, vol. 7.

[114] E. G. Kardakos, C. K. Simoglou, and A. G. Bakirtzis, "Optimal offering strategy of a virtual power plant: A stochastic bi-level approach," *IEEE Transactions on Smart Grid*, vol. 7, no. 2, pp. 794–806, 2016.

[115] A. Mnatsakanyan and S. W. Kennedy, "A novel demand response model with an application for a virtual power plant," *IEEE Transactions on Smart Grid*, vol. 6, no. 1, pp. 230–237, 2015.

[116] J. Johnson, J. Flicker, A. Castillo, C. Hansen, M. El-Khatib, D. Schoenwald, M. A Smith, R. Graves, J. Henry, T. Hutchins, J. Stamp, D. Hart, A. Chavez, M. Burnett, J. Tabarez, C. Glatter, B. Xie, A. Meliopoulos, P. Huynh, and K. Davis, "Design and evaluation of a secure virtual power plant," *Sandia Technical Report, SAND2017-10177*, 09 2017.

[117] F. Borrelli, A. Bemporad, and M. Morari, *Predictive control for linear and hybrid systems*. Cambridge University Press, 2017.

[118] I. A. Hiskens and B. Gong, "Mpc-based load shedding for voltage stability enhancement," *Proceedings of the 44th IEEE Conference on Decision and Control*, pp. 4463–4468, Dec 2005.

[119] M. Amini and M. Almassalkhi, "Corrective dispatch of uncertain energy resources using chance-constrained receding horizon control," *arXiv preprint arXiv:1810.08685*, 2018.

[120] A. M. Ersdal, L. Imsland, and K. Uhlen, "Model predictive load-frequency control," *IEEE Transactions on Power Systems*, vol. 31, no. 1, pp. 777–785, 2016.

[121] NIST, *NIST Framework and Roadmap for Smart Grid Interoperability Standards, Release 3.0*, Sep 2014. [Online]. Available: https://www.nist.gov/sites/default/files/documents/smartgrid/NIST-SP-1108r3.pdf

[122] S. Xin, Q. Guo, H. Sun, B. Zhang, J. Wang, and C. Chen, "Cyber-physical modeling and cyber-contingency assessment of hierarchical control systems," *IEEE Transactions on Smart Grid*, vol. 6, no. 5, pp. 2375–2385, Sept 2015.

[123] A. Teymouri, S. H. Fathi, and F. Karbakhsh, "An advanced hysteresis controller to improve voltage profile of power system with pv units: A smart grid power exchange framework," in *2015 30th International Power System Conference (PSC)*. IEEE, 2015, pp. 79–85.

[124] National Institute of Standards and Technology Smart Grid Interoperability Panel, *NIST-IR 7628 Volume 1, Guidelines for Smart Grid Cyber Security*, 2010, no. September. [Online]. Available: http://permanent.access.gpo.gov/gpo1900/nistir-7628_total.pdf

[125] A. Teymouri, A. Mehrizi-Sani, and C.-C. Liu, "Cyber security risk assessment of solar pv units with reactive power capability," in *IECON 2018-44th Annual Conference of the IEEE Industrial Electronics Society*. IEEE, 2018, pp. 2872–2877.

[126] R. M. Hermans, A. Jokić, M. Lazar, A. Alessio, P. P. Van den Bosch, I. A. Hiskens, and A. Bemporad, "Assessment of non-centralised model predictive control techniques for electrical power networks," *International journal of control*, vol. 85, no. 8, pp. 1162–1177, 2012.

[127] H. Jafari, M. Mahmodi, and H. Rastegar, "Frequency control of micro-grid in autonomous mode using model predictive control," in *Iranian Conference on Smart Grids*, May 2012, pp. 1–5.